Kinetics and Mechanism of The Photocycle of Photoactive Yellow Protein

Chandra P. Joshi

A dissertation submitted for the degree

of the Doctor of Natural Science at the

Department of Physics of the

Free University Berlin

5 July 2006

First referee	Prof. Dr. Maarten P. Heyn
Second referee	Prof. Dr. Robert Bittl
Date of defense	5 July 2006

Table of Contents

Table of Contents

[1]Abbreviations:

PYP	**P**hotoactive **Y**ellow **P**rotein
WT	**W**ild **T**ype
Hr. Halophila	***Halo****r**hodospira Halophila*
PAS	**P**ER-**A**RNT-**S**IM, acronym formed from the names of the first three proteins of this family (**p**eriod clock protein, **a**ryl hydrocarbon receptor nuclear translocator, **s**ingle minded protein)
NMR	**N**uclear **M**agnetic **R**esonance
FTIR	**F**ourier **T**ransform **I**nfrared **S**pectroscopy
RR	**R**esonance **R**aman
CD	**C**ircular **D**ichroism
SAXS	**S**mall **A**ngle **X**-ray **S**cattering
pCA	**p**ara-**C**oumaric **A**cid
PR	**P**hoto**r**eversal Signal
SVD	**S**ingular **V**alue **D**ecomposition
BFTB	**B**lue **F**lash data acquisition **T**riggered on **B**lue flash
DFTB	**D**ouble **F**lash data acquisition **T**riggered on **B**lue flash
DFTV	**D**ouble **F**lash data acquisition **T**riggered on **V**iolet flash
BFTV	**B**lue **F**lash data acquisition **T**riggered on **V**iolet flash
VFTV	**V**iolet **F**lash data acquisition **T**riggered on **V**iolet flash
GFTG	**G**reen **F**lash data acquisition **T**riggered on **G**reen flash

List of amino acids:

A	Alanine (Ala)
C	Cysteine (Cys)
D	Aspartic acid (Asp)
E	Glutamic acid (Glu)
F	Phenylalanine (Phe)
G	Glycine (Gly)
H	Histidine (His)
I	Isoleucine (Ile)
K	Lysine (Lys)
L	Leucine (Leu)
M	Methionine (Met)
N	Asparagine (Asn)
P	Proline (Pro)
Q	Glutamine (Gln)
R	Arginine (Arg)
S	Serine (Ser)
T	Threonine (Thr)
V	Valine (Val)
W	Tryptophan (Trp)
Y	Tyrosine (Tyr)

Abstract

The kinetics and intermediates of the photocycle and photoreversal of photoactive yellow protein were investigated from pH 4.6 to 11 by time-resolved absorption spectroscopy. At pH 7, three intermediate states: I_1 (λ_{max} ~ 460 nm), I_2 (λ_{max} ~ 370 nm) and I_2' (λ_{max} ~ 350 nm) were observed. I_2' is the signaling state of this photoreceptor. The time courses and the spectra of these intermediates were constructed using the extrapolated difference method. From the rise of I_2' (~ 1.0 ms) to the end of the cycle, I_1, I_2 and I_2' are in equilibrium. The equilibrium between I_2 and I_2' is pH dependent. Upon increasing the pH from 4.6 to 8.4, the I_2 population decreases whereas I_2' increases with a pK_a of ~6.4. This pK_a might be assigned to the carboxylate side chain of E46. Due to the pH dependent I_2/I_2' equilibrium, the ground state recovery rate is also pH dependent with the same pK_a.

At pH 10, three intermediate states: I_1, I_1' and I_2' were observed. The spectrum of I_1' (λ_{max} ~ 425nm) was determined. From the rise of I_2' (~ 1.0 ms) to the end of the cycle, I_1, I_1' and I_2' are in a pH dependent equilibrium with a pK_a of ~ 9.9. Upon increasing the pH from 8 to 11, the I_1/I_1' population increases whereas I_2' decreases. This pK_a is assigned to the deprotonation of the phenol of the exposed chromophore. I_2 contributes minimally in this pH range. The rate constant for the ground state recovery also has a pK_a of ~ 10 suggesting that $k_3 \sim [I_2']$. Thus, the pH controls the accumulation of the signaling state I_2'.

The kinetics of photoreversal from the I_1, I_2 and I_2' intermediates was investigated with double flash excitation. A first flash, at 430 nm, initiated the photocycle. After a variable time delay, the I_1 intermediate was photoreversed by a second flash, at 500 nm, or a mixture of I_2 and I_2' intermediates was photoreversed by a second flash, at 355 nm. The photoreversal times from the I_1, I_2 and I_2' intermediates are respectively <1 μs (unresolved), 57 μs and 380 μs at pH 6. The first step in photoreversal is unresolved *cis-trans* isomerization of the chromophore. The respective delay dependent photoreversal amplitudes corresponding to 57 μs and 380 μs confirmed the temporal variation of the I_2 and I_2' intermediates of the normal cycle, and I_2 and I_2' are in equilibrium after 5 ms. Measurement of the pH dependent photoreversal amplitudes with 355 nm as a second flash applied with a delay of 20 ms, and at pH range from 4.6 to 8.5 produced a pK_a ~6.1. This confirms the normal cycle I_2/ I_2' equilibrium. Depending on the progression of the photocycle, reversal becomes slower with the time delay, thus mirroring the individual steps of the forward photocycle. Photoreversal experiments at pH 10 with the second flash at 355 nm confirm the presence of the I_1' and I_2' intermediates and absence of the I_2.

Chapter 1

Introduction

In this study, the mechanism of the photocycle kinetics of the blue light photoreceptor photoactive yellow protein (PYP[1]) from *Halorhodospira Halophila* is investigated in detail. Transient absorption spectroscopy with single and double flash excitation is used to investigate the photocycle of wild type (WT[1]) PYP. For an understanding of the mechanism of the photocycle it is necessary to determine the spectra of the intermediates and their temporal interconversions.

This thesis is organised as follows: basics about PYP related to the structure, function and dynamics are discussed in Chapter 1. In addition, the specific aims of this investigation are highlighted in this Chapter. Chapter 2 reports about the details of the materials and methods applied in this investigation. The experimental results of the photocycle kinetics are presented in Chapter 3 where the results are divided according to the pH ranges: acid/neutral and alkaline pH. These observations are supported by the experimental results with the double flash excitation as described in Chapter 4. Finally, a summary and outlook of this investigation are presented.

1.1 Photoactive Yellow Protein (PYP)

During the extraction of all coloured proteins from halophilic, photosynthetic purple bacteria *Ectothiorhodospira* (now *Halorhodospira*) *Halophila*, Terry E. Meyer discovered photoactive yellow protein (PYP) in the cytoplasm of this bacterium **[Meyer, 1985]**. This protein is highly soluble in water and has a brilliant yellow colour at neutral pH. PYP absorbs blue light with an absorbance maximum at 446 nm, Figure 1.1, with a high extinction coefficient (ε=45000 $M^{-1}cm^{-1}$). This protein has a reversible photo bleaching (photocycle) upon blue light illumination **[Meyer, 1987]**. At neutral pH, the initial dark state is resumed within sub-s time range after the bleach **[Meyer, 1987]**.

These bacteria, *Hr. Halophila*[1], accumulate in photosynthetic green light **[Sprenger, 1993]** and the video analysis of freely swimming bacteria shows that they swim out of intense (but nondamaging) blue light. This physiological action is reversible upon reducing light intensity indicating that physiological action is inhibited by light. The action spectrum of this physiological reaction is similar to the absorption spectrum of PYP indicating that PYP might be mediating this action. *Hr. Halophila* exhibits a repellent response to blue light, presumably to select the optimal light levels and living conditions **[Sprenger, 1993]**. Recently hybrid PYP/Phytochrome photoreceptors have been discovered with well-defined functions **[Kyndt, 2004]**.

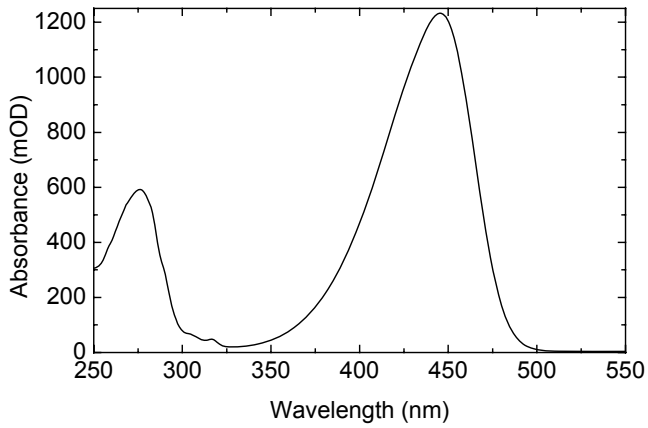

Figure 1.1: Absorption spectrum of an aqueous solution of photoactive yellow protein from *Hr. halophila*.

Photo-bleaching of PYP with blue light initiates the structural changes **[Meyer, 1989]** (for details, see below) of this protein (similar to partial unfolding). This structurally altered protein is supposed to bind to a response regulator (still unidentified) during signal transduction, a signaling process similar to that of other sensory proteins like rhodopsin, bacteriorhodopsin, phytochrome and phototropin **[Meyer, 1989]**. Therefore, PYP and its photocycle have been studied in considerable detail since its discovery, to elucidate this signal transduction mechanism up-to atomic level (detail later). In addition, the structural motif of PYP is found to be similar to that of PAS[1] domain proteins (detail later) which are sensory modules found in signaling proteins of all kingdoms of life. Therefore, PYP is proposed as the structural prototype of this universal domain. A variety of biophysical techniques have been used to study the structure and dynamics of PYP. Foremost of them are: time resolved X-ray Laue crystallography, NMR[1] in solution, FTIR[1] in crystal and solution, RR[1], CD[1], SAXS[1], fluorescence and transient absorbance spectroscopy. Structure, function and dynamics of PYP were recently reviewed in **[Cusanovich, 2003]** and **[Hellingwerf, 2003]**.

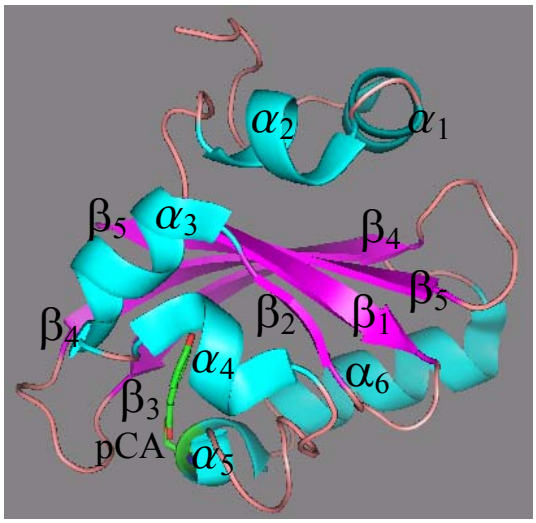

Figure 1.2: A ribbon representation of the secondary structure of PYP from *Hr. halophila*. pCA[1] chromophore is shown in green and red sticks. Color code of the secondary structure: random coils-brown, helices-cyan (labeled with: α_1- α_6), central anti-parallel β sheet-pink (labeled with: β_1- β_5). Structure was acquired from **[Ihee, 2005]**. The crystal structure data are deposited in the protein data bank: http://pdbbeta.rcsb.org/pdb/ with PDB ID: 1TS6. Figure was produced using molecular visualisation system PyMOL: http://pymol.org/.

The secondary structure of PYP determined from X-ray crystallography at 1.6 Å spatial resolution **[Ihee, 2005]** shows that it has a mixed α/β fold with a five-stranded central anti-parallel β–sheet flanked by six α–helices, as shown in the Figure 1.2.

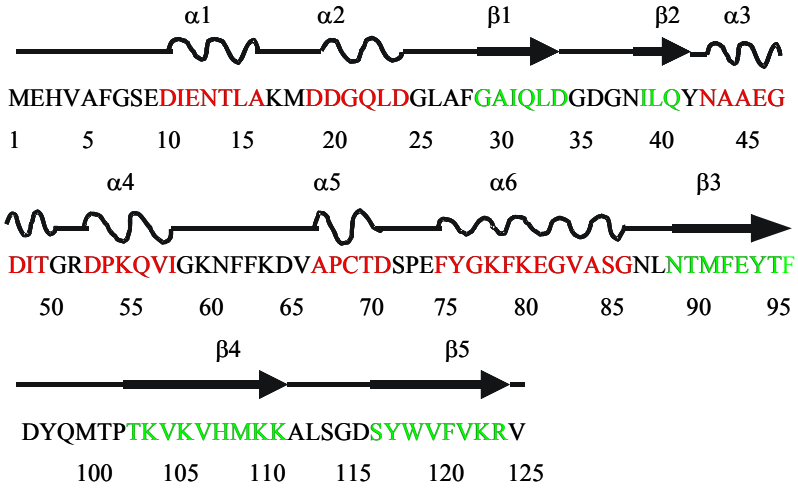

Figure 1.3: Sequence and corresponding secondary structure of photoactive yellow protein **[Ihee, 2005]**. Corresponding secondary structures: random coils (black), α helices (red) and β strands (green) are indicated above this sequence and are represented by straight line, wave form and thick arrow respectively. Names of the corresponding secondary structure elements: alpha helices, α_1-α_6, and beta strands (β_1-β_5) are placed on the top.

The solution structure of PYP was also resolved with NMR resulting in an ensemble of 26 structures **[Düx, 1998]**. The solution and the crystal structures are essentially the same **[Hellingwerf, 2003]**.

Blue light absorption of PYP is due to its 4-hydroxycinnamoyl chromophore also called para-coumaric acid (pCA[1]) **[Hoff, 1994]**, which is covalently attached to a unique

cysteine located at the position 69 in helix α_5 via a thioester bond **[Hoff, 1994]**, Figures 1.2 and 1.4.

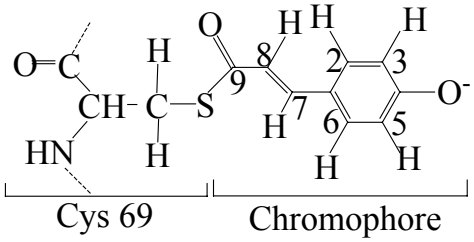

Figure 1.4: Chemical structure of PYP chromophore linked to Cys-69 of the apoprotein via a thiol ester bond.

The primary structure of this protein consists of a sequence of 125 amino acids as shown in Figure 1.3. The chemical structure of the PYP chromophore is shown in Figure 1.4. The molecular weight of this protein, determined by ionisation mass spectroscopy, is 14020 Daltons **[Baca, 1994]**.

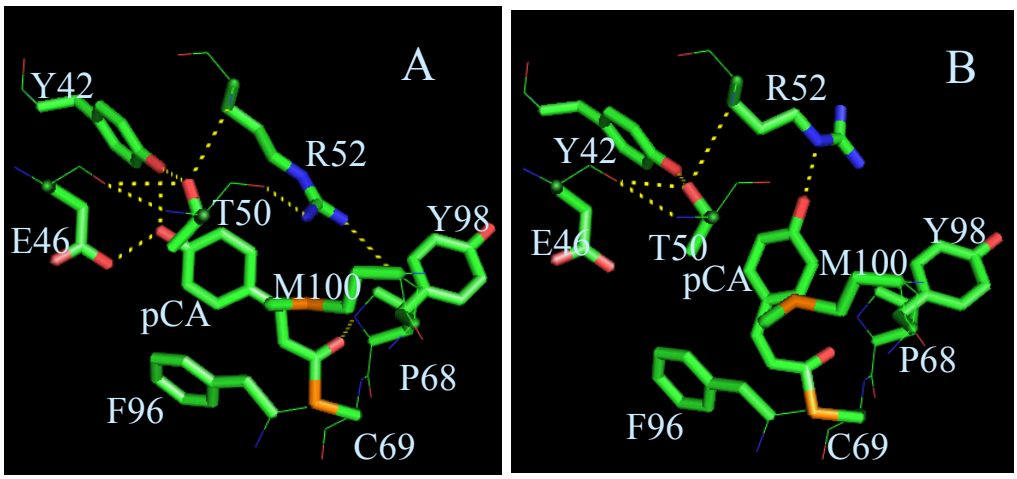

Figure 1.5: Structure of the chromophore binding pocket of PYP in (A) dark and (B) I_2 intermediate. Hydrogen bonds are shown as yellow dotted lines. Carbon, oxygen, nitrogen and sulphur atoms are shown as sticks (thick: side chain, thin: main chain) with green, red, blue and orange colours respectively. Figure A is the detailed structure around the chromophore of Figure 1.2. The structural data for Figure B are acquired from PDB ID:1TS6.

The chromophore is buried in a hydrophobic pocket inside the protein surrounded by amino acids T50, E46, Y42, R52, M100, Y98, F96 (see abbreviations) as shown in Figure 1.5. The chromophore is anchored by three hydrogen bonds, two of them between the phenolate oxygen and the protonated side chains of Y42 and E46, Figure 1.5A. The third one is between the chromophore carbonyl and the backbone amide proton of C69.

In the dark the chromophore is in the anionic form **[Baca, 1994]**, **[Kim, 1995]** and in the *trans* configuration **[Borgstahl, 1995]**, **[Genick, 1997A]**. The side chain oxygen of T50

forms a hydrogen bond with the hydroxyl group of Y42 and the main chain carbonyl oxygen of the E46 **[Borgstahl, 1995]**. In addition, the guanidinium group of R52 forms hydrogen bonds with the main chain oxygens of T50 and Y98. The chromophore is separated from the solvent only by the side chain of R52. The tight packing of the protein core strongly constrains the chromophore mobility and limits the *trans* to *cis* isomerization which occurs in fs only after light absorption **[Genick, 1997A]**.

Free coumaric acid in water at neutral pH absorbs maximally at 284 nm **[Kroon, 1996]**. Native PYP denatured with 4 M GdnHCl absorbs maximally at 339 nm and 397 nm at pH 3 and pH 11 respectively with a pK_a of 8.9 of phenolate oxygen. The red-shift of the absorbance maximum from 284 nm to 339 nm is due to binding of pCA covalently to Cys-69 of PYP. Deprotonation of the phenolate oxygen of bound pCA further red-shifts the absorbance maximum to 397 nm, which is at 446 nm for the buried pCA (deprotonated) inside the folded native protein. Thus the additional blue shift of ~49 nm is due to protein chromophore interaction **[Kroon, 1996]**.

The absorbance maximum of native PYP at pH 2 is blue-shifted by ~96 nm to 350 nm (close to the absorbance maximum of the denatured form) and the chromophore is protonated indicating that the protein is partially denatured at low pH. The pK_a of this chromophore protonation is 2.8 **[Meyer, 1985]**. PYP is indeed denatured with strong acid and gets hydrolysed above pH 11. In the active site of PYP the deprotonated form of the phenolate oxygen is stabilized, Figure 1.5A, indicating that the ionisation constants for both E46 and the chromophore are shifted strongly in opposite directions from their solution pK_a values (4.5 and 9) **[Baca, 1994]**. For the bound chromophore the pK_a is lowered to 2.8. Although the exact nature of the protein-chromophore interaction and of this unusual pK_a is unclear, it is argued that the anion form of the chromophore is stabilized in the dark by forming unusually short hydrogen bonds with Y42 and E46 in this highly packed area **[Xie, 2001]**, where hydrogen bonds acquire significant covalent character **[Anderson, 2004]**.

The interaction of the chromophore with the protein dramatically changes the photochemical properties of this cofactor (see below). ApoPYP may be reconstituted with anhydrides of various chromophore analogues **[Kroon, 1996]**. Analogues lacking the 4-hydroxy substituent lack both chromophore deprotonation and chromophore protein interaction (hybrid PYPs have only the protonated form of the chromophore analogue) confirming the importance of this substituent in the spectral tuning of PYP. Hydroxy and methoxy substitutions in the 3- and/or 5- position, Figure 1.4, donot disrupt strong interactions with the protein (hybrid PYPs have both the protonated and anionic form of the

chromophore analogue) but increase their pK_a for protonation and fluorescence quantum yield **[Kroon, 1996]**.

This protein is highly stable against heating as it can be heated at 90°C for 10 minutes without permanent damage **[Meyer, 1987]**. The protein denatures in 4 M urea, thus also shows high stability against denaturation.

PYP enters a photocycle upon blue light excitation. During the photocycle, thermally unstable and spectrally distinguishable intermediates are formed in the dark, which are in their electronic ground state. The photocycle events of PYP in solution at neutral pH and room temperature can be divided into four parts, as shown in Figure 1.6:

1. Photo-isomerization around the C_7-C_8 double bond: This is the early event just after reaching the Franck-Condon state with a short blue laser pulse. Using ultrafast infrared spectroscopy, it was shown that the electronic excited state, P*, decays to the early photointermediate I_0 (λ_{max}~510 nm) in 3 ps **[Heyne, 2005]**. Structural changes on the femtosecond time scale are probably restricted to the closely packed chromophore within the hydrophobic binding pocket leading to breaking of the hydrogen bond between the carbonyl oxygen of the covalent thiol ester and the backbone amide hydrogen of the Cys 69, Figure 1.5A, along with a partial twist of the thioester bond **[Heyne, 2005]**, **[Genick, 1998]**. This movement is associated with complete isomerization about the C_7=C_8 bond attached to the phenolic ring, Fig 1.4, without significant relocation of this phenolate moiety **[Heyne, 2005]**. This leads to the formation of the more relaxed planar chromophore **[Heyne, 2005]**, **[Genick, 1998]**. Trans to cis isomerization process upon excitation is driven via charge translocation from the phenolic oxygen toward the ethylene chain, weakening of the isomerizabale C_7=C_8 bond and thus leading to the isomerization **[Groot, 2003]**.

The fluorescence quantum yield from P* at room temperature is very low ~ 10^{-3} **[Meyer, 1991]** suggesting that the photocycle processes occur with high efficiency **[Groot, 2003]**. I_0 decays with 1 ns life time to form the relatively stable intermediate I_1 **[Groot, 2003]**.

I_1 absorbs maximally at 460nm **[Meyer, 1987]**, **[Yeremenko, 2006]** and in this intermediate the carboxyl group of Glu 46 remains protonated **[Brudler, 2001]** and the hydrogen bond to the chromophore's phenolate oxygen is further strengthened **[Perman, 1998]**, **[Genick, 1998]**, **[Brudler, 2001]**, **[Unno, 2000]**, **[Ren, 2001]**, **[Pan, 2004]**. The chromophore configuration as a whole is altered significantly (photon energy is stored and the resulting chromophore is in a higher energy state).

2. Proton uptake and chromophore protonation: In 370 μs, I_1 decays to I_2, Figure 1.6, where the protein takes up one proton from solvent **[Meyer, 1993]**, **[Borucki, 2002]**. The phenolate

oxygen of the chromophore, in *cis* form, is protonated in I_2 **[Imamoto, 1997]**, **[Unno, 2002]**, **[Unno, 2003]** and the local protein environment is altered **[Brudler, 2001] [Xie, 2001]**, **[Unno, 2003], [Pan, 2004]** blue-shifting the absorption maximum to λ_{max}=370nm **[Otto, 2005]**, **[Yeremenko, 2006]**, **[Shimizu, 2006]**. Both hydrogen bonds with the phenolate oxygen are broken **[Genick, 1997A]**, **[Ihee, 2005]**, and the phenolate moiety of the chromophore is exposed to the solvent **[Genick, 1997A]**, **[Brudler, 2001] [Xie, 2001]**, **[Pan, 2004], [Unno, 2003]** allowing it to move towards Arg 52 forming an hydrogen bond with its side chain **[Genick, 1997A]**, Figure 1.5B. The carbonyl part of the chromophore flips back towards the backbone reforming the hydrogen bond with the main chain of cysteine **[Pan, 2004], [Ihee, 2005]**.

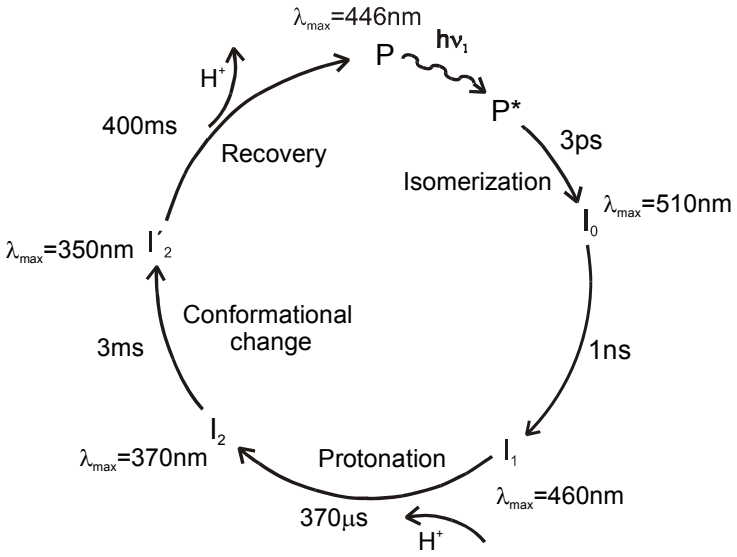

Figure 1.6: Photocycle of PYP in solution from *H. halophila* at neutral pH and room temperature. P is the ground state and P* the excited state. Intermediate states are shown along with the values of their absorption maxima and half-lifes. I_0, and I_1 are states with a *cis* form of the deprotonated chromophore and I_2 and I_2' are *cis* states with protonated chromophore. The values of the absorption maximum and half-life of I_0 state were acquired from **[Groot, 2003]** and the remaining from **[Joshi, 2005]**. Key photocycle events associated with various transitions are shown in the interior part of the scheme.

There are a variety of explanations for the chromophore protonation mechanism. Whether the chromophore is protonated intramolecularly from the putative proton donor, E46 **[Xie, 2001]** or from the solvent upon outer exposure of the chromophore **[Borucki, 2002]** is still to be established.

The kinetics of proton uptake and formation of the I_2 intermediate was shown to be synchronised in flash photolysis experiments with a pH indicator dye, suggesting that protonation of the chromophore occurs by proton transfer from the solvent **[Borucki, 2002]**.

According to a different explanation of the chromophore protonation mechanism, formation of I_2 involves intramolecular proton transfer from Glu-46 to the phenolate oxygen

whereby the strong hydrogen-bonding interaction between the chromophore and E46 is lost **[Imamoto, 1997]**, **[Xie, 2001]**. Therefore, I_1-to-I_2 transition is likely to be the stage where the stored photon energy is transferred from the distorted chromophore to the protein, producing a relaxed I_2 chromophore structure.

3. Signaling state formation: Recent time-resolved FTIR **[Brudler, 2001]**, **[Xie, 2001]**, UV/Vis transient absorption spectroscopy **[Yeremenko, 2006]** and dye binding **[Borucki, 2002]**, **[Hendriks, 2002]** studies showed that about 3 ms after flash excitation I_2 decays to another blue-shifted intermediate with a protonated chromophore, I_2' (decay time ~400 ms), Figure 1.6. This transition is associated with a major conformational change of the protein as indicated by structural and spectroscopic methods in solution such as NMR **[Rubinstenn, 1998]**, FTIR (**[Xie, 2001], [Hoff, 1999]**), SAXS (**[Sasaki, 2002]**, **[Imamoto, 2002]**), and CD (**[Sasaki, 2002]**, **[Lee, 2001]**, **[Ohishi, 2001]**). The global structural change from I_2 to I_2' has also been described as a partial unfolding **[Van Brederode, 1996]** and the absorbance maximum is further blue shifted to ~350nm **[Otto, 2005]**. In I_2', a hydrophobic surface area is exposed **[Meyer, 1989]**, **[Borucki, 2002]** which is found to be near the chromophore binding site **[Genick, 1997A]**, **[Hendriks, 2002]** as well as the N-terminal cap **[Rubinstenn, 1998]**, Figure 1.7.

Long-lived I_2 (more precisely a photostationary mixture of I_2 and I_2') intermediate shows considerable disorder in solution structure mainly in the N-terminal domain **[Rubinstenn, 1998]**. Movement of the N-terminal cap in the I_2 to I_2' transition allows the exposure of a hydrophobic area which presumably involves the anti-parallel β-sheet of the PAS core.

A partial loss of ellipticity is observed in I_2' **[Lee, 2001]**, and assumed to be due to the swinging away of the N-terminus from the central β-sheet, and the associated structural change, Figure 1.7.

The conformational change detected by X-ray diffraction in the I_2 intermediate, was found to be limited to the chromophore and the binding pocket **[Genick, 1997A]**, **[Ihee, 2005]**. In I_2 the chromophore reorients by about 60°, bringing its oxygen close to the protein surface **[Genick, 1997A]**. It is likely that in crystals packing constraints prevent the formation of I_2' and that the crystal structure of ref **[Genick, 1997A]** and of Figure 1.5B both refer to I_2.

The structurally altered I_2' state is supposed to be the signalling state where a response regulator (unidentified to date) binds via hydrophobic contact during the signal transduction process **[Cusanovich, 2003]**.

The dyes bromocresol purple **[Borucki, 2002]** and Nile red **[Hendriks, 2002]** bind transiently to the surface of the structurally altered I_2' intermediate but not in I_2. Indicating that the long-living I_2' intermediate rather than I_2 is the activated or signaling state.

Direct comparison of the time-resolved FTIR spectroscopic data in solution and in crystals also showed that the structure of the putative signaling state is not developed in crystals **[Xie, 2001]**.

PYP contains two hydrophobic pockets one on each side of the central β sheet **[Borgstahl, 1995]**, **[Düx, 1998]**. The chromophore is buried inside the larger one of the pockets, Figure 1.2. Another hydrophobic pocket keeps the N-terminal cap attached to the central β sheet, Figure 1.7. The N-terminal domain is the region where the largest conformation change is observed during the formation of I_2' and presumably the binding site with the response regulator **[Cusanovich, 2003]**.

Structural changes at the chromophore (yellow sticks, Figure 1.7) in the I_1 state (formed upon absorption of the photon energy) trigger the structural alteration surrounding the chromophore on one side of the the β sheet (during I_2 transition), Figure 1.7 (β_5–β_6). This results in global structural changes in the subsequent transition to I_2' on the other side of the β sheet causing the transmission of the signal from the ligand-binding site to the interacting N-terminal part (pink). This signal transduction mechanism is still unclear and many hypotheses concerning such long range interactions have been proposed.

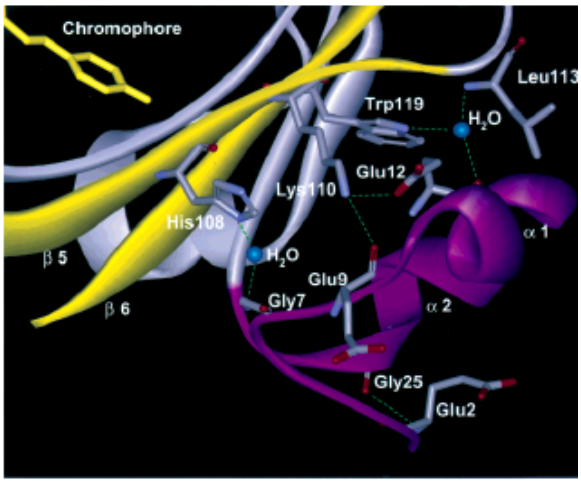

Figure 1.7: The local structural changes around the chromophore (yellow sticks) located on one side of the β-sheet (β_5–β_6, yellow) are due to the ismerization of the chromophore and its subsequent protonation during I_2 formation. This triggers the structural changes also on the other side of the β-sheet in the N-terminal cap (pink) during I_2' formation **[Harigai, 2003]**.

One of them is the hydrophobic collapse model where the N-terminal cap of PYP is supposed be involved in signaling via N-terminal disorder induced by photo-activation of the chromophore followed by the breakage of the E46/chromophore hydrogen bond and by movement of the chromophore out of the hydrophobic cavity **[Cusanovich, 2003]**. This results in the collapse of this cavity which causes the distortion of the central β-sheet. This

distortion in turn causes the N-terminal cap to dissociate from the β–sheet **[Cusanovich, 2003]**. From the salt dependence of the I_2 to I_2' transition it was recently discovered that a salt linkage between the conserved residues K110 and E12 needs to be broken in the formation of I_2' **[Borucki, 2005]**. Breaking of this "ionic lock" allows the N-terminal cap to dissociate from the β-sheet.

Another molecular mechanism of PYP activation is the protein quake model **[Xie 2001], [Pan, 2004]**. According to this model, the resulting conformational change following light absorption around the chromophore in the I_1 state triggers the chromophore rearrangement that results in the enhancement of proton affinity in the I_1 state which causes direct proton transfer from E46 to the chromophore during the formation of I_2 without changes in global protein conformation. The resulting negative charge on E46 is embedded in the highly hydrophobic cavity and thus energetically unstable, hence triggering a large amplitude protein quake with the epicentre located at the new buried charge, COO^- of E46 **[Xie, 2001]**.

4. Ground state recovery: The signalling state decays to the initial state in 400 ms, Figure 1.6. During recovery of the ground state, several processes have to occur. The chromophore has to re-isomerize to the *trans* form, the protonation state of chromophore has to change, and the protein conformation has to return to its ground state fold. Although all these events may occur in distinct steps, they appear to occur simultaneously. Re-isomerization of the chromophore could be the rate-limiting step **[Devanathan, 1998]**. Photoreversal, light induced reisomerization of the chromophore from cis-to-trans, during the photocycle leads to a 1000-fold increase in the recovery to P **[Joshi, 2005]**. In the M100A mutant, the light–activated recovery rate is 6 orders of magnitude faster than dark thermal recovery where I_2^{trans} is formed probably in ps time scale **[Devanathan, 1998]**. I_2^{trans} differs only in chromophore conformation. This shows that a large change of the protein fold and the state of protonation can be achieved quickly once the chromophore has been isomerised **[Devanathan, 1998]** and thus that chromophore isomerization could be the rate determining step during ground state recovery. However, the sequence of the events during recovery (e.g., reisomerization and deprotonation of chromophore, proton release to solvent and protein conformational reset) is still to be established.

The the solution photocycle bleach and recovery are strongly affected by alcohols and by the viscosity, indicating the protein conformationl change that exposes hydrophobic region to solvent **[Meyer, 1989]**. A change in heat capacity inferred from curved Arrhenius plots for recovery of photobleached PYP as a function of temperature **[Meyer, 1989]** also indicates

that hydrophobic region (23% of the amide groups which are buried in P are exposed in I_2') is exposed to solvent during the photocycle **[Hoff, 1999]**.

There is a remarkable pH dependence for both bleach and recovery **[Genick, 1997]**, **[Demchuk, 2000]**. The pH dependence of the recovery rate constant was observed to be bell-shaped with two pK_a's of 6.4 and 9.4 and assigned to E46 and the chromophore respectively. Glu 46 and the chromophore have pK_a values of 4.5 and 9 respectively in solution **[Genick, 1997]**. This is quite different from the chromophore pK_a in the dark titration of 2.8.

Crystalline PYP was shown to undergo a different photocycle than the PYP in solution at pH 6.5 **[Yeremenko, 2006]**. The signaling state, I_2' develops only minimally in the crystal. The majority of molecules return to P from I_2, whose lifetime is shortened by a factor of about ~18 (20 ms in the crystal, 360 ms in solution) compared to the recovery in solution (branching). This implies that the crystal kinetic model is not applicable to the solution kinetic model **[Yeremenko, 2006]**. The crystallographic structures are thus only relevant up to and including the I_2 intermediate.

From crystallography, it is found that the residues most likely to effect the properties of the chromophore are Y42, E46, T50, R52, Y98 and M100 (see abbreviations), Figure 1.5. Single site mutants Y42F, Y42A, E46Q, E46A, E46D, T50V, T50A, R52A, R52Q, M100A, M100L, M100K, M100E, Y98Q, Y98F have been constructed and partially characterized **[Meyer, 2003]**, **[Imamoto, 2001]**, **[Borucki, 2002]**, **[Borucki, 2003]**, **[Borucki, 2005]**. Some of the results that are relevant for this thesis are described below.

Major effects of the mutations at Y42 are on the spectral properties and less on the kinetics of the formation where formation of I_2 is faster by a factor 2 and recovery slowed by half in the Y42F mutant **[Brudler, 2000]**. In the absorption spectrum of the ground state of Y42F, an additional peak appears at 390nm, where the major absorption band has its λ_{max} at 458 nm, i.e. red-shifted by 12 nm with respect to WT. Y42F shows a biphasic transition with pK_as of 4.4 and 6.4 during titration in the dark. This is likely due to the loss of the Y42 hydrogen bond **[Brudler, 2000]**.

The major effect of the E46Q mutant (λ_{max}=460nm) is on the photocycle kinetics, in which both formation and decay of the I_2 intermediate are significantly accelerated with increasing pH in contrast to WT **[Borucki, 2003]**, **[Genick, 1997]**. The pH dependence of the recovery rate of WT is bell-shaped while that of E46 mutants is sigmoidal (pK_a=8.3). The corresponding pK_a is due to chromophore ionisation **[Borucki, 2003]**. The pK_a of the chromophore in the dark folded protein is increased significantly in E46Q (from 2.7 to 4.8)

and even further in E46A (to 7.9) **[Borucki, 2003]** and E46D (to 8.6), which approach that of the chromophore in solution (~ 9) **[Devanathan, 1999A]**.

Mutants T50V and R52A show small red-shifts in the absorption maximum at 457 nm and 452 nm respectively and have minimal effects on the photocycle kinetics **[Brudler, 2000]**, **[Genick, 1997]**. T50 hydrogen bonds with Y42 in WT but directly hydrogen bonds to the chromophore in Y42F **[Brudler, 2000]**. The double mutant Y42F/T50V has a greater proportion of 390 nm intermediate than the Y42F mutant. Thus, Y42 and T50 stabilize the chromophore in the 446 nm form. The minimal effect of the mutation at T50 indicates that it is less important than Y42 and other active site residues. Negative charge on the chromophore was supposed to be stabilized partially by the nearby positive charge on R52, but minimal effects of mutation suggest that this is not the case **[Imamoto, 2001]**.

Mutations M100A, M100L and M100K have dramatic effects in slowing the recovery of the photocycle by at least 3 orders of magnitude such that room light is sufficient to produce steady-state bleach **[Devanathan, 1998]**. The more rapid photoreversal versus dark recovery suggests that cis-trans isomerization of the chromophore could be catalysed by the M100 sulphur **[Devanathan, 1998]**.

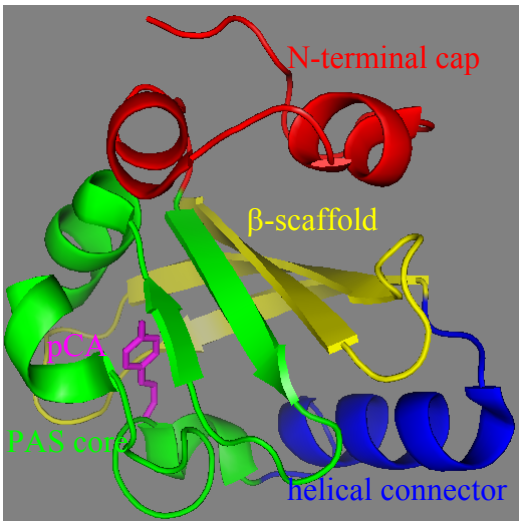

Figure 1.8: 3D folding of the PYP molecule can be divided into four parts **[Pellequer, 1998]**: 1) N-terminal cap, coloured in red, contains 1-28 residues (α_1 and α_2 helices). 2) PAS core, coloured in green, spanning 29-71 residues (first two beta strands and helices: α_3 and α_4 including α_5-chromophore binding loop). 3) Helical connector, coloured in blue, spans 72 to 87 residues. 4) β-scaffold, coloured in yellow, spaning residues from 88 to 125 (contains last three antiparallel beta strands). Chromophore is shown by pink coloured sticks.

PAS domains are the structural modules that can be found in proteins from all kingdoms of life **[Taylor, 1999]**, **[Pellequer, 1998]**. These domains are sensory modules, sensing typically oxygen, redox potential, or light intensity, and have a common structural motif: PAS core , β-scaffold, helical connector. Although the amino acid sequences of the different PAS domains are different, their 3D structures are conserved **[Pellequer, 1998]**. Since all of the PAS domains resemble the structure of PYP, Figure 1.8, PYP is proposed as the PAS structural prototype **[Pellequer, 1998]** as it is the best studied upto now. Highly

diffracting crystals of the dark state as well as of many intermediates are available. Moreover, PYP is highly stable against heating, denaturant and light intensity. Understanding the mechanism of converting photon energy to conformational alteration by PYP may help to understand the signal transduction mechanism of PAS domain super family in general.

PYP's have been identified in seven organisms up-to now: *Halorhodospira. halophila* (*Hr. halophila*), *Rhodothallasium salexigens* (*Rt. salexigens*), *Halochromatium salexigens* (*Hc. Salexigens*), *Rhodobacter capsulatus* (*Rb. capsulatus*), *Rhodobacter sphaeroides* (*Rb. sphaeroides*), *Rhodocista centenaria* (*Rc. centenaria*, Ppr) and *Thermochromatium tepidum* (*Tc. tepidum,* Ppd) **[Kyndt, 2004]**, **[Cusanovich, 2003]**. All of the results presented in this thesis were obtained with the PYP from *Hr. halophila*.

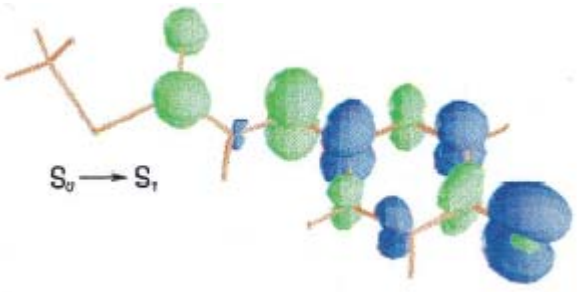

Figure 1.9: Differential electronic density for the vertical electronic transition $S_0 \rightarrow S_1$ of the dark state of PYP **[Molina, 2001]**. Electronic charge density moves from blue (decrease) to green (increase) areas during the transiton.

In quantum–chemical studies, **[Molina, 2001]**, applying second order perturbation theory to the experimentally determined available structure **[Genick, 1998]**, it was shown that the π–π^* transition to the lowest excited state is related to the typical blue light absorption observed at 446 nm. Differential electronic density for the vertical electronic transition between the ground state, S_0, and the lowest singlet excited state, S_1, of the dark ground-state of PYP is as shown in Figure 1.9, where, overall electronic charge shift takes place from the phenolate oxygen (blue, decrease) to the carbonyl group (green, increase) during this transition **[Molina, 2001]**.

1.2 Specific Aims of the Investigation

It is apparent from the discussion in the previous section that upon light activation, PYP forms a signaling state during the photocycle, in which a large structural change takes place and the protein is partially unfolded. The mechanism leading to the formation and the decay of this signaling state at the atomic level is still unclear. For an understanding of the functional mechanism of PYP as a photoreceptor, a detailed characterization of its photocycle, in terms of the kinetic mechanism is essential. The kinetics of the photocycle mechanism consists of the detection of the number of intermediate states, via their characteristic absorption spectra or three dimensional structures, the connectivity among

them, and the rate constants by which these states interconvert. Therefore, a general question about PYP and the major aim of this thesis is:

- ***What is the reaction mechanism of this blue light photoreceptor PYP?***

The answer will be discussed on the basis of the experimental results in Chapter 3. Detection of the temporal evolution of the three dimensional structures formed after laser excitation is one way to answer this question. These structures might be followed using time-resolved X-ray crystallography in crystals **[Ihee, 2005]**. In particular, signaling pathways have been determined via structural progression of intermediates using time-resolved X-ray crystallography from ns to seconds **[Ihee, 2005]**. However, the photocycle kinetics in crystals differs strongly from that in the solution **[Xie, 2001]**, **[Yeremenko, 2006]**. The signaling state I_2' is not well developed in the crystal, probably due to crystal packing constrains **[Xie, 2001]**, **[Yeremenko, 2006]** of the PYP molecules in the crystal lattice. Since, PYP is in the aqueous state under physiological conditions, the relevance of the studies in crystals is questionable.

Alternatively, the sequential structures might be tracked by measuring some specific property, e.g. the change of the chromophore absorption or protein vibrational spectra using time resolved electronic **[Meyer, 1987]**, **[Hendriks, 2003]** or vibrational (FTIR: **[Brudler, 2001] [Xie, 2001]**, Resonance Raman: **[Pan, 2004]**) spectroscopy. Changes in secondary and tertiary structures have also been detected by CD and SAXS. Detection of the structural progression of the intermediates in the solution during dark relaxation after light activation is still in an early stage. The structural and the dynamic changes during the photocycle are also studied by NMR in solution **[Rubinstenn, 1998]**, where the solution structure of the dark and the signaling state are resolved in the presence of background illumination. Time resolved absorption or vibrational spectroscopy is one way to track the intermediates under the physiological conditions to elucidate the activation mechanism of the photoreceptor.

In this investigation, time-resolved absorption spectroscopy with ns time resolution (section 2.2) is used to study the photocycle kinetics, where absorbance change is measured after laser excitation with a ns pulse at a wavelength near the absorbtion maxima, Figure 1.1. This absorbance change is due to the formation and decay of the various spectrally distinguishable intermediates during the photocyle. The purpose of this investigation is to characterize the intermediates spectrally from the measured data of the transient absorbance changes. Recently developed extrapolated difference method (section 2.4.1) and an alternative method scaled subtraction (section 2.4.2) will be used to determine the spectra of the intermediates. This is the key information to acquire the time courses of the intermediates

that determine the interconversion of the intermediates (sections 3.1.1 and 3.2.1), leading to a plausible reaction mechanism.

This technique is comparable to the determination of signaling pathways via the transient structures in X-ray crystallography. Furthermore, this method has an advantage over X-ray crystallography. Transient absorption measurements are carried out in solution i.e. under the physiological conditions. Moreover, the photocycles in solution and crystal differ as described earlier.

During this investigation particular emphasis is given to the pH effect on the photocycle (sections 3.1.2 and 3.2.2). In earlier studies of the photocycle a bell-shaped recovery rate was observed with two pKa's ~ 6.4 and ~ 9.4 **[Genick, 1997]**. In this study, these pK_a's will be explained in terms of titration curves of the intermediate populations, and assigned to particular functional groups. Thus, the extensive data set measured with ns time resolution from ns to s, in pH region 4.6 to 11, and the wavelength range from 320 nm to 510 nm will be explained in terms of the number of intermediates, their characteristic spectra and the interconnectivity. Detailed photocycle models will be proposed based on these observations.

Photoreceptors with their chromophores photoisomerizable around a specific bond have numerous features in common. One of these is that many photointermediates, in particular the signaling state, can be reversed by light directly back to the initial dark state. This is called photoreversal. Photoreceptors with this property are called photochromic: they can be switched back and forth by light between the inactive dark and active signaling states. Examples are rhodopsin, phytochrome, phototropin and PYP. Photoreversal is a common, almost universal, property of photoreceptors. Photoreversible reactions play a key role in signal transduction. In addition to its intrinsic biological significance, this photochromic molecular switching property is of potential technological interest in the development of optical storage and switching devices.

The mechanism of the photocycle kinetics is also supported by double flash excitation experiments. During a double flash experiment, the sample is excited by two flashes of the selected wavelengths applied with an appropriate time delay. Selection of these two parameters depends upon the absorption spectra and the kinetics of the photocycle intermediates. The first flash, usually a blue flash at 430 nm starts the cycle. The effect of the second flash applied during the photocycle is photoreisomerization of the chromophore followed by a rapid dark relaxation to the initial state through photoreversal process.

The photoreversal signal (PR[1]) may be resolved by triggering the data acquisition on the second flash. The second question considered during this investigation is:

- ***What might be deduced from the effect of a second flash of the proper wavelength applied at a suitable time during the photocycle?***

The answer will be discussed on the basis of the experimental results in chapter 4. It will be shown that the answer to this question assists to verify the reaction mechanism of the normal photocycle described in chapter 3.

The choice of the wavelength of the second flash is important to be considered for this experiment. The largest effect is expected on the I_2 (370 nm) and I_2' (350 nm) intermediates when a violet flash at 355 nm is applied during the photocycle, Figure 1.6. Similarly, the effect of a green flash at 500 nm might excite I_1 selectively, as other intermediates including the dark state absorb minimally around this wavelength. Moreover, the I_1 and I_2/I_2' intermediates are formed respectively in ~ μs and ms time scale during photocycle, Figure 1.6. A larger effect of a green flash on I_1 and a violet flash on I_2/I_2' is expected, when the second flash is applied respectively with a ~ μs and a ms time delay.

The effect of the second flash will be defined in terms of the photoreversal signal (section 4.1.1). This signal represents the photoback reaction kinetics. The kinetics may be time resolved if photoreversal is slower than the experimental time resolution. Spectral characterization of the photoreversal signal (section 4.1.3) describes of the photo-backreaction kinetics via the photoreversal intermediates involved. The delay dependence of the photoreversal amplitudes acquired from the fit of this signal (section 4.1.2) may follow the temporal variation of the normal cycle intermediate from which the photoreversal signal originates, when excited selectively. In this way, double flash excitation experiments facilitate the investigation of the normal photocycle, and contribute to an understanding of the reaction mechanism of the photoreceptor.

The initial evidence for photoreversals in PYP are from single flash kinetic experiments with a photostationary mixture of I_2 and the ground state in wild type **[Miller, 1993]**, **[Hendriks, 1999]** and in the mutant M100A **[Devanathan, 1998]**. Transient absorption measurements with excitation at 355 nm and nanosecond time resolution showed that rapid unresolved photoisomerization occurred, converting I_2 (which is the *cis* isomer) to an I_2^{trans} form. I_2^{trans} then decayed monoexponentially to the initial dark state (P) with an exponential time constant of 147 μs at room temperature **[Hendriks, 1999]**. Compared to the thermal decay, the light-induced decay of I_2 in wild-type PYP is approximately 10^3 times faster. In the mutant M100A the return to P via the photo-backreaction from I_2 was also

monoexponential with a time constant of 230 μs **[Devanathan, 1998]**. At that time the existence of two I_2- like intermediates, I_2 and I_2' was not recognised. So in these early experiments an undefined photostationary equilibrium of I_2 and I_2' was photoreversed.

The double flash experiments presented in this investigation are superior to the earlier reported photoreversal experiments (**[Miller, 1993]**, **[Hendriks, 1999]**, **[Devanathan, 1998]**) where a photostationary mixture of intermediates was subjected to a single UV flash. Moreover these experiments were limited to the conditions where the cycle is slow enough to accumulate the intermediates in sufficient amounts.

The next three chapters report the details of the experimental and data analysis methods (Chapter 2), and the results of the single (Chapter 3) and double flash excitation (Chapter 4) experiments.

Chapter 2

Materials and Methods

The mechanism of the photocycle kinetics of PYP was studied in detail using time resolved absorption spectroscopy, also known as flash photolysis. In this technique, the sample is excited with a short laser pulse and dark relaxation of the protein is monitored via time resolved absorbance changes. In this chapter, the principles of the transient absorbance changes will be explained (section 2.2.1) and the experimental set up used to measure such changes in single or double flash excitation experiments will be described (section 2.2.2). The aim of the data analysis is to determine the spectra and time courses of the intermediates as described in section 2.4. Spectra of the intermediates formed during the photocycle and the intermediate time courses can be calculated from the measured time resolved absorbance changes using the extrapolated difference method (section 2.4.1) or the scaled subtraction method (section 2.4.2). A photocycle model can be proposed from the fit of the time courses with a sum of exponentials. As some of the photocycle intermediates are in equilibrium during the photocycle, the time courses were also measured for various values of a certain parameter such as pH, to identify the nature of the equilibria. Moreover, pH dependent equilibria and associated decay rates are related in section 2.5.2, which explains the underlying cause of the pK_a of the pH dependent decay rates.

2.1 Sample Preparation

Wild type PYP was investigated in this study and acquired from Terry E. Meyer/ Michael A. Cusanovich, University of Arizona, USA. Native PYP from *H. halophila* was prepared as described **[Meyer, 1989]**. *H. halophila* holo-PYP was produced also by the use of the biosynthetic enzymes TAL and pCL and subsequently purified from *Escherichia coli* BL21(DE3) as described in **[Kyndt, 2003]**.

2.2 Flash Photolysis

2.2.1 Transient Absorbance Changes

When monochromatic light is passed through an absorbing material, the transmitted intensity is proportional to the incident intensity I, the concentration c of the absorbing material, the infinitesimal path length dx and the characteristic extinction coefficient ε(λ):

$$dI = -\varepsilon(\lambda)\, c(x)\, I(x)\, dx \qquad \textbf{(2.1)}$$

If the concentration c is constant over the path d, integration of this relation leads to the Lambert-Beer law:

$$I = I_0 10^{-\varepsilon(\lambda)\, cd} \Leftrightarrow A(\lambda) = \varepsilon(\lambda)\, cd = \log\left(\frac{I_0}{I}\right) \qquad \textbf{(2.2)}$$

The wavelength dependence of the extinction coefficient ε(λ) (unit: $M^{-1}cm^{-1}$) determines the absorption spectrum of the species. The dimensionless exponent ε(λ)cd is called absorption and also measured in the unit of OD (optical density). To measure the absorption spectrum, the light intensity of monochromatic light produced by a monochromator has to be measured before (I_0) and after (I) the sample for every wavelength of the measuring light. In a two beam spectrophotometer, instead of measuring the light intensity I_0, the transmitted intensity through a reference sample (usually water), placed in one of the beams of the spectrophotometer, is measured to calculate the absorption. A typical absorption spectrum of PYP is as shown in Figure 1.1.

In general, during the photocycle after laser excitation, a spectrally distinguishable mixture of species i, each with a distinct spectrum $\varepsilon_i(\lambda)$, is formed transiently. In that case, the absorption is a function of both time and wavelength:

$$A(\lambda,t) = \sum_{i=1}^{n} A_i(\lambda,t) = \sum_{i=1}^{n} \varepsilon_i(\lambda) c_i(t) d \qquad \textbf{(2.3)}$$

In time resolved absorption spectroscopy, the absorbance change before and after laser excitation is measured rather than the absolute absorption. In these measurements, the transmitted intensity of the measuring light at a selected wavelength after laser excitation is measured, and transient recording of the intensity I(λ,t) is started after the laser flash. In this case, the absorbance change during the photocycle is calculated using the relation:

$$\Delta A(\lambda,t) = A(\lambda,t) - A_P(\lambda) = \log\left(\frac{I(\lambda)}{I(\lambda,t)}\right) \qquad \textbf{(2.4)}$$

where,

$$A_P(\lambda) = \varepsilon_P(\lambda)\, c_T\, d \qquad \textbf{(2.5)}$$

is the ground state (dark state, P) absorption and I(λ) is the transmitted intensity from the sample before laser excitation. c_T is the initial PYP concentration (total). In this case, measurement of the intensity I_0 before the sample is not necessary. Substituting the values of A(λ,t) and $A_P(\lambda)$ in eq 2.4 from 2.3 and 2.5 respectively:

$$\Delta A(\lambda,t)= \sum_{i=1}^{n} \varepsilon_i(\lambda) c_i(t) d - \varepsilon_P(\lambda)\, c_T\, d \qquad \textbf{(2.6)}$$

where, the absorbance change is a function of the transient concentration changes of the intermediates. Since,

$$c_T = \sum_{i=1}^{n} c_i(t) \qquad \textbf{(2.7)}$$

Eq 2.6 becomes:

$$\Delta A(\lambda,t)= \sum_{i=1}^{n} [\varepsilon_i(\lambda) - \varepsilon_P(\lambda)]\; c_i(t)\, d \qquad \textbf{(2.8)}$$

and further,

$$\Delta A(\lambda,t)= \sum_{i=1}^{n} [\varepsilon_i(\lambda) - \varepsilon_P(\lambda)] \left(\frac{1}{c_T}\right) c_i(t)\, d * c_T \qquad \textbf{(2.9)}$$

with,

$$n_i(t)= \frac{c_i(t)}{\sum_{i=1}^{n} c_i(t)} \qquad \textbf{(2.10)}$$

as the relative concentration, eq 2.9 becomes:

$$\Delta A(\lambda,t)= \sum_{i=1}^{n} [A_i(\lambda) - A_P(\lambda)]\, n_i(t) \qquad \textbf{(2.11)}$$

Thus, the absorbance change from the time resolved absorption measurements at any wavelength λ is the sum of the difference spectra multiplied by the associated relative concentrations of the intermediates. When the coupled system is described with first order kinetics, the rate of change of the concentration depends linearly on the concentration itself:

$$\frac{d}{dt} n_i = \sum_{j=1}^{m} K_{ij} n_j \qquad \textbf{(2.12)}$$

$$\text{with } K_{ii} = -\sum_{j=1, j\neq i}^{m} K_{ij}; \quad i = 1, \ldots\ldots\ldots\ldots, m$$

where K_{ij} is the decay rate from the j to i intermediate. The general solution of this system of coupled linear differential equations can be written as the sum of r exponentials:

$$n_i(t)=\sum_{j=1}^{r} C_{ij}e^{-k_j t} \qquad \textbf{(2.13)}$$

with decay rates k_j. Substituting the solutions for $n_i(t)$ from eq 2.13 in eq 2.11 we obtain:

$$\Delta A(\lambda,t)=\sum_{j=1}^{r}\sum_{i=1}^{n} C_{ij}\,[A_i(\lambda)-A_p(\lambda)]\,e^{-k_j t}=\sum_{j=1}^{r} B_j(\lambda)e^{-k_j t} \qquad \textbf{(2.14)}$$

where,

$$B_j(\lambda)=\sum_{i=1}^{n}\,[A_i(\lambda)-A_p(\lambda)]\,C_{ij} \qquad \textbf{(2.15)}$$

is the amplitude spectrum corresponding to the j^{th} transition which depends upon the kinetic parameters C_{ij} and the difference spectra.

In matrix notation, relations (2.11) and (2.15) are:

$$\Delta\mathbf{A}=(\mathbf{A}-\mathbf{A}_P)\mathbf{n} \qquad \textbf{(2.16)}$$

$$\mathbf{B}=(\mathbf{A}-\mathbf{A}_P)\mathbf{C} \qquad \textbf{(2.17)}$$

The row index of $\Delta\mathbf{A}$, **B**, **A** and $\mathbf{A}_p$ corresponds to the wavelength λ, the column index of $\Delta\mathbf{A}$ and **n** corresponds to the time t, the column index of **B** and **C** to the j^{th} component and the column index of **A**, $\mathbf{A}_p$ and row index of **C** and **n** to intermediate i. Matrix $\mathbf{A}_p$ consists of identical columns of the ground state spectrum.

The purpose of the analysis of the photocycle kinetics is to extract the spectra of the intermediates, $\boldsymbol{\varepsilon}_i(\lambda)$, their time courses $n_i(t)$ and, under favourable circumstances, the reaction scheme from the exponential fit of $n_i(t)$. The extrapolated difference method (section 2.4.1) and the subtraction method (section 2.4.2) are the methods used to obtain the spectra of the intermediates, i.e. matrix $\mathbf{A}-\mathbf{A}_P$. Corresponding time courses of the intermediates can be obtained from the measured absorbance changes (time traces) using the matrix inversion of the eq 2.16:

$$\mathbf{n}=(\mathbf{A}-\mathbf{A}_P)^{-1}*\Delta\mathbf{A} \qquad \textbf{(2.18)}$$

2.2.2 Experimental Set Up for the Measurement of Transient Absorbance Changes with Single and Double Flash Excitation

The experimental set up for the measurement of transient absorbance changes with single or double flash excitation is shown in Figure 2.1. The whole experiment was controlled through a PC (486, 133 MHz, 8 MB RAM) via a homemade software, an algorithm developed in C++ **[Dickopf, 1997]**. For the efficient excitation of the ground state to start the photocycle, a short laser pulse at the wavelength near the absorption maximum of 446 nm is required. This is produced through a excimer pumped dye laser. When the measurement is

started, an I/O serial port (Fa. Kolter) transmits a TTL pulse to a home made delay generator (DG), Figure 2.1, via an interface (home made).

The excimer laser (Radiant Dyes, RD-EXC-100), EL, with XeCl as laser medium can be started using two pulses P_1 and P_2 at a delay of 33 ms produced by the delay generator. An output laser pulse at 308 nm of about 100 mJ pulse energy and 10 ns pulse length is used to excite the dye (Stilbene 3 dissolved in methanol, Radient Dyes) DC, which produces a laser pulse at 430 nm (blue flash), energy of which is increased further to 4-6 mJ by using a mirror (m_1) on one side of the beam, Figure 2.1.

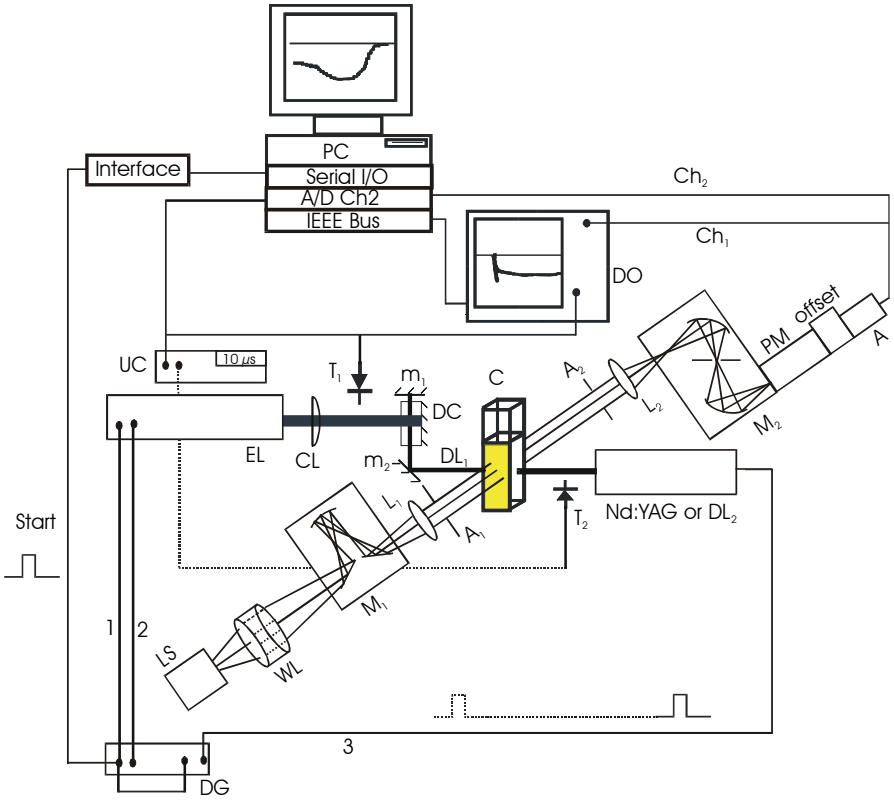

Figure 2.1: Experimental set up for single or double flash excitation. DG: delay generator. 1,2: two pulses with a delay of 33 ms to start excimer laser (EL). 3: delayed trigger pulse to start second laser (Nd:YAG, 355nm or second excimer laser). LS: light source. WL: water lens. M_1: first monochromator. L_1, L_2: lens. A_1,A_2: apertures. C: cuvette. T_1,T_2: photodiodes. DL_1: dye laser (blue, 430 nm). DL_2: dye laser (green, 500 nm). M_2: double monochromator. PM: photomultiplier. A: amplifier. Ch_1/Ch_2 : output channels from PM. DO: digital oscilloscope. UC: universal counter. CL: cylindrical lens. m_1,m_2 : mirrors. DC: dye cuvette

Mirror m_2 was used to align this beam to excite the sample placed in the cuvette, C (5X5 mm, Quartz glass, Helma, QS 1.000). The beam diameter was adjusted with two lenses (6 cm diverging and 16 cm converging lens, not shown) which was about 1 cm at the sample cuvette. Beam profile and intensity adjustment before the sample cuvette and beam alignment

were made by optimising the output signal of the photomultiplier (see below) measured by an oscilloscope with the sample in the cuvette.

The volume of the protein solution in the cuvette was 500-700 µl. The temperature of the sample was controlled by a thermostat (Julabo Labortechnik GmbH) with the circulation around the cuvette holder.

A 100 W tungsten-halogen lamp (Spindler and Hoyer) was used as a source of measuring light (LS). This is highly stable and durable with sufficient light intensity in the spectral range of 320-800 nm which is one of the requirements of the flash photolysis experiment. The light beam passed through an infrared filter, from water lens (WL), that suppresses heat radiation, was incident on the monochromator M_1 (Jobin-Yvon, "division d' instruments" SA, H10 VIS, spectral bandwidth (FWHM) of 6 nm with 1 mm slits).

The beam is further collimated by a lens L_1, limited by an aperture A_1 (5-7 mm diameter) and passed through the sample cuvette (path length 5 mm) crossing through almost the same volume and at right angles to the excitation beam. The transmitted beam is further limited with a bit larger aperture A_2 (10-12 mm diameter) and focussed on the double monochromator, M_2 (Jobin-Yvon, "division d' instruments" SA, H10 VIS, spectral resolution of 6 nm with 2 mm width of all three slits) by a lens L_2. The photomultiplier, PM (Hamamatsu S4710 1 GHz bandwidth) was placed at the exit of this monochromator. The double monochromator, M_2 was used to suppress the light of the laser flash scattered in the direction of the photomultiplier.

The light intensity of the measuring beam was 100 $\mu W/cm^2$ at 450 nm at the sample after the first monochromator. Attenuation of the intensity of the measuring beam had no effect on the observed kinetics (see later), suggesting that the intensity was small enough to avoid the build up of photostationary states. The spectral bandwidth of the monochromators in the measuring beam was ± 6 nm which is the spectral resolution of the experiment.

As the monochromator M_2 doesn't suppress fully the scattered light, the photomultiplier detects the saturation intensity as the flash effect in the time range of < 100µs at the wavelength of the laser pulse (± 6 nm). To reduce further this artefact, the light intensity of the measuring light has to be increased so that the scattered light intensity is negligible compared to the measuring light intensity. This can also be done by using slits of larger widths in the monochromator M_1 and M_2. However, with measuring light of higher intensity, a photostationary mixture of the ground state and the photointermediates was observed at pH values where the photocycle is slow (see below). In that case, the measuring

light intensity has to be further reduced. To overcome the problem with lower signal to noise ratio in this case, the number of measuring scans were increased (see below).

The photomultiplier voltage, V(t) is proportional to the intensity I(t) transmitted through the sample. In this experiment, the absorbance change is measured rather than the absolute absorbance which depends upon the measured voltage, V(t) with respect to the reference voltage, V_r. In this case, a voltage of opposite sign V_o is applied to the photomultiplier so that signal is combined with the V_o, and V_r is compensated ($V_o \approx V_r$). Then, the time course of the measured voltage, $V^M(t)$, after laser excitation is:

$V^M(t) = V(t) + V_o$ and $V_r^M = V_r + V_o$ **(2.19)**

Absorbance change of eq 2.4 is obtained using the following relation:

$$\Delta A(\lambda,t) = -\log\left(\frac{I(\lambda,t)}{I(\lambda)}\right) = -\log\left[\frac{V_r + V^M(t) - V_r^M}{V_r}\right] \quad \textbf{(2.20)}$$

To measure V_r, the voltage of opposite sign V_0 has to be switched off for a defined time interval and V_r^M is the voltage just before the trigger (pretrigger value). Before the start of the measurement, the photomultiplier voltage is increased so that the offset is 200 mV. During measurement a photomultiplier voltage of the typical range of 200-500 volts was necessary with this additional offset voltage, V_r of ~ 200 mV. Photomultiplier voltage depends upon the intensity of the transmitted light which in turn depends on the type of the sample and the other experimental conditions (e.g. slit width, measuring light intensity, geometry of optical set up etc.). Once the photomultiplier is sensitive to the transmitted light, output signal from the photomultiplier is produced. As the absorption of the sample changes during the photocycle after laser excitation, the output of the photomultiplier changes accordingly.

The signal from the photomultiplier is amplified (amplifier, AD9610, Analog Devices) by a factor of 40, passed through a low pass filter and divided in two channels (Ch_1,Ch_2, Figure 2.1) for digitalization via two overlapping channels. The corresponding ranges of the sampling rate of the fast and slow channels are 10^8-10^7 s^{-1} and 10^5-10^4 s^{-1} respectively. Data acquisition, signal processing, and digitalization were performed as described **[Dickopf, 1997]**, **[Borucki, 1999]**.

Output (data acquisition) from the two channels is converted into signals of different time base using a Analog-Digital converter. One of the channels is connected to the fast oscilloscope (Lecroy 9350A, DO: Figure 2.1), which has an analog band width of 500 MHz and sampling rate of 1 GHz, 8-bit amplitude resolution and equipped with memory capacity of 100kbyte. The saved data were read via IEEE-interface (488-PC2, Meilhaus) to the PC for

further processing. Data acquisition for the slower channel is done with data acquisition board (T512, IMTEC). This has 12-bit resolution, 4 Mega samples storage capacity and 200 ns time resolution.

Both data acquisition units, the oscilloscope and the A/D card of the PC, can be triggered simultaneously by the output signal from photodiode T_1 which is triggered by the scattered light of the laser flash. This is the zero time of the measurement. The measured time range in this experiment is 1 ns to 50 s with a sufficient overlap of both channels. The effective time resolution during the laser flash is limited to the range of 20-50 ns due to the rise time of the photomultiplier and the amplifier.

$2x10^5$ data points per flash are collected at the temporary memory of the PC after triggering of the data acquisition units which is the input for further data processing.

Each measurement produces a large amount of data (above 8 MByte). To describe the exponential relaxation with time after laser excitation, fewer time points per time interval are sufficient (logarithmically equidistant 100 data points per decade are sufficient to produce a adequately smooth time trace, see below). Therefore, logarithmic data reduction of measured data points is valuable. Data reduction is also useful to enhance the efficiency of the PC. To reduce the data points measured on the linear time scale to logarithmically equidistant time patterns with 100 data points per decade the following relation can be used:

$t_i=10^{i/100}$ ns, i=0,……,1000 **(2.21)**

In this way, measured linear time points are converted to logarithmic time patterns. The total number of data points is about 700 after data reduction of $2x10^5$ measured data points. Then, the absorbance change is calculated from V_r, V_r^M and the temporal variation voltage V^M using equation 2.20. Due to slightly different amplification factors of the two channels, the two signals deviate slightly in the overlap region and an offset is used to correct the mismatch. Signals from the 2 channels are merged into a single curve. To increase further the signal to noise ratio, measurements are repeated many times, generally 10 or 20 scans, and the averages of all the scans are saved.

Due to this averaging process, the scattered data points produce more or less continuous time traces. As more linear data points contribute to a measured logarithmic time point at later times than at early times, the signal to noise ratio of the later time point is much better than that of the early time point, (Figure 3.3). For this reason a slower process will have a higher accuracy than a faster one. This effect was taken into account in the data analysis by using appropriate weighting factors which increase the weight of the later data points (see below).

To investigate the effect of a second flash applied during the photocycle, double flash experiments were performed. In this experiment, the sample is excited with a second flash at a selected wavelength after a suitable time delay. Selection of these two parameters depends upon the absorption spectra and the kinetics of the photocycle intermediates. In general, the effect of the second flash applied during the photocycle is a fast isomerization followed by return to the initial state which is faster than the thermal relaxation in the normal cycle. This is called photoreversal. In PYP, intermediates like I_1 (λ_{max}=460nm), I_2 (λ_{max}=370nm) and I_2' (λ_{max}=350nm) are formed during the photocycle on the μs and ms time scales respectively. The largest effect is expected on the I_2 and I_2' intermediates when a violet flash at 355 nm is applied between 200 μs and 20 ms, Figure 4.1, after initiation of the photocycle (as other intermediates as well as the ground state have smaller extinction coefficients at this wavelength). A green flash around 500 nm wavelength applied at a μs time delay might excite selectively the I_1 intermediate (as I_2 and ground state have practically zero absorbance at this wavelength).

For photoreversal experiments on I_2 and I_2', the sample was excited with a second laser pulse at 355 nm (Q-switched frequency tripler of Nd:YAG Laser, Spectra-Physics Inc., GCR-16, pulse energy 10 mJ/pulse, pulse width 5-6 ns), Figure 2.1. The delay generator (DG) produced two pulses- 2 and 3 from the start pulse with defined delay which were used to start the lasers. First pulse- 2 starts the excimer pumped dye laser (430 nm) which initiates the photocycle of PYP. Second pulse- 3 starts the Nd:YAG Laser laser at a defined time delay during the photocycle.

The time delay between the two pulses was checked by an universal counter (Philips PM6666) UC, using the output pulse from the photodiode for the excimer laser and the electronic pulse synchronized to the Q-switch for the violet flash. Since the fluctuation of time delay between the triggers is around ±200 ns, time delays larger than 1 μs are accurate. A delay generator (DG) allowed delays to be set between the two laser pulses from 1 μs to 50 s with an accuracy of 100 ns.

To resolve the kinetics of photoreversal after the second flash, data acquisition was also triggered on the second flash. This was the Q-switch synchronized pulse for the violet flash.

For the photoreversal of I_1, the sample was excited with a second laser pulse at 500 nm from an excimer pumped dye laser (Lambda Physik, EMG 50E, pulse width 10 ns, average energy 100 mJ/pulse). Coumarine 307 dissolved in methanol was used as the laser

dye. The laser energy in front of the dye cuvette was 13 mJ/pulse. Photodiode T_2 was used to monitor the delay and used for triggering of the data acquisition.

The dark spectrum (A_P) was measured by using a double beam UV-Vis spectrophotometer (Shimadzu Corporation, Japan, UV-260). The pH was controlled with a glass electrode of a digital pH-Meter (Knick). Titrations were carried out by the addition of the small amounts of HCl or KOH.

2.3 Amplitude Spectra of the Transitions

The amplitude spectra $B_j(\lambda)$ of eq 2.15 can be obtained from the measured transient absorbance changes $\Delta\mathbf{A}(\lambda,t)$ with the following two methods: global fit analysis and singular value decomposition (SVD[1]). Amplitude spectra of the transitions are further used in the extrapolated difference method (see section 2.4.1) or scaled subtraction method (see section 2.4.2) to estimate the spectra of the intermediates of eq 2.16 and to calculate their time courses from eq 2.18.

2.3.1 Global Fit Analysis

Absorbance changes $\Delta A\ (\lambda,t)$, in general, can be represented with the sums of r exponentials with apparent rate constants k_l and amplitudes a_l.

$$\Delta A\ (\lambda,t)= \sum_{l=1}^{r} a_l(\lambda)e^{-k_l t} + a_0(\lambda) \qquad \textbf{(2.22)}$$

In global fit analysis, the weighted sum of squared differences f between the fit with r rate constants k_l and the data points at n_w measured wavelengths λ_i and N times t_j is minimized **[Heßling, 1993]**:

$$f=\sum_{i=1}^{n_w} \sum_{j=1}^{N} [W_i(t_j)]^2 * [\Delta A_{measured}(\lambda_i, t_j) - \sum_{l=1}^{r} a_l(\lambda_i)e^{-k_l t_j} - a_0(\lambda_i)]^2 \qquad \textbf{(2.23)}$$

The assumption in this procedure is that the rate constants are the same for all spectral elements. The number of rate constants r is chosen, along with the optimal weight, with the criterium that the residual plot has a random distribution with r rate constants, however this plot results a systematic deviation with r-1 rate constants. The weight is chosen with respect to the estimated noise using the relation:

$$W_i(t_j)=\frac{(w_i)^j}{\sum_{j=1}^{N}(w_i)^j} * N\ ; \qquad j=1,2,\ldots..,N \qquad \textbf{(2.24)}$$

with associated error, $E_i(t_j)=\frac{1}{W_i(t_j)}$. Here N is the total number of measured time points, and the value of w_i of eq 2.24 is chosen from the range of $1<w_i<1.05$ which is the same for all wavelengths λ_i and differs for different time points t_j. This is because in the measured absorbance changes, the signal to noise ratio increased with increasing time which is due to the averaging procedure during data acquisition (explained in section 2.2.2). A proper choice of weights produces the best fit across the whole time range. Optimisation is done using software Microcal origin 7.5. The amplitudes from the fit according to eq 2.22 represent the amplitude spectra:

$$B_l(\lambda)=a_l(\lambda) \qquad \textbf{(2.25)}$$

which are equal to the amplitude spectra described in eq 2.15 and 2.27.

In general, a global fit analysis was used to obtain the amplitude spectra from the single and double flash excitation measurements of PYP.

2.3.2 Singular Value Decomposition

Another method to obtain the amplitude spectra of transitions is singular value decomposition **[Henry, 1992]**. Transient absorbance changes measured at various wavelengths covering the whole spectral range of the photocycle are arranged in a matrix $\Delta\mathbf{A}$. This matrix has dimensions $m*n$ where m time traces (m is the number of wavelengths) are arranged in n columns for each time point. A column represents the transient absorbance change at a particular time point for the measured spectral range. Singular value decomposition of the matrix $\Delta\mathbf{A}$ is the decomposition of this matrix into the product of three matrices **U**, **S** and **V** in such a way that **[Henry, 1992]**:

$$\Delta\mathbf{A}= \mathbf{U}\,\mathbf{S}\,\mathbf{V}^T$$

where, **U** and **V** are unitary matrices having the property $\mathbf{U}^T*\mathbf{U} = \mathbf{V}^T*\mathbf{V} =\mathbf{I}_n$ where $\mathbf{I}_n$ is identity matrix. The columns of **U** (dimension $m*n$) and **V** (dimension $n*n$) represent the orthonormal basis vectors corresponding to the amplitude spectra (time independent) and the time traces respectively. The third matrix **S** (dimension $n*n$) is a diagonal matrix with the diagonal elements arranged in decreasing order called singular values. The smallest value of the magnitude of the difference $\|\Delta\mathbf{A}-\mathbf{U}_k\mathbf{S}_k\mathbf{V}^T_k\|$ is feasible with a suitable choice of the number of singular values k (also called significant singular values) of the diagonal matrix **S**. An important property of SVD is that for all $k\leq n$, the first k columns of **U**, along with the corresponding columns of **V** and the rows and columns of **S**, provide the best least square

approximation to the matrix $\Delta\mathbf{A}$. The number of singular values k is chosen, with the criterium that the difference $\|\Delta\mathbf{A}-\mathbf{U}_k\mathbf{S}_k\mathbf{V}^T_k\|$ has a random distribution with k columns of **U**, **S** and **V** matrices, however this difference results a systematic deviation with k-1 columns. The remaining data matrix contains mainly the noise (up to the point at which a particular subset of significant singular values and the vectors is chosen). Thus, singular value decomposition acts as a mechanism-independent filter of noise. Time traces of the basis vectors $V_l(t)^T$, with l=1, 2, 3,….., k ($\mathbf{V}_k^T$ has a dimension of k∗n), weighted by the corresponding singular values S_l can be fitted simultaneously by a sum of r exponentials:

$$S_lV_l(t)^T=G_{l0}+\sum_{j=1}^{r} G_{lj}e^{-kj*t} \qquad \textbf{(2.26)}$$

where, k_j represents the rate constant of the j^{th} transition. From the amplitudes G_{l0} and G_{lj} of this fit and the basis spectra $U_l(\lambda)$ ($\mathbf{U}_k$ has dimension of m∗k), the amplitude spectra $B_j(\lambda)$ can be calculated **[Borucki, 2003A]** from:

$$B_j(\lambda)=\sum_{l=1}^{k} [U_l(\lambda)]*G_{lj} \ ; \qquad \textbf{(2.27)}$$

which, in matrix notation is:

$$\mathbf{B}=\mathbf{U}_k\mathbf{G} \qquad \textbf{(2.28)}$$

Here, $B_j(\lambda)$ (**B** has a dimension of m∗r) represents the amplitude spectrum corresponding to the j^{th} transition in total of r transitions. In general for PYP, the amplitude spectrum corresponding to the infinite time, G_{l0} is negligible compared to the amplitude spectra of the other transitions as the absorbance change vanishes after completion of the photocycle. Another advantage of SVD is that the number of data points to be analysed is greatly reduced (m∗n data points before SVD vs m∗k after SVD). This procedure provides information about the number of significant spectral components (k) and the corresponding transitions (r) during the photocycle.

Matrix calculations were performed with Matlab version R12.1. Fitting the weighted basis vectors of time traces with sums of exponentials was carried out with Microcal Origin 7.5.

2.4 Spectra and Time Courses of the Intermediates

Two independent methods, the extrapolated difference and the scaled subtraction methods, use the amplitude spectra $B_j(\lambda)$ of eq 2.25 or eq 2.27 to obtain the matrix containing

the difference spectra of intermediates $\mathbf{A}$-$\mathbf{A}_P$ as described below. The matrix of the corresponding time courses **n**, can be obtained using eq. 2.18.

2.4.1 Extrapolated Difference Method

SVD analysis of the measured transient absorbance changes shows that there are three significant singular values and thus three spectrally distinguishable intermediates contributing in the photocycle of PYP, with three transitions (see sections 3.1.1 and 3.2.1), mainly I_1, I_2 and I_2' in the acid/neutral pH range (pH 4.6 to 8.4, section 3.1.2) and I_1, I_1' and I_2' in the alkaline pH range (pH 8 to 11, section 3.2.2). I_1 decays partially to I_2 (at acid pH) or to I_1' (at alkaline pH) in the first transition. The mixture of I_1/I_2 or I_1/I_1' decays together to I_2' in the second transition in acid or alkaline pH respectively. All intermediates in the respective pH range are in equilibrium after about ~20 ms and in turn, decay to P in the third transition.

The amplitude spectra $B_j(\lambda)$ of eq 2.25 or 2.28 are arranged in columns ordered from low to high apparent time constants, to form the amplitude matrix **B** of eq 2.17. From the columns of **B** and **C** new matrices, $\tilde{\mathbf{B}}$ and $\tilde{\mathbf{C}}$ are formed by linear combinations of sum of columns starting with index k to index r in the following way:

$$(\tilde{B})_k = \sum_{j=k}^{r} (B)_j \; ; \qquad (\tilde{C})_k = \sum_{j=k}^{r} (C)_j ; \qquad k = 1,2,....,r \qquad \textbf{(2.29)}$$

The columns of $\tilde{\mathbf{B}}$ represent the extrapolated absorption difference spectra, **[Borucki, 1999]** and the columns of $\tilde{\mathbf{C}}$ of eq (2.30), contain the relative contributions of the intermediates in these difference spectra.

$$\tilde{\mathbf{C}} = \begin{pmatrix} x_1 & x_2 & x_3 \\ y_1 & y_2 & y_3 \\ z_1 & z_2 & z_3 \end{pmatrix} \qquad \textbf{(2.30)}$$

x_i, y_i, z_i represent the relative contributions of the respective spectral components x, y and z in the i^{th} transition. The matrix equation for $\tilde{\mathbf{B}}$ follows from eq 2.15 and 2.17:

$$\tilde{\mathbf{B}} = (\mathbf{A} - \mathbf{A_p})\tilde{\mathbf{C}} \qquad \textbf{(2.31)}$$

and can be solved for **A**:

$$\mathbf{A} = \tilde{\mathbf{B}}\tilde{\mathbf{C}}^{-1} + \mathbf{A_p} \qquad \textbf{(2.32)}$$

Once the $\tilde{\mathbf{C}}^{-1}$ matrix, the inverse of the matrix $\tilde{\mathbf{C}}$, defined in eq 2.33, is known, the spectra of the intermediates can be calculated.

$$\tilde{\mathbf{C}}^{-1} = \begin{pmatrix} (\tilde{\mathbf{C}}^{-1})_{11} & (\tilde{\mathbf{C}}^{-1})_{12} & (\tilde{\mathbf{C}}^{-1})_{13} \\ (\tilde{\mathbf{C}}^{-1})_{21} & (\tilde{\mathbf{C}}^{-1})_{22} & (\tilde{\mathbf{C}}^{-1})_{23} \\ (\tilde{\mathbf{C}}^{-1})_{31} & (\tilde{\mathbf{C}}^{-1})_{32} & (\tilde{\mathbf{C}}^{-1})_{33} \end{pmatrix} \qquad \textbf{(2.33)}$$

For each column $(\tilde{\mathbf{C}}^{-1})_i$ the related spectrum $\mathbf{A}_i$ can be calculated from column i of the matrix eq 2.32:

$$(\mathbf{A})_i = \tilde{\mathbf{B}}(\tilde{\mathbf{C}}^{-1})_i + (\mathbf{A}_p)_i \qquad \textbf{(2.34)}$$

In general, it is not possible to find a unique solution for the unknown elements of $\tilde{\mathbf{C}}$ and **A** from these equations, since the columns of $\tilde{\mathbf{B}}$ are not linearly independent. However, spectra of intermediates, i.e. columns of **A**, can be calculated by introducing the following constraints on the intermediate spectra **A** and the $\tilde{\mathbf{C}}^{-1}$ matrix:

1. The sum of the contributions of the intermediates in the extrapolated difference spectra (columns of $\tilde{\mathbf{B}}$) is constant and equals the fraction of molecules cycling, η, provided that the time constants of the relaxations are sufficiently separated. This means that the sum of x, y and z for each extrapolated difference spectrum equals η, or that the sum of the matrix elements of each column of $\tilde{\mathbf{C}}$ equals η:

$$\sum_{i=1}^{3} \tilde{\mathbf{C}}_{ij} = \eta \Leftrightarrow \sum_{i=1}^{3} \tilde{\mathbf{C}}^{-1}{}_{ij} = 1/\eta \qquad j = 1,2,3 \qquad \textbf{(2.35)}$$

here, η is the fraction of cycling molecules which is assumed to be conserved during these transitions.

2. The absorption of I_2' is identical to zero for wavelengths larger than or equal to 410 nm: $A_{I2'}$ ($\lambda \geq 410$nm) $\equiv 0$. This is because I_2' has its S_0 to S_1 transition around 355 nm. No higher wavelength transition thus occur. Assuming that the spectra of all intermediates have similar bandwidths, one can then estimate from the spectrum of P, which does not absorb beyond 500 nm, that I_2' does not absorb beyond 410 nm.

Taking into account the second constraint, we consider eqs 2.31, 2.32 and 2.34 only in the wavelength region $\lambda \geq 410$nm, i.e. we drop the rows which are related to smaller wavelengths. Hence the third column of the reduced matrix **A** corresponding to I_2' intermediate is the null vector $(\mathbf{A})_3 = \vec{0}$. Since $(\mathbf{A})_3$ is zero, eq 2.34 allows to determine $(\tilde{\mathbf{C}}^{-1})_3$, the third column of $\tilde{\mathbf{C}}^{-1}$. Provided that the number of wavelength points is larger than 3, eq 2.34 is an over determined system of linear equations, for which the least squares solution

may be found by multiplication with the pseudoinverse matrix $\tilde{\mathbf{B}}^{-1}$ from the left and rearranging:

$$(\tilde{\mathbf{C}}^{-1})_3 = -(\tilde{\mathbf{B}})^{-1}(\mathbf{A}_p)_3 \qquad \textbf{(2.36)}$$

Considering eq 2.34 not only for λ≥410nm but in the full spectral range, $(\tilde{\mathbf{C}}^{-1})_3$ allows to determine the spectrum of the I_2' intermediate. Using the conservation constraint of eq 2.35, $(\tilde{\mathbf{C}}^{-1})_3$ also provides η, the fraction of cycling molecules or the excitation efficiency of the laser flash.

By making the very reasonable assumption that only I_1 contributes in the first extrapolated state $\tilde{\mathbf{B}}_1$ (which is also verified with an independent method, see section 2.4.2), the problem is simplified with $y_1=0= z_1$ in eq 2.30. The elements of $(\tilde{\mathbf{C}}^{-1})_1$, of eq 2.33, can be expressed in terms of $(\tilde{\mathbf{C}}^{-1})_2$, $(\tilde{\mathbf{C}}^{-1})_3$ and the elements of the first column of $\tilde{\mathbf{C}}$ using the matrix relation $\tilde{\mathbf{C}}^{-1}\,\tilde{\mathbf{C}}=\mathbf{I}$, where we get:

$$\left.\begin{aligned}(\tilde{\mathbf{C}}^{-1})_{11} &= (1-(\tilde{\mathbf{C}}^{-1})_{12} * y_1 - (\tilde{\mathbf{C}}^{-1})_{13} * z_1)/x_1\\ (\tilde{\mathbf{C}}^{-1})_{21} &= -((\tilde{\mathbf{C}}^{-1})_{22} * y_1 + (\tilde{\mathbf{C}}^{-1})_{23} * z_1)/x_1\\ (\tilde{\mathbf{C}}^{-1})_{31} &= -((\tilde{\mathbf{C}}^{-1})_{32} * y_1 + (\tilde{\mathbf{C}}^{-1})_{33} * z_1)/x_1\end{aligned}\right\} \qquad \textbf{(2.37)}$$

and thus,

$$(\tilde{\mathbf{C}}^{-1})_1 = \begin{pmatrix} 1/x_1 \\ 0 \\ 0 \end{pmatrix} \qquad \textbf{(2.38)}$$

Here, the conservation constraint of eq 2.35 is applied, from which it follows that x_1 is fraction of cycling molecules η. Hence, from eq 2.34 (where i=1), with known $(\tilde{\mathbf{C}}^{-1})_1$, the I_1 spectrum is determined.

It is an experimental observation that the second column of the $\tilde{\mathbf{B}}$ matrix, $\tilde{\mathrm{B}}_2$ has no contribution from I_2' (detail in the section 3.1.1), implying $z_2=0$ in $\tilde{\mathbf{C}}$ matrix of eq 2.30. As we already know the $(\tilde{\mathbf{C}}^{-1})_1$ and $(\tilde{\mathbf{C}}^{-1})_3$, elements of $(\tilde{\mathbf{C}}^{-1})_2$ can be expressed in terms of $(\tilde{\mathbf{C}}^{-1})_1$, $(\tilde{\mathbf{C}}^{-1})_3$ and elements of the second column of $\tilde{\mathbf{C}}$ using the matrix relation $\tilde{\mathbf{C}}^{-1}\,\tilde{\mathbf{C}}=\mathbf{I}$, where we get:

$$\left.\begin{aligned}(\tilde{\mathbf{C}}^{-1})_{12} &= -((\tilde{\mathbf{C}}^{-1})_{11} * x_2 + (\tilde{\mathbf{C}}^{-1})_{13} * z_2)/y_2\\ (\tilde{\mathbf{C}}^{-1})_{22} &= (1-(\tilde{\mathbf{C}}^{-1})_{21} * x_2 - (\tilde{\mathbf{C}}^{-1})_{23} * z_2)/y_2\\ (\tilde{\mathbf{C}}^{-1})_{32} &= -((\tilde{\mathbf{C}}^{-1})_{31} * x_2 + (\tilde{\mathbf{C}}^{-1})_{33} * z_2)/y_2\end{aligned}\right\} \qquad \textbf{(2.39)}$$

Again, the conservation constraint of eq 2.35 implies: $x_2+y_2+z_2=\eta$. Thus $(\tilde{\mathbf{C}}^{-1})_2$ can be expressed as a function of y_2:

$$(\tilde{\mathbf{C}}^{-1})_2 = \begin{pmatrix} -\dfrac{(\eta - y_2)}{\eta * y_2} \\ \dfrac{1}{y_2} \\ 0 \end{pmatrix} \qquad \textbf{(2.40)}$$

Since every element of the $\tilde{\mathbf{C}}$ matrix can take only positive values and the conservation constraint has to be obeyed, y_2 can have values between 0 and η. Now, from eq 2.34 (in this case i=2), the I_2 (at acid/neutral pH) or I_1' (at alkaline pH) spectrum is calculated for various values of y_2. Physically meaningful absorption spectra are those which have positive absorbance. Of the many possible spectra one is selected which has a reasonable spectral bandwidth (see section 3.1.1 and 3.2.1).

The completely determined spectra of intermediates in the matrix of difference $\mathbf{A}$-$\mathbf{A}_P$ provides information about the ratio of concentrations of the intermediates in the extrapolated states and can be used to calculate their time courses, **n**, using eq 2.18.

The extrapolated difference method was developed by Dr. B. Borucki **[Borucki, 1999]** and successfully applied to the photocycle of bacteriorhodopsin **[Borucki, 1999]**. See **[Borucki, 1999]** for further details.

2.4.2 Scaled Subtraction Method

A different method to obtain the intermediate spectra from the amplitude spectra of eq. 2.25 or 2.28 is the scaled subtraction method. This method is used for the data set at pH 10 (contributing I_1, I_1' and I_2' spectra, section 3.2.1). Details of this procedure are explained in the section 3.2.1.2.

To start with this method, a correct I_1 spectrum is essential. It is an experimental observation that the initial bleach $\Delta A(\lambda,\sim 1\mu s)$, which is also the I_1-P difference spectrum, is the same for acid/neutral pH as well as alkaline pH, showing that I_1 is the same for the whole pH range (see $\tilde{\mathbf{B}}_1$ (▲) of Figure 3.3 and 3.10). To obtain the I_1 spectrum, the proper amount of dark spectrum has to be added to this bleach (detail in section 4.1.1, Figure 4.1C). This amount depends upon the excitation efficiency and can be approximated by scaling the dark spectrum to the bleached signal $\Delta A(\lambda \geq 430nm,\sim 10\ ms)$ at pH 6 assuming that mainly I_2/I_2'

contribute in this time range, which do not absorb beyond λ≥430nm, as well as I_1 contribute minimally in this time range.

When the I_1 contribution (Figure 3.9A, ■) is subtracted from the amplitude spectrum of the first transition $(\mathbf{B})_1$ [●, Figure 3.9A], the pure I_1' spectrum (Figure 3.9A, ○) can be obtained. This subtraction is done by matching the scaled I_1 spectrum and the $(\mathbf{B})_1$ amplitude spectrum in the spectral range λ≥485 nm as shown in Figure 3.9A. In successive subtraction of the I_1 contribution from the other two amplitude spectra $(\mathbf{B})_2$ [□, Figure 3.9A], and $(\mathbf{B})_3$ [○, Figure 3.9B], the mixtures of I_1'/I_2' (Figure 3.9C, □) and $I_1'/I_2'/P$ (Figure 3.9B, ●) amplitude spectra are obtained respectively.

Using the pure I_1' spectrum (Figure 3.9A, ○), the pure I_2' spectrum (Figure 3.9C, ■) can be calculated upon subtraction of the I_1' contribution (Figure 3.9C, ⊠) from I_1'/I_2' mixture (Figure 3.9C, □) by matching in the spectral range λ≥430 nm as shown in Figure 3.9C.

The I_2' spectrum can also be calculated from the $I_1'/I_2'/P$ amplitude spectrum (Figure 3.9B, ●), see above. In this case, the dark state contribution (P, ✳: Figure 3.9B) has to be subtracted at first from the $I_1'/I_2'/P$ mixture (Figure 3.9B, ●), where this $I_1'/I_2'/P$ amplitude spectrum and P match in λ≥465 nm range as shown in Figure 3.9B. This subtraction results in the I_1'/I_2' amplitude spectrum (Figure 3.9C, ○). Finally, the I_2' spectrum can be calculated from this I_1'/I_2' amplitude spectrum upon subtraction of the I_1' contribution (Figure 3.9C, ●) by matching in the spectral range λ≥430 nm as shown in Figure 3.9C.

The relative contributions of the corresponding factors obtained during the subtraction procedure are the elements of the matrix **C** of eq. 2.17. Thus, **n** can be obtained using eq 2.18, once the matrix $\mathbf{A}\text{-}\mathbf{A}_P$ is known from the subtraction procedure.

2.5 pH Dependent Time Courses of the Intermediates

As we will describe in detail in section 3.1.1 and 3.2.1, during the photocycle the I_1, I_2 and I_2' intermediates are in equilibrium at pH 6 and I_1, I_1' and I_2' at pH 10 after about ~20 ms. It is further investigated whether this equilibrium is pH dependent. For that purpose, transient absorbance changes $\Delta\mathbf{A}(\lambda,t)$ are measured for various pH values and the pH dependent time courses of the intermediates I_1, I_2 or I_1' and I_2' were obtained using combined singular value decomposition (section 2.5.1). The equilibrium of the I_2/I_2' states is pH dependent at acid/neutral pH (see section 3.1.2). Likewise the $I_1/I_1'/I_2'$ states are in equilibrium in the alkaline pH (see section 3.2.2). In addition, the decay rates of these equilibria to P are also strongly pH dependent. Both observations might be related with the photocycle scheme as described below (section 2.5.2).

2.5.1 Combined Singular Value Decomposition

It is possible to perform the singular value decomposition of the combined data matrix constructed from the large data set measured at the various pH values. This is particularly useful if the same number of intermediates are involved in the whole pH range **[Borucki, 2002]**. The large matrix, $\Delta\mathbf{A}$, can be constructed by joining successively the matrices $\Delta\mathbf{A}_1(\lambda,t_1)$, $\Delta\mathbf{A}_2(\lambda,t_2)$,……, $\Delta\mathbf{A}_n(\lambda,t_m)$ from the measured data sets of the n individual pH values. Under the condition that the same spectral components contribute throughout the whole pH range, it is necessary to have the time traces in exactly the same spectral range for every pH. In this case, kinetics might change with the pH, i.e., the number of measured time points might differ. The number of the rows in this large matrix is the number of wavelengths and the number of columns is the sum of the time points from the whole pH range. Singular value decomposition of such a combined matrix $\Delta\mathbf{A}$ is:

$$\Delta\mathbf{A} = [\Delta\mathbf{A}_1(\lambda,t_1) \quad \Delta\mathbf{A}_2(\lambda,t_2) \quad \ldots\ldots\ldots \quad \Delta\mathbf{A}_n(\lambda,t_m)] = \mathbf{U}_k\mathbf{S}_k\mathbf{V}^T_k \qquad \textbf{(2.41)}$$

where, $$\mathbf{V}^T_k = [\mathbf{V}_{k1}(t_1) \quad \mathbf{V}_{k2}(t_2) \quad \ldots\ldots\ldots \quad \mathbf{V}_{kn}(t_m)]^T \qquad \textbf{(2.42)}$$

with $\mathbf{U}_k$ and $\mathbf{V}_k$ the unitary matrices. The best fit to the data matrix for the individual pH data set $\Delta\mathbf{A}_i(\lambda,t_j)$ can be obtained from the matrix product $\mathbf{U}_k\mathbf{S}_k\mathbf{V}^T_{ki}(t_j)$ with the significant singular values k. The advantage of the combined singular value decomposition is that the error is distributed over the whole data set during the matrix decomposition. The time course of the intermediates, $\mathbf{n}_i(t_j)$, can be calculated from the following relations:

$$\Delta\mathbf{A} = \mathbf{U}_k\mathbf{X}^{-1}\mathbf{X}\mathbf{S}_k\mathbf{V}^T_k \qquad \textbf{(2.43)}$$

where,

$$\mathbf{U}_k\mathbf{X}^{-1} = \mathbf{A}\text{-}\mathbf{A}_P \qquad \textbf{(2.44)}$$

and,

$$[\mathbf{n}_1(t_1) \quad \mathbf{n}_2(t_2) \ldots\ldots\ldots \quad \mathbf{n}_n(t_m)]^T = \mathbf{X}\mathbf{S}_k\mathbf{V}^T_k \qquad \textbf{(2.45)}$$

if the transformation matrix, $\mathbf{X}$ is known. Here, the matrix $\mathbf{X}$ is required because this matrix transforms the basis vectors of the spectral part ($\mathbf{U}_k$) to the spectra of intermediates (eq 2.44), and the basis vectors of the temporal part ($\mathbf{V}^T_k$) to the time courses of the intermediates (eq 2.45). The advantage with this matrix $\mathbf{X}$ is that this is a single transformation matrix for the whole measured data set subjected to the combined SVD. This matrix $\mathbf{X}$ might be determined from the basis spectra, $\mathbf{U}_k$ and known difference spectra $\mathbf{A}\text{-}\mathbf{A}_P$ using eq 2.44. The difference spectra $\mathbf{A}\text{-}\mathbf{A}_P$ in turn, can be obtained from the analysis of the data set at a particular pH using the extrapolated difference spectra method or scaled subtraction method (section 2.4).

Combined SVD of the data set from pH 4.6 to 8.4 shows that three spectral components I_1, I_2 and I_2' contribute during the photocycle where I_2 and I_2' are in pH dependent

equilibrium (after ~20 ms) with increasing I_2' at higher pH (section 3.1.2). Data sets from pH 8 to 11 show that three spectral components I_1, I_1' and I_2' contribute in this pH range where I_1' and I_2' are in pH dependent equilibrim with increasing I_1' at higher pH (section 3.2.2.). In the overlapping pH range 8 to 8.5, all four intermediates I_1, I_1', I_2 and I_2' might contribute. However, the major contribution is due to I_2'.

2.5.2 pH Dependence of Equilibrium and Decay Rate

During the photocycle of PYP, I_1' (deprotonated form of chromophore) and I_2' (protonated form of chromophore) are in pH dependent equilibrium (section 3.2.2). In addition, the decay rate of this equilibrium to the initial state P is also pH dependent with similar pK_a. The pH dependence of this rate constant can be related to the relative population of the species with the following analysis using the reaction scheme of Figure 2.2**, [Kenneth, 1990]**.

I_1' and I_2' are in pH dependent equilibrium:

$$[I_1'] + [H^+] \Leftrightarrow [I'_2] \qquad \textbf{(2.46)}$$

The acid dissociation constant is:

$$K_a = \frac{[H^+][I_1']}{[I'_2]} = 10^{-pK_a} \qquad \textbf{(2.47)}$$

The normalized fractions of I_1' and I_2' are respectively:

$$F_{I1'} = \frac{[I_1']}{[I_1'] + [I_2']} = \frac{K_a}{[H^+] + K_a} = \frac{1}{1 + 10^{-n(pH - pK_a)}} \qquad \textbf{(2.48)}$$

$$F_{I2'} = \frac{[I_2']}{[I_1'] + [I_2']} = \frac{[H^+]}{[H^+] + K_a} = \frac{1}{1 + 10^{n(pH - pK_a)}} = 1 - F_{I1'} \qquad \textbf{(2.49)}$$

where, $[H^+]=10^{-pH}$ and n is the Hill coefficient. Thus, $F_{I1'}$ and $F_{I2'}$ are sigmoidal functions of the pH.

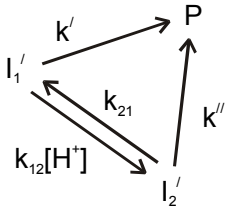

Figure 2.2: A reaction scheme showing pH dependent equilibrium between I_1' and I_2' and transition to P with decay rates k′ and k″ respectively.

Let us suppose that I_1' and I_2' decay to P with decay rates of k′ and k″ respectively and that the I_1'/I_2' equilibrium formation is very fast compared to these two rates. Under these conditions, the decay rate of the sum of the states I_1' and I_2' can be expressed as their sum weighted by respective rate constants:

$$-\frac{d([I_1'']+[I_2''])}{dt} = k''[I_1''] + k''[I_2''] \quad \textbf{(2.50)}$$

Replacing the values for $[I_1'']$ and $[I_2'']$ using eq 2.48 and 2.49:

$$-\frac{d([I_1'']+[I_2''])}{dt} = \left\{k''\left(\frac{1}{1+10^{-n(pH-pK_a)}}\right) + k''\left(\frac{1}{1+10^{n(pH-pK_a)}}\right)\right\}([I_1'']+[I_2'']) \quad \textbf{(2.51)}$$

Thus, the apparent rate constant for the ground state (P) recovery is:

$$k = \left\{k''\left(\frac{1}{1+10^{-n(pH-pK_a)}}\right) + k''\left(\frac{1}{1+10^{n(pH-pK_a)}}\right)\right\} \quad \textbf{(2.52)}$$

Under the condition that $k'' \gg k'$, the apparent rate constant k is a sigmoidal function of pH, the same as that of the I_2'' population in the I_1''/I_2'' equilibrium. Thus,

$$k = k''\left(\frac{1}{1+10^{n(pH-pK_a)}}\right) \quad \textbf{(2.53)}$$

So, the pK_a of the I_1''/I_2'' equilibrium and of the decay rate of this I_1''/I_2'' equilibrium to P are identical under these conditions.

Chapter 3

Photocycle Kinetics Mechanism of Photoactive Yellow Protein

The experimental results of the measurements on the pH dependence of the photocycle kinetics of photoactive yellow protein are presented in this Chapter. They are divided into two parts covering the acid/neutral (pH 4.6 to 8.4) and the alkaline (pH 8 to 11) pH ranges. In the whole pH range and the measured time window of 50 ns to 50 s, three transitions are observed. The intermediates, I_1 and I_2' contribute over the whole pH range. However, I_2 and I_1' contribute only in the acid and alkaline pH range respectively.

Spectra and time courses at pH 7 (section 3.1.1) and at pH 10 (section 3.2.1.1) are determined using the extrapolated difference method. Moreover, the spectra at pH 10 are confirmed with an independent method, scaled subtraction (section 3.2.1.2). The pH dependent time courses in the acid/neutral pH range (section 3.1.2) were determined using the I_1, I_2 and I_2' intermediate spectra acquired at pH 7. The corresponding pH dependent time courses in the alkaline pH range (section 3.2.2) were calculated using the I_1, I_1' and I_2' spectra obtained at pH 10. Finally, the intermediate populations measured at about ~20 ms during the cycle confirmed the pH dependent equilibrium between the I_2 and I_2' intermediates in the acid/neutral pH range and between the I_1' and I_2' intermediates in the alkaline pH range respectively. From these observations and the measured pH dependent decay rates photocycle models are proposed for both the acid/neutral (section 3.1.3) and alkaline pH (section 3.2.3) range. A different photocycle model is proposed for each pH range, since the intermediates contributing are different (I_2' and I_1' contributing only in the acid and alkaline pH ranges respectively).

3.1 Photocycle Kinetics at Acid/Neutral pH

The intermediate spectra are determined at pH 7. I_1, I_2 and I_2' contribute to the photocycle at this pH. Using these spectra, the corresponding pH dependent time courses of the photocycle intermediates in the pH range 4.6 to 8.4 are calculated. We find that the pH dependent intermediate populations are related to the transition rates. A photocycle model is proposed based on these observations.

3.1.1 Spectra and Time Courses of Intermediates at pH 7

Transient absorbance changes were measured at pH 7 at 19 wavelengths, ranging from 330 to 510 nm, in the time range from 50 ns to 5 s, Figure 3.1A. For clarity, only eight of the time traces are shown.

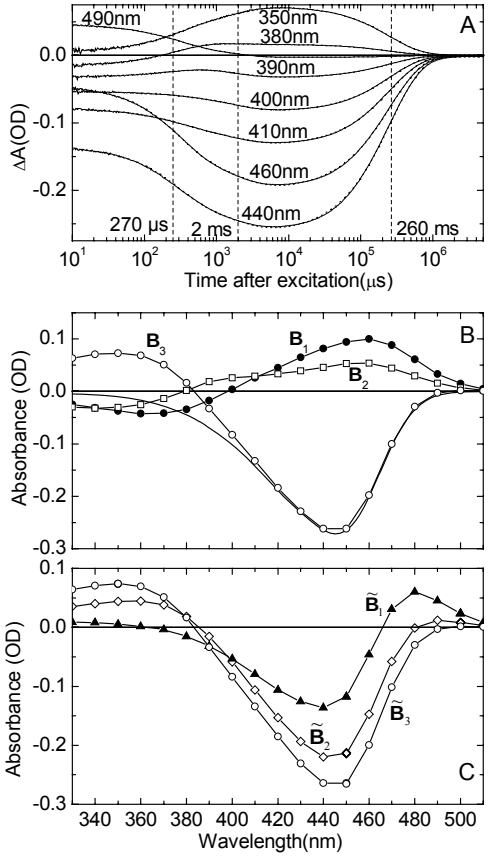

Figure 3.1: (A) Transient absorption changes after excitation at 430 nm at 19 wavelengths varying from 330 to 510 nm. For clarity, only the traces at the indicated wavelengths are shown. The vertical dashed lines indicate the time constants for a global fit to the weighted SVD time traces with a sum of three exponentials. τ_1 = 270 μs is the rise time of I_2, τ_2 = 2.0 ms is the rise time of I_2', and τ_3 = 260 ms is the return to P. The dotted lines, only distinguishable from the data in the μs-time range, are the fits. Conditions: pH 7, 20 °C, 50 mM KCl and 50 mM Tris. PYP concentration: 35 μM. (B) Amplitude spectra $B_i(\lambda)$ calculated from the amplitudes of the exponential fits to the SVD time traces and the corresponding basis spectra of the data in (A). The three amplitude spectra correspond to the following time constants: τ_1 =270 μs (●), τ_2 = 2.0 ms (□), τ_3 = 260 ms (○). The solid curve is a scaled and inverted ground state spectrum. (C) Extrapolated difference spectra obtained from the amplitude spectra of (B) as described in the text: $\tilde{\mathbf{B}}_1$ (▲), $\tilde{\mathbf{B}}_2$ (◇), $\tilde{\mathbf{B}}_3$ (○).

The complete data set in the time range 10 μs to 5 s was subjected to SVD analysis as described in section 2.3.2. The first six singular values were: 11.2, 1.8, 0.14, 0.05, 0.03, and 0.02. We consider the first three to be significant, suggesting the presence of only three spectrally distinguishable intermediates. The additional components, corresponding to the

singular values s_4, s_5 and s_6 show very noisy time traces and were thus neglected. The three weighted time traces from SVD were fitted simultaneously, as described in eq 2.26, starting at 10 μs with a sum of three exponentials with time constants τ_1 = 270 μs, τ_2 = 2.0 ms and τ_3 = 260 ms. These times are marked by vertical dashed lines in Figure 3.1A. The dotted lines in Figure 3.1A, which can barely be distinguished from the data, represent these fit curves for the individual time traces. From the fit to the SVD time traces with the sum of three exponentials and the corresponding basis spectra, the amplitude spectra $B_j(\lambda)$ were calculated using eq. 2.27. These are presented in Figure 3.1B. The amplitude spectra provide considerable insight into the spectra of the intermediates. $B_1(\lambda)$ clearly describes the transition from I_1 (λ_{max} ~ 460 nm) to I_2 with a λ_{max} value above 360 nm. $B_2(\lambda)$ is apparently a transition from an equilibrium of I_1 and I_2 to I_2' with I_2' blue-shifted with respect to I_2. $B_3(\lambda)$ represents the ground state recovery and suggests that I_2' has its λ_{max} value near 350 nm. Comparison of the negative minimum of $\mathbf{B}_1$ with the positive maximum of $\mathbf{B}_3$, suggests that the transition from I_2 to I_2' is associated with a blue-shift of the order of ~ 20 nm.

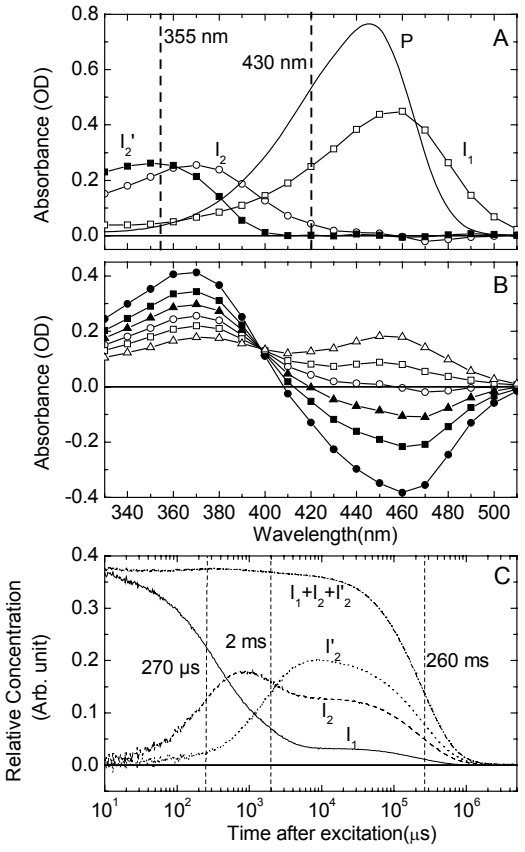

Figure 3.2: (A) Intermediate spectra I_1 (□), I_2 (○) and I_2' (■) calculated from the extrapolated difference spectra of Figure 3.1C. The solid curve represents the spectrum of dark state P for comparison. Vertical dashed lines indicate the wavelengths of the blue (430 nm) and violet (355 nm) excitation flashes used. (B) I_2 and I_2' spectra for various allowed values of y_2 as described in the text. y_2= 0.12 (●), y_2 = 0.15 (■), y_2 = 0.18 (▲), y_2 = 0.22 (○), y_2 = 0.27 (□) and y_2 = 0.37 (Δ). (C) Time-courses of the relative concentrations of I_1 (—), I_2 (---), and I_2' (····) calculated according to eq 2.18. The time-courses of the sum of the relative concentrations of I_1, I_2 and I_2' is indicated by —· —. The vertical dashed lines indicate the time constants from the global SVD fit of Figure 3.1A.

The three amplitude spectra $\mathbf{B}_1$, $\mathbf{B}_2$ and $\mathbf{B}_3$ were used to construct the $\tilde{\mathbf{B}}$ matrix according to eq 2.29. $\tilde{\mathbf{B}}_1$ is the sum of amplitude spectra $\mathbf{B}_1$, $\mathbf{B}_2$ and $\mathbf{B}_3$ (arranged in

columns). $\tilde{\mathbf{B}}_2$ is the sum of amplitude spectra $\mathbf{B}_2$ and $\mathbf{B}_3$, and $\tilde{\mathbf{B}}_3$ is the same as $\mathbf{B}_3$. The three columns, $\tilde{\mathbf{B}}_1$, $\tilde{\mathbf{B}}_2$ and $\tilde{\mathbf{B}}_3$, representing the extrapolated difference spectra, are presented in Figure 3.1C. $\tilde{\mathbf{B}}_1$ equals the initial absorbance change right after the flash, and suggests that the initial bleach led to the formation of the I_1 intermediate (positive absorbance change near 480 nm).

Using the second constraint as described in Materials and Methods (section 2.4.1), that I_2' does not absorb beyond 410 nm, eq 2.34 is considered only in the range $\lambda > 410$ nm, i.e. the rows for the shorter wavelengths are dropped. Then the third column of the reduced matrix **A**, corresponding to the spectrum of I_2', is the null vector: $(\mathbf{A})_3 = \vec{0}$. Since $(\mathbf{A})_3$ is zero, we can solve eq 2.34 for $(\tilde{\mathbf{C}}^{-1})_3$ resulting in eq 2.36. In this way, the third column of $\tilde{\mathbf{C}}^{-1}$ is determined. Using the first constraint described in the section 2.4.1, the sum of these matrix elements equals η^{-1}. In this way, the fraction of cycling molecules, $\eta = 0.371$, is determined. Finally, using $\tilde{\mathbf{B}}$ and $\mathbf{A}_p$ for the whole spectral range allows us to calculate the spectrum of I_2' from $(\tilde{\mathbf{C}}^{-1})_3$ using eq 2.34. The result is shown in Figure 3.2A (■). The λ_{max} value of the spectrum is at about 350 ± 5 nm .

Since only I_1 contributes to $\tilde{\mathbf{B}}_1$ (see Figure 3.1C), the elements $\tilde{C}_{21} = y_1$ and $\tilde{C}_{31} = z_1$ of $\tilde{\mathbf{C}}$ of eq 2.30 are given by $y_1 = z_1 = 0$. This allows us to calculate the elements of the first column of $\tilde{\mathbf{C}}^{-1}$ of eq 2.33. The result is $\tilde{C}^{-1}_{11} = 1/x_1$, $\tilde{C}^{-1}_{21} = 0$, $\tilde{C}^{-1}_{31} = 0$. Since the sum of these elements equals $1/\eta$ (eq 2.35, conservation constraint), we have $x_1 = \eta = 0.371$. With $(\tilde{\mathbf{C}}^{-1})_1$ now completely known, we can calculate the spectrum of I_1 from $(\tilde{\mathbf{C}}^{-1})_1$, $\tilde{\mathbf{B}}$ and $\mathbf{A_p}$ using eq 2.34. The result is shown in Figure 3.2A (□). This spectrum of I_1 is in good agreement with that obtained at pH 10 (Figure 3.8A (□), below).

To calculate the spectrum of the third spectral species, I_2, the procedure is as follows. From Figure 3.1B, we note that $\mathbf{B}_1$ reflects a transition between two intermediates with λ_{max} values of about 460 nm (decay of I_1) and 370 nm (rise of I_2). Since there is apparently no contribution from the more blue-shifted species I_2' (λ_{max} about 350 nm) in $\mathbf{B}_1$, which is well known to be formed from I_2 in the next transition **[Xie**, **2001]**, I_2' does not contribute to $\tilde{\mathbf{B}}_2$ either. Moreover, dye binding experiments showed that the formation of the signaling state I_2' is delayed with respect the formation of I_2 **[Borucki**, **2002]**. Therefore it is concluded that I_2' is not involved in the first transition and thus $z_2 = 0$ in eq 2.30. The elements x_2, y_2, z_2 of the second column of $\tilde{\mathbf{C}}$ of eq 2.30 can now be expressed in terms of x_2, y_2, and η with the

help of $\tilde{\mathbf{C}}^{-1}\tilde{\mathbf{C}} = \mathbf{I}$ as described in eq 2.39. Using the conservation constraint, $x_2 + y_2 = \eta$ of eq 2.35, we finally obtain for the elements of the second column of $\tilde{\mathbf{C}}^{-1}$ (eq 2.40): $\tilde{C}_{12}^{-1} = -(\eta - y_2)/\eta y_2$, $\tilde{C}_{22}^{-1} = 1/y_2$, $\tilde{C}_{32}^{-1} = 0$. So we have now determined all elements of the second column of $\tilde{\mathbf{C}}^{-1}$, the only free parameter remaining is y_2 (eq 2.40). Since x_i, y_i and z_i can only assume positive values and $x_2 + y_2 = \eta$, y_2 is restricted to values between 0 and η. The spectrum of I_2 can now be calculated from $(\tilde{\mathbf{C}}^{-1})_2$, $\tilde{\mathbf{B}}$ and $\mathbf{A}_p$ using eq 2.34. The results are shown in Figure 3.2B for six values of y_2 from 0.12 to 0.37 (~η). Since the extinction coefficient has to be positive, physically meaningful absorption spectra are only obtained for $y_2 \geq 0.22$. Of the spectra remaining in Figure 3.2B, we pick the one associated with $y_2 = 0.22$, since it has the smallest spectral bandwidth.

For y_2 considerably larger than 0.22, the spectral bandwidth becomes much larger than for P and I_1 and a secondary absorption maximum develops near 460 nm. This contradicts the original assumption that the UV transitions of I_2 and I_2' are the longest wavelength transitions of these intermediates, which precludes transitions at higher wavelengths. The spectrum of I_2 for $y_2 = 0.22$ is redrawn in Figure 3.2A (○). Its λ_{max} value is at about 370 ± 5 nm. We note that the value of λ_{max} is independent of the choice of y_2.

Using the spectra of I_1, I_2 and I_2', the time courses of the intermediates were calculated from the experimental $\Delta A(\lambda,t)$ data by using eq 2.18. The time-dependence of the relative concentrations of the I_1, I_2 and I_2' intermediates at pH 7 are shown in Figure 3.2C.

I_1 partially decays to I_2 in 270 µs. I_1 and I_2 then further decay around 2 ms to an $I_1/I_2/I_2'$ equilibrium. This equilibrium finally decays to P in 260 ms. Also shown is the sum of the relative concentrations of these intermediates (dash-dot line). To a good approximation, this sum is constant over the entire time range before the decay to P, validating the data analysis. Its value is very close to η = 0.371, the fraction cycling, showing the internal consistency of the analysis.

The matrix containing the relative contributions of the intermediates, $\tilde{\mathbf{C}}$ of eq. 2.30, it's inverse, $\tilde{\mathbf{C}}^{-1}$ of eq. 2.33, and the coefficient matrix, **C** of eq. 2.17 calculated in this analysis are:

$$\tilde{\mathbf{C}} = \begin{pmatrix} 0.371 & 0.151 & 0.032 \\ 0 & 0.22 & 0.13 \\ 0 & 0 & 0.209 \end{pmatrix},$$

$$\tilde{\mathbf{C}}^{-1}=\begin{pmatrix} 2.7 & -1.85 & 0.742 \\ 0 & 4.55 & -2.83 \\ 0 & 0 & 4.78 \end{pmatrix} \text{ and}$$

$$\mathbf{C}=\begin{pmatrix} 0.22 & 0.119 & 0.032 \\ -0.22 & 0.09 & 0.13 \\ 0 & -0.209 & 0.209 \end{pmatrix} \text{ respectively.}$$

3.1.2 pH Dependence

To answer the question whether the equilibrium between I_1, I_2 and I_2' observed at 20 ms during photocycle (Figure 3.2C) is pH dependent, and to learn more about the nature of the transition between the acid and the neutral pH regimes, the photocycle kinetics were measured at the following fifteen pH values: 4.6, 4.8, 5.1, 5.4, 5.7, 6.0, 6.3, 6.6, 6.75, 6.9, 7.35, 7.7, 7.9, 8.1 and 8.4. With excitation at 430 nm, time traces were collected at the seven wavelengths 340, 370, 390, 410, 450, 490, and 500 nm over the time range from 50 ns to 50 s. Results for selected wavelengths are shown in Figure 3.3. Note that the panels of Figure 3.3 have very different vertical scales, and correspondingly different signal to noise ratios. The smallest pH-induced absorbance changes are at 500 nm. The initial absorbance change is almost pH independent at every wavelength, suggesting that the amount of I_1 formed is independent of pH in this range. At each pH, the absorbance changes at all wavelengths could be fitted simultaneously with a sum of three exponentials. The first time constant was virtually constant in this pH range, varying between 200 and 350 μs. The second time constant varied between 1.3 (pH 8.4) and 10.6 ms (pH 5.1), and is pH dependent. As we saw above, the first transition is due to the decay of I_1 to I_2 and the second transition is due to the decay of I_1/I_2 to the $I_1/I_2/I_2'$ equilibrium. The data of Figure 3.3 show that the third time constant, the return of the $I_1/I_2/I_2'$ equilibrium to P, is also strongly pH dependent, slowing down with decreasing pH. The pH dependent rate constants k_2 and k_3 are plotted in Figure 3.5B and D respectively.

Some preliminary conclusions on the pH dependence of the I_1, I_2, I_2' intermediate populations may be drawn by inspection of these data. At 340 nm, the extinction coefficient of I_2' is larger than that of I_2 (Figure 3.2A). Although the sequence of time traces is not entirely regular, the absorbance at 340 nm around 10 ms (Figure 3.3A) seems to increase with pH, suggesting an increase in the relative amount of I_2'. At 370 nm, the extinction coefficient of I_2 is larger than that of I_2' (Figure 3.2A). The decrease in absorbance at 370 nm

with pH in the ms time range (panel B of Figure 3.3), may thus be interpreted as a decrease in the relative amount of I_2.

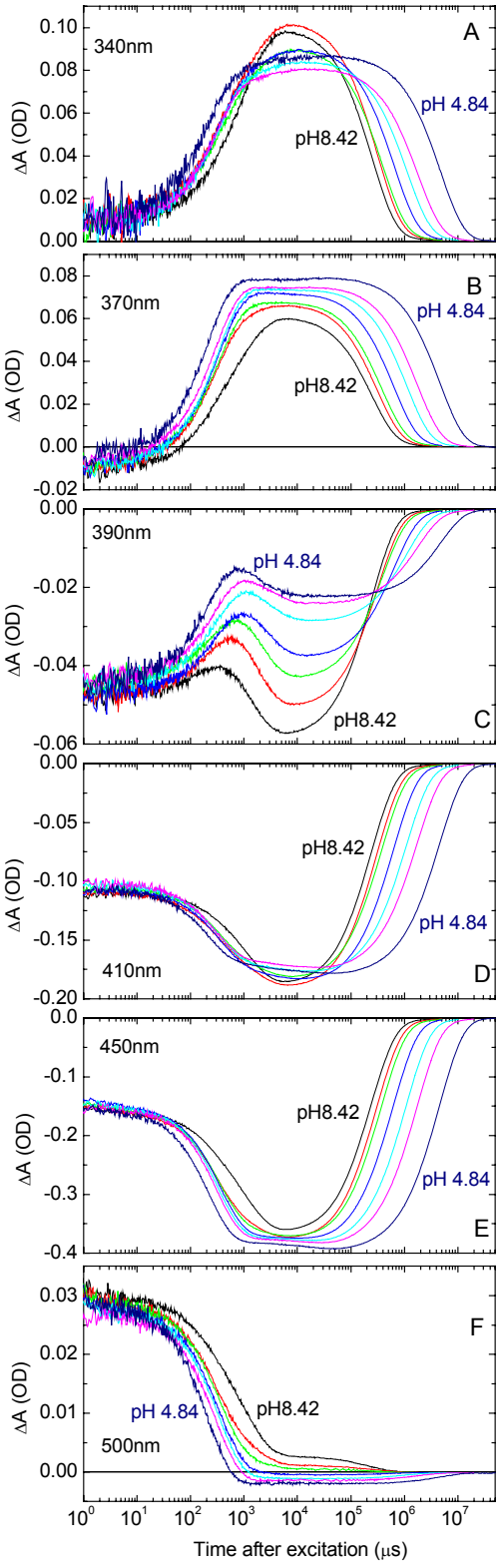

Figure 3.3: pH dependence of the transient absorbance changes after excitation at 430 nm at various wavelengths. (A): 340 nm (characteristic for I_2'), (B): 370 nm (characteristic for I_2), (C): 390 nm (characteristic for I_2), (D): 410 nm (characteristic for I_1'), (E): 450 nm (characteristic for P) and (F): 500 nm (characteristic for I_1). The color code for the pH values in each panel are: black, pH 8.4; red, pH 6.9; green, pH 6.6; blue, pH 6.0; light blue, pH 5.7; pink, pH 5.4; dark blue, pH 4.8. Conditions: 50 mM MES, 50 mM KCl, 20°C. PYP concentration: 53 μM.

At 390 nm, the difference in extinction coefficient between I_2 and I_2' is even larger. This wavelength is therefore diagnostic for the I_2 to I_2' transition and for pH effects on this

transition. Panel C of Figure 3.3 shows the increase in absorbance below 1 ms due to the I_1 to I_2 transition (the extinction coefficient of I_2 is larger than that of I_1 at this wavelength, see Figure 3.2A). The amount of I_2 formed apparently decreases with increasing pH judging from the amplitude of the absorption change below 1 ms in Figure 3.3C. Around 2 to 3 ms there is a large decrease in absorbance due to the I_2 to I_2' transition. The amplitude of this transition increases with pH, suggesting that more I_2' is formed at alkaline pH. Panel D shows time traces at 410 nm. This wavelength is appropriate for monitoring the I_1' intermediate which occurs at alkaline pH (section 3.2.1). These traces indicate that this intermediate is absent in this pH range. The traces at 500 nm (Panel F) are characteristic for I_1. They suggest that, with increasing pH, more I_1 remains after the I_1/I_2 to I_2' transition. This is also supported by the traces at 450 nm (panel E) indicating that the ground state depletion decreases with pH.

To obtain the time courses of the intermediate populations, it was assumed that the spectra of I_1, I_2 and I_2' of Figure 3.2A are pH independent and that no other intermediates contribute in the pH range from 4.6 to 8.4. The Eq 2.18 was then used to calculate the time traces $n_i(t)$ for each intermediate at each pH value from the absorbance changes $\Delta A(\lambda, t)$ and the spectra $A_i(\lambda)$ by matrix inversion. The time dependencies of the populations of I_1, I_2 and I_2' at seven of the fifteen pH values are shown in panels A, B and C of Figure 3.4. They confirm what was suggested by the data of Figure 3.3: I_1 decays partially to I_2; I_1 and I_2 then partially decay to I_2'; beyond 10 ms I_1, I_2 and I_2' are in equilibrium and return together to P. Figure 3.4D shows that the sum of the populations is approximately constant in time and equal to the fraction cycling. Whereas the population of I_1 in equilibrium with I_2 and I_2' is only slightly pH dependent (see traces of Figure 3.4A around 10 ms), the concentrations of I_2 and I_2' show a strong and opposite pH dependence. With increasing pH, the amount of I_2' increases at the expense of a corresponding decrease in the I_2 population.

To quantify the observed pH dependence of the equilibrium populations, the relative concentrations of the intermediate populations corresponding to the different transitions were derived from the $\tilde{\mathbf{C}}$ matrix of eq 2.31. The columns of this matrix, as shown in eq 2.30, contain the relative concentrations of the intermediates in the difference spectra $\tilde{\mathbf{B}}$. For every pH, the amplitude spectra were derived from the simultaneous fit of the measured transient absorbance changes at 340 nm, 370 nm, 390 nm, 410 nm, 450 nm 490 nm and 500 nm of Figure 3.3, with a sum of three exponentials. These amplitude spectra were arranged, with increasing order of the transitions, in the columns of matrix **B**. Extrapolated difference

spectra $\tilde{\mathbf{B}}$ matrix of eq 2.31 was obtained from the **B** matrix by adding the columns as defined in the eq 2.29.

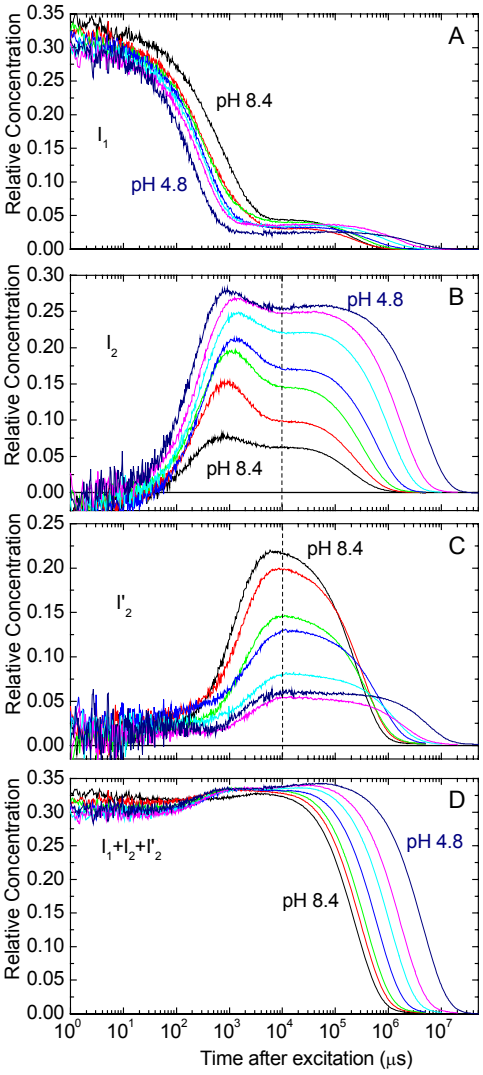

Figure 3.4: Time courses of the relative concentrations of the I_1 (A), I_2 (B) and I_2' (C) intermediates at various pH values calculated using eq 2.18 as explained in the text. (D): time course of the sum of the populations of I_1, I_2 and I_2'. Color code as in Figure 3.3. The values read off at the vertical dashed lines at 10 ms in B and C are plotted in Figure 3.5C.

The corresponding elements of the $\tilde{\mathbf{C}}$ matrix defined by eq 2.30 were acquired by matrix inversion of eq 2.31 where $\mathbf{A}$-$\mathbf{A}_p$ was derived from Figure 3.2A. The columns of $\tilde{\mathbf{C}}$ matrix defined in eq 2.30 represent, in order, the relative concentrations of the I_1, I_2 and I_2' species in the respective transition. Before the first transition, only I_1 is present (i.e. $y_1=0=z_1$) as shown in Figure 3.4A-C (~ 10 μs). The first and second row of the second column (x_2 and y_2) of the $\tilde{\mathbf{C}}$ matrix represent the respective relative concentrations of the I_1 and I_2 intermediates, before the second transition. The pH dependence of these values are plotted in Figure 3.5A. The solid curves are the results of a simultaneous fit with the Henderson-Hasselbalch equation. The fit parameters were pK_a ~ 7 and n ~ 0.97 indicating that I_1 and I_2

are in a pH-dependent equilibrium. Before the second transition, I_2' makes a minimal contribution, as shown by Figure 3.4C (i.e. z_2=0).

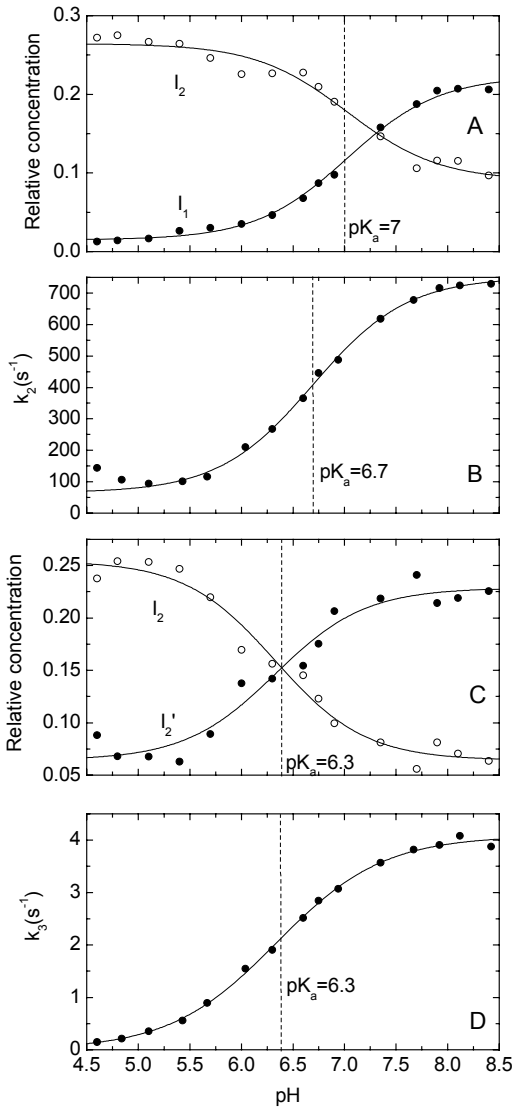

Figure 3.5: (A) pH dependence of the equilibrium concentrations of the I_1(•) and I_2(o) intermediates derived from the $\tilde{\mathbf{C}}$ matrix as described in the text. The solid curves are the simultaneous fits of these titration curves with the Henderson-Hasselbalch equation with pK_a = 7 and n ~ 0.97. (B) pH dependence of the decay rate k_2 of I_1/I_2 equilibrium to $I_1/I_2/I_2'$ equilibrium. For every pH, the decay rates k_2 and k_3 were derived from the simultaneous fit of the measured transient absorbance changes at 340 nm, 370 nm, 390 nm, 410 nm, 450 nm 490 nm and 500 nm with a sum of three exponentials. The solid curve is the fit of the decay rate with the Henderson-Hasselbalch equation with pK_a = 6.7, n ~ 0.95. (C) pH dependence of the equilibrium concentrations of the I_2(o) and I_2' (•) intermediates derived from the $\tilde{\mathbf{C}}$ matrix as described in the text. The solid curves are the simultaneous fits of these titration curves with the Henderson-Hasselbalch equation with pK_a = 6.3 and n ~ 0.98. (D) pH dependence of the decay rate k_3 of the ground state recovery. The solid curve is the fit of the decay rate with the Henderson-Hasselbalch equation with pK_a = 6.3, n ~ 0.84.

The formation of the I_1/I_2 equilibrium before the second transition is directly evident from the 390 nm traces of the Figure 3.3C where the height of the hill at about ~ 500 µs increases with decreasing pH. This is due to the I_1 to I_2 transition (I_2' does not yet contribute to the cycle) with I_2 decreasing at higher pH. The next transition to the $I_1/I_2/I_2'$ equilibrium from the I_1/I_2 equilibrium may also be discerned from the same Figure. Moreover, this is mirrored in the I_2 time courses with the bump between 500 µs and 1 ms, Figure 3.4B. The I_1/I_2 equilibrium is also evident from the $\tilde{\mathbf{B}}_2$ (positive absorbance for λ≥ 500 nm and around λ ~ 360 nm) which is the extrapolated difference spectrum before the second transition. The decay of the I_1/I_2 equilibrium during the second transition could not be visually inspected

from the I_1 time course in Figure 3.4A, or from the 500 nm trace of Figure 3.3F. This is because I_1 continues to decay in both of the first and second transitions.

The decay rate corresponding to the second transition slows down upon decreasing pH, Figure 3.3. The rate constant k_2 for this transition was determined from a global fit of the data of Figure 3.3 at all seven wavelengths. Its pH dependence is plotted in Figure 3.5B. A fit with the Henderson-Hasselbalch equation results in a pK_a of ~ 6.7 and n ~ 0.95. The apparent decay rate corresponding to the second transition thus seems to be proportional to the I_1 population in the I_1/I_2 equilibrium, compare Figure 3.5A and B. This relationship is expected in the framework of a simple model presented in the discussion (scheme I).

The second and third row of the third column (y_3 and z_3) of the $\tilde{\mathbf{C}}$ matrix represent the respective relative concentrations of I_2 and I_2' intermediates, before recovery. The pH dependence of their concentrations is plotted in Figure 3.5C. The x_3 value represents the relative I_1 population before the third transition (~ 10 ms) and is weakely pH dependent. This is consistent with the observation presented in Figure 3.4A. The corresponding relative concentrations of I_2, I_2' intermediates plotted in Figure 3.5C are very similar to the corresponding values of the I_2 and I_2' intermediates read off at 10 ms of Figure 3.4B and C respectively (vertical dashed lines), as it should be. The solid curves are the results of a simultaneous fit with the Henderson-Hasselbalch equation. The fit parameters were pK_a ~ 6.4 and n ~ 0.98. I_2 and I_2' are thus in a pH-dependent equilibrium.

The ground state recovery slows down with decreasing pH, Figure 3.3. The rate constant k_3 for this recovery is plotted in Figure 3.5D. A fit with the Henderson-Hasselbalch equation results in a pK_a of ~ 6.3 and n ~ 0.8 . The apparent decay rate for the dark-state recovery thus seems to be proportional to the I_2' population in the $I_1/I_2/I_2'$ equilibrium. This relationship is also described later in the discussion with a simple model (scheme II).

In summary, the I_1/I_2 equilibrium is formed from I_1 during the first transition with about ~ 350 µs life time, and is pH dependent with pK_a ~7. The I_1/I_2 equilibrium decays to another pH dependent equilibrium $I_1/I_2/I_2'$ in the second transition. During recovery, the $I_1/I_2/I_2'$ equilibrium decays to P with a pK_a ~ 6.3. A detailed photocycle model based on these observations is shown in Figure 3.6. We note that the transitions of the Figure 3.5A and C are incomplete. The possible reasons for this observation are presented later in the discussion.

3.1.3 Discussion

From measurements of the pH dependence of the photocycle and photoreversal (see section 4.2) kinetics of PYP between 4.6 and 8.4, the following results were obtained: 1) the

spectra of the signaling state I_2' (350 nm) and its precursor I_2 (370 nm) differ by about 20 nm, 2) at about 500 µs, I_1 and I_2 are in pH dependent equilibrium with pK_a ~7, 3) the decay rate of the second transition is pH dependent with pK_a ~6.7, 4) from several ms (formation of I_2') to the end of the cycle the three intermediates I_1, I_2 and I_2' are in equilibrium, 5) the pK_a of the pH-dependent equilibrium between I_2' and its precursor I_2 is ~ 6.4 from photocycle kinetics and ~ 6.1 from photoreversal kinetics (see section 4.2). The pH is thus an important parameter that controls the amount of receptor in the active state. This is analogous to the case of the photoreceptor rhodopsin where the equilibrium between the signaling state M_{II} and its precursor M_I is also strongly pH dependent **[Dickopf**, **1998]**. In **[Borucki**, **2005]** we showed that the I_2/I_2' equilibrium also depends on the salt concentration.

The existence of two distinguishable I_2 intermediates with protonated chromophore was first demonstrated by time-resolved FTIR **[Xie**, **2001]**, **[Brudler**, **2001]**. I_2 decays to I_2' in about 2 – 3 ms **[Xie**, **2001]**, **[Brudler**, **2001]**. This transition to the signaling state I_2' is characterized by a global conformational change **[Xie**, **2001]**, **[Brudler**, **2001]**. Here, we showed that this transition may also be monitored by transient electronic absorption spectroscopy and determined the absorption spectra of I_2 and I_2' by the extrapolated difference method **[Borucki**, **1999]**. The λ_{max} values of I_2 and I_2' are 370 ± 5 and 350 ± 5 nm, respectively. Absorption spectra for I_2 and I_2' at pH 8.1 were presented in **[Hendriks**, **2003]**. No λ_{max} values were provided, but the spectrum of I_2 was said to be "slightly red-shifted" with respect to I_2', in agreement with our results. The spectrum of I_2 presented in **[Hendriks**, **2003]** is so noisy that it is difficult to estimate λ_{max} . The poor quality of this spectrum is probably due to the fact that at pH 8.1 the contribution of I_2 in the equilibrium is very low, as we showed here (Figure 3.5C). Our I_2 and I_2' spectra are comparable to those presented in **[Otto, 2005]**, **[Yeremenko, 2006]** and **[Shimizu, 2006]**, which were obtained by different methods and published after conclusion of our experiments.

Using these spectra and assuming that they are pH independent in the pH range from 4.6 to 8.4, we obtained the time dependence of the concentrations of I_1, I_2 and I_2' (Figure 3.4).

At about 500 µs, I_1, I_2 are in equilibrium and decay together to the I_1, I_2 and I_2' equilibrium during the second transition, Figure 3.4A-C. The equilibrium intermediate populations of I_1 and I_2 are pH dependent with a pK_a of ~ 7, Figure 3.5A. Below the pK_a, I_2 is the major species, above the pK_a the opposite holds.

The decay rate k_2 of the second transition, is also pH dependent with a pK_a of 6.7, i.e. very close to that for the I_2/I_2' equilibrium as shown in Figure 3.5A. This relationship might be explained using the scheme I, as discussed in section 2.5.2.

During the second transition I_1 and I_2 decay to I_2', forming the $I_1/I_2/I_2'$ equilibrium. Under the assumption that the I_1/I_2 equilibrium is formed (scheme I) much faster than the respective individual microscopic rates k' and k'' for decay of I_1 and I_2 to I_2', the apparent rate $k_2 \sim [I_1]$, when $k' \gg k''$. Analysis of this reaction scheme I, as described in section 2.5.2, shows that the apparent rate constant for the decay rate corresponding to the second transition (k_2 of Figure 3.5B) has the observed sigmoidal pH dependence, and a pK_a equal to that for the I_1/I_2 equilibrium. The observed pH dependence of the recovery rate is thus a consequence of the pH dependence of the intermediate equilibria. Since the protonation of the chromophore changes in this equilibrium, the simplest interpretation is that this pK_a~ 7/6.7 might be due to the phenol group of chromophore. This value of pK_a lies within the range of the chromophore pK_a, inside the protein (~ 2.8) and free in the solution (~ 9). The I_1/I_2 equilibrium is also observed in the E46Q mutant with a pK_a ~ 8.2 **[Borucki, 2003]**, and also assigned to the phenolate oxygen of the chromophore.

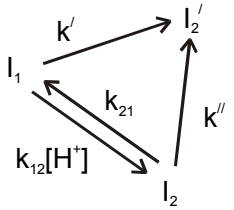

(I)

The I_1 to I_2 transition is incomplete at high pH (Figure 3.5A). This might be due to one of the following reasons. First, the time constant of the first (~ 370 µs) and second transition (about 1-10 ms) are not well separated. So, the I_1/I_2 equilibrium might not be formed completely in the I_1 to I_2 decay during the first transition. Additionally, we note that this equilibrium decays further to the another equilibrium $I_1/I_2/I_2'$ in the second transition. A method to separate these two time constants further (e.g. by a change of the temperature) would help to confirm this argument. Second, there is a I_1' contribution at alkaline pH (above pH 8), replacing I_2 at acid/neutral pH, Figure 3.11. Both I_1 and I_1' increase with increasing pH in the alkaline pH range. This is reflected by the increase of I_1/I_2 at pH > 8 (Figure 3.5A), leading to the incomplete titration curves in this pH region. Third, since the I_1' and I_2 contributions are small at pH 8-8.5 and the cycle is also the fastest, a precise determination of the relative contributions of all four intermediates I_1, I_1', I_2 and I_2' might not be possible. Here, it is assumed that no I_1' contributes in this pH range.

From about 5 ms onwards, I_1, I_2 and I_2' are in equilibrium and decay together to the initial dark state P, Figure 3.4A-C. The equilibrium intermediate populations of I_2 and I_2' are pH dependent with a pK_a of ~ 6.4, Figure 3.5C. Below the pK_a, I_2 is the major species, above the pK_a the opposite holds.

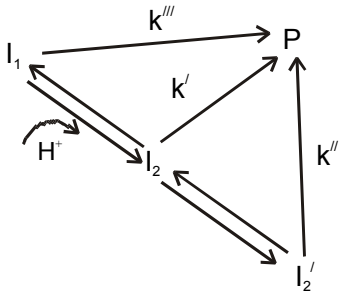

(II)

As is well known (e.g. from **[Genick**, **1997]**), the rate k_3, for the ground state recovery, is also pH dependent with a pK_a of 6.3, i.e. within experimental error equal to that for the I_2/I_2' equilibrium (6.4 and 6.1, from single flash photolysis and photoreversal measurements (section 4.2), respectively). Thus, k_3 seems to be proportional to the I_2' population (compare Figures 3.5C and 3.5D). Such a proportionality might be explained with the scheme II as described in section 2.5.2, and is expected under the following conditions: 1) the equilibration rates between I_1, I_2 and I_2' are rapid compared to the microscopic rates of return from each intermediate to the ground state, 2) the latter are pH independent, and 3) the rate from I_2' to P is much larger than from the other intermediates ($k'' \gg k'$, $k'' \gg k'''$). A similar model is also proposed to explain the pH dependence of the rate of ground state recovery at alkaline pH, section 3.2.2. At alkaline pH, the I_1, I_1', and I_2' intermediates are in equilibrium (section 3.2.2). The pK_a of the I_1' to I_2' equilibrium is ~9.9, the ground state recovery rate constant k_3 has a pK_a of 9.7, and is proportional to the I_2' population. There is thus a striking similarity between the behaviour at high and low pH. For both branches of the bell-shaped pH dependence of k_3, it seems that k_3 is proportional to $[I_2']$. This proportionality is not exact however, since k_3 approaches zero at low pH, whereas $[I_2']$ approaches a constant value unequal to zero. A more detailed model thus seems to be required. Nevertheless this symmetry between low and high pH behaviour is worth pointing out and the underlying model provides a lowest order explanation.

The proposed reaction scheme for the kinetics and equilibria of the photocycle in this pH range combining the results of the scheme (I) and (II) and the photoreversal results (see sections 4.1 and 4.2) is presented in Figure 3.6.

The pH dependence of the absorption spectrum of a photostationary mixture of P, I_2 and I_2' produced by background illumination was recently analysed by SVD **[Otto**, **2005]**, **[Shimizu**, **2006]**. It was shown that I_2 and I_2' are in a pH dependent equilibrium with a pK_a of 6.3, and that the spectrum of the high pH species I_2' is blue shifted with respect to that of the low pH species I_2 **[Otto**, **2005]**, **[Shimizu**, **2006]**. The I_2 and I_2' intermediates also differ with regard to the fluorescence lifetime of the single tryptophan of PYP, W119 **[Otto**, **2005]**. In I_2, the lifetime is long (0.82 ns). In I_2', the life time is much shorter (0.04 ns). Using background illumination, it was shown that the fluorescence decay in the photostationary state is pH dependent with I_2 dominating at low pH and I_2' at high pH **[Otto**, **2005]**. The pK_a was ~ 6.3. Combining the pH dependence of the fluorescence amplitudes with that of the photostationary absorption, absorption spectra were calculated for the I_2 and I_2' species. These had λ_{max} values of ~370 and ~350 nm for I_2 and I_2', respectively **[Otto**, **2005]**, in good agreement with the results reported in this work.

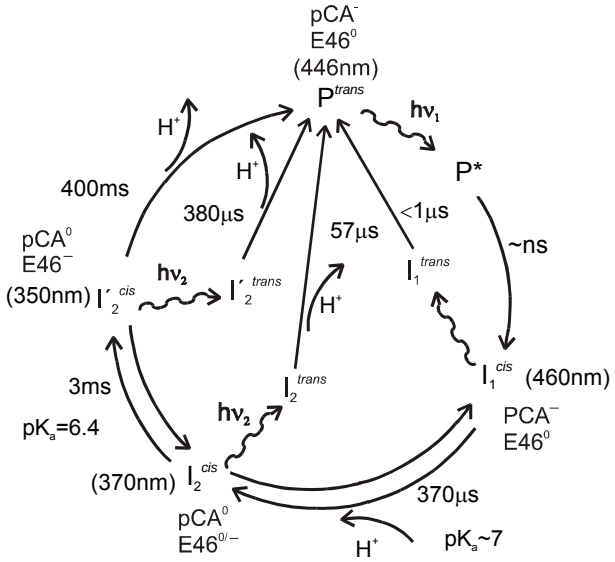

Figure 3.6: Proposed model for the kinetics of the photocycle and photoreversal (described in sections 4.1 and 4.2) of PYP in the pH range from 4.6 to 8.4. Note the equilibria between I_1, I_2 and I_2'. For each intermediate, the chromophore configuration state: *cis* or *trans* is denoted in the superscript. The I_2^{cis} and $I_2'^{cis}$ intermediates are in a pH dependent equilibrium and photoreverse to P^{trans} with exponential time-constants of 57 and 380 µs (section 4.1.2). The pK_a of the I_2^{cis} / $I_2'^{cis}$ equilibrium is 6.4. Reisomerization from I_1^{cis} to I_1^{trans} is with a time constant < 1µs (section 4.1.4). The I_1^{cis} and I_2^{cis} intermediates are in a pH dependent equilibrium with pK_a of ~7. These three intermediates I_1, I_2 and I_2' decay together to P. For each of the intermediates, protonation states of the chromophore (pCA) and the residue E46 are represented by 0, protonation and –, deprotonation in the superscript. For clarity the short-lived intermediates I_0 and $I_0^{\ddagger}$ between P* and I_1 are not shown. The corresponding values of the absorbance maxima are indicated in the brackets.

These results were recently confirmed in **[Shimizu**, **2006]**. Analysis of the photostationary absorption spectra by a scaled subtraction procedure yielded a pK_a of 6.4 and λ_{max} values of 367 and 356 nm for I_2 and I_2', respectively **[Shimizu**, **2006]**. These authors showed moreover from CD and small angle X-ray scattering experiments that the

global structural transition occurs between these two intermediates with a pK_a of 6.4. Together with the kinetics results from time-resolved absorption spectroscopy presented here, these complementary methods lead to a comprehensive picture of the I_2 to I_2' equilibrium.

In a related study **[Yeremenko, 2006]** spectra and time courses of the photocycle intermediates were presented at pH 6.5 in solution and crystals of WT and the mutant E46Q. The I_1, I_2 and I_2' spectra of Figure 3.2A are comparable to those presented in **[Yeremenko, 2006]**. Moreover, the time constants associated with various transitions are also similar. However, the time courses corresponding to different intermediates differ significantly from our work (Figure 3.4A-C). In **[Yeremenko, 2006]** I_1 decays partially to I_2 during the first transition, which is similar to that shown in Figure 3.4A,B. During the second transition, I_1 and I_2 decay completely to I_2', which is different to what is observed here (Figure 3.4B). At pH 6.5, from about ~ 10 ms and onwards, only I_2' contributes in the photocycle **[Yeremenko, 2006]**. In contrast in our work, at pH 6.5 which is near the pK_a ~6.4 between I_2 and I_2', I_2 makes a significant contribution (about 50%). This pH dependent equilibrium is also established in **[Otto, 2005]** by measurement of the tryptophan fluorescence, in **[Shimizu, 2006]** by CD measurements, and in our own separate investigation by measurements of the photoreversal kinetics using double flash excitation (see section 4.2). The discrepancy is probably due to the data analysis method used: target analysis **[Yeremenko, 2006]**. In target analysis, different pre-defined photocycle models are tested to fit the measured data **[Yeremenko, 2006]**, where rate constants and the spectra are the input parameters. Therefore, this analysis accepts many possible parameters leading to many equally likely photocycle models. In contrast, in our study, first of all the spectra of the intermediates contributing to the photocycle were determined from the measured time traces using only two well established plausible assumptions, which is the key information to elucidate the kinetics mechanism from the transient absorption measurement. Knowledge of the spectra of the intermediates leaves not too many possibilities for the photocycle model. Moreover, the time courses of the intermediates determined in this way from the measured absorbance changes and the spectra of intermediates (eq. 2.18) indicate precisely the interconversion of the intermediates during the photocycle (Figure 3.2C).

An important question concerns the group responsible for the pK_a of ~6.4. The similar pK_a for the recovery rate k_3 is commonly attributed to the carboxyl group of E46 **[Demchuk, 2000]**, **[Meyer, 2003]**. We now need to discuss this pK_a in the context of the underlying I_2/I_2' equilibrium. What is the mechanism whereby the change in protonation of

E46 shifts the equilibrium from I_2 to I_2'? In I_2 the chromophore is already protonated and has moved away from E46 towards the surface **[Genick**, **1997A]**. If E46 is the internal proton donor for the chromophore, its carboxyl group is presumably already deprotonated in I_2, in accordance with some observations from time-resolved FTIR **[Xie**, **2001]**. In I_2' the chromophore remains protonated, but the protein structure is changed in a major way. It is unclear how the deprotonated E46 could affect the I_2/I_2' conformational equilibrium. If however, E46 is not the internal proton donor, and the chromophore is protonated from the external medium, as suggested **[Borucki**, **2002]**, E46 could remain protonated in I_2 and be deprotonated in I_2'. In other time-resolved FTIR measurements **[Brudler**, **2001]** a positive band was observed at 1759 cm^{-1} with a risetime of 113 μs (formation of I_2) and assigned to an environmental shift of the protonated E46. The authors of **[Brudler**, **2001]** were not aware of the I_2/I_2' equilibrium and concluded from the fact that the amplitude of the positive band was significantly smaller than that of the negative band due to the initial dark state, that only a fraction of the molecules cycling had a protonated E46 in I_2. Their experiments were however performed in buffer at pH 7. At this pH the I_2/I_2' equilibrium is far on the side of I_2' (see Figure 3.5C), so that only a minority of molecules would have been in the I_2 state. It is thus consistent with the experimental results of **[Brudler**, **2001]** to conclude that in I_2 the carboxyl group of E46 is protonated.

In fact, recent photostationary FTIR measurements showed that E46 is at least partially protonated in I_2 **[Shimizu**, **2006]**. A role of E46 in controlling the I_2/I_2' equilibrium is thus plausible. In the absence of the carboxyl group, in the mutant E46Q, the conformational change in I_2' is much smaller or absent **[Xie**, **2001]** and the absorption maximum at pH 7 is at 368 nm **[Imamoto**, **2001A]**, i.e. I_2-like. These results suggest that in the absence of E46 the I_2/I_2' equilibrium is predominantly or entirely on the side of I_2 (**[Borucki**, **2003]**, **[Shimizu**, **2006]**) and further support the idea that E46 is responsible for the wild type pK_a of 6.4. We note that this reinterpretation of the FTIR results is consistent with a mechanism of chromophore protonation from the external medium **[Borucki**, **2002]**. Following this model, the protonation states of the chromophore (pCA) and the residue E46 are represented by 0, protonation and –, deprotonation in the superscript in Figure 3.6, for each of the intermediate.

Another residue that might be involved is H108. In **[Hendriks**, **1999A]** the pH dependence of the steady-state proton uptake was investigated. From the observed pH dependence, a pK_a of 6.6 was obtained, which was attributed to histidine 108. This residue is located on the central β-scaffold (Figure 1.7, blue sticks) and may be involved in the

interaction between the β-scaffold and the N-terminal domain (Figure 1.7). It was recently postulated, on the basis of the observation that the I_2 to I_2' transition is blocked at low salt concentrations, and that the loss of this interaction is a prerequisite for the formation of I_2' **[Borucki**, **2005]**.

Recently two forms of I_1 could be distinguished on the basis of their resonance Raman spectra, which are in a pH-dependent equilibrium with a pK_a of ~ 6.2 **[Unno**, **2004]**. The low pH form (I_1^{ℓ}) lacks the hydrogen bond with E46, whereas the high pH form (I_1^{h}) has both hydrogen bonds. It is possible that the pH dependence observed here for the I_2/I_2' equilibrium is due to the pH dependence of the preceding I_1^{ℓ}/I_1^{h} equilibrium.

3.2 Photocycle Kinetics at Alkaline pH

The intermediate spectra were determined at pH 10. Using these spectra the corresponding pH dependent time courses of the photocycle intermediates in the pH range 8 to 11 were calculated. A photocycle model is proposed from these observations.

3.2.1 Spectra and Time Courses of Intermediates at pH 10

The intermediate spectra at pH 10 were determined by two independent methods: extrapolated difference method and scaled subtraction method.

3.2.1.1 Extrapolated Difference Method

Panels A and B of Figure 3.7 allow a comparison between the transient absorption changes at pH 10 (A) and pH 6 (B) at a number of selected wavelengths. The data show striking differences between these two pH values in the time range between 200 μs and 2 ms, for wavelengths between 390 and 420 nm. It will be argued that this difference at pH 10 is due to the transient formation and decay of an intermediate called I_1' which absorbs maximally around 425 nm, and has rise- and decay-times of 330 μs and 1 ms, respectively (the first two vertical dashed lines of panel A). Comparing the trace in panel A at 340 nm (rise of I_2' intermediate) with those at 390 - 420 nm, we note that the additional contribution in the latter traces develops prior to the rise of the I_2' intermediate (about 1 ms).

The transient absorbance changes at pH 10 were measured at 33 wavelengths, ranging from 330 to 510 nm, in the time range from 100 ns to 5 s. Only eight of these traces are shown in Figure 3.7A. The complete data set was subjected to SVD analysis as described in section 2.3.2. The first six singular values were: 11.8, 2.6, 0.28, 0.071, 0.059 and 0.051.

Since the contributions from s_4, s_5 and s_6 are within the noise level, we consider only the first three components as significant. This suggests the presence of only three spectrally distinguishable intermediates. The three weighted time traces from SVD were fitted simultaneously starting at 8 μs with a sum of three exponentials with time constants τ_1 = 330 μs, τ_2 = 1 ms and τ_3 = 830 ms. The solid lines in Figure 3.7A represent these fit curves for the individual time traces. From the fit to the SVD time traces and the corresponding basis spectra, the amplitude spectra $B_j(\lambda)$ were calculated using eq 2.27. These are presented in Figure 3.7C.

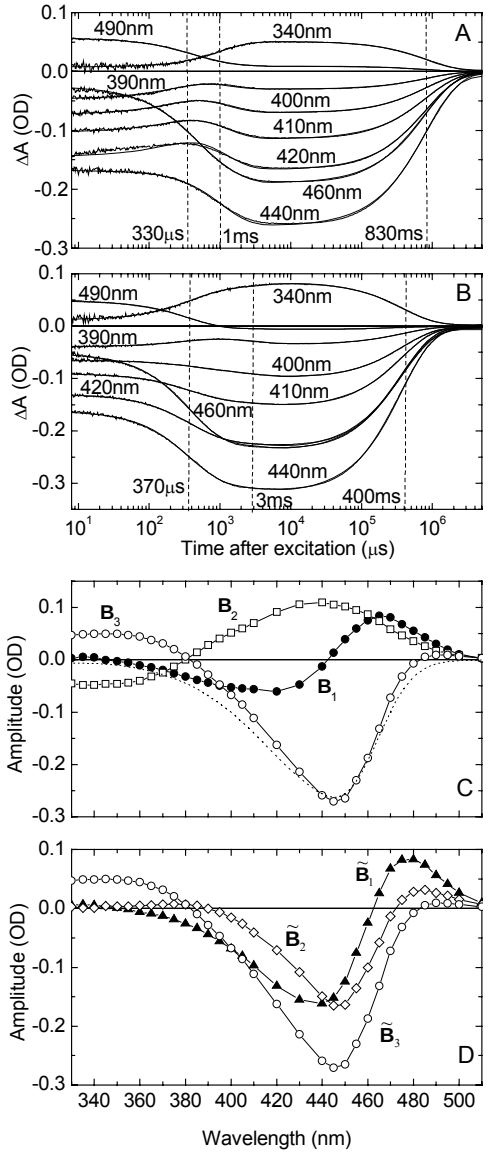

Figure 3.7: (A) Transient absorption changes after excitation at 430 nm at wavelengths varying from 330 to 510 nm. For clarity, only the traces at the indicated wavelengths are shown (8 out of 33 wavelengths measured). The vertical dashed lines indicate the time constants for a global fit to the weighted SVD time traces with a sum of three exponentials. τ_1 = 330 μs is the rise time of I_1', τ_2 = 1 ms is the rise time of I_2', and τ_3 = 830 ms is the return to P. The solid lines, only distinguishable from the data in the μs-time range, are the fits. Conditions: pH 10, 20 °C, 50 mM KCl and 20 mM Tris. PYP concentration: 58 μM. (B) The corresponding data at pH 6. PYP concentration: 43 μM. (C) Amplitude spectra $B_i(\lambda)$ calculated from the amplitudes of the exponential fits to the SVD time traces and the corresponding basis spectra of the data in (A). The three amplitude spectra correspond to the following time constants: τ_1 = 330 μs (●), τ_2 = 1ms (□), τ_3 = 830 ms (○). The dotted line is a scaled and inverted ground-state spectrum. (D) Extrapolated difference spectra obtained from the amplitude spectra of (C) according to eq 2.29: $\widetilde{\mathbf{B}}_1$ (▲), $\widetilde{\mathbf{B}}_2$ (◊), $\widetilde{\mathbf{B}}_3$ (○).

The amplitude spectrum $B_1(\lambda)$ associated with the 330 μs life time, has a positive peak near 465 nm and negative peak near 420 nm with no contribution in the UV (350 nm). The data thus clearly show that in this transition I_1 is converted to I_1' without the formation of

I_2'. This conclusion follows directly from inspection of the data (i.e. the amplitude spectrum $B_1(\lambda)$) and is model-independent. The amplitude spectrum $B_2(\lambda)$ associated with the 1 ms life time has a very broad positive contribution between 380 and 500 nm and a negative contribution in the UV (350 nm). $B_2(\lambda)$ thus strongly suggests that in this later transition an I_1/ I_1' equilibrium decays to I_2'. Note that the scaled ground state spectrum in Figure 3.7C(…) does not fit to $B_3(\lambda)$ for $\lambda > 410$ nm, indicating the presence of I_1 and I_1' in equilibrium with I_2' before recovery.

The three amplitude spectra, $\mathbf{B}_1$, $\mathbf{B}_2$ and $\mathbf{B}_3$, were used to construct the $\tilde{\mathbf{B}}$ matrix according to eq 2.29. $\tilde{\mathbf{B}}_1$ is the sum of amplitude spectra $\mathbf{B}_1$, $\mathbf{B}_2$ and $\mathbf{B}_3$ (arranged in columns). $\tilde{\mathbf{B}}_2$ is the sum of amplitude spectra $\mathbf{B}_2$ and $\mathbf{B}_3$, and $\tilde{\mathbf{B}}_3$ is same as $\mathbf{B}_3$. The three columns, $\tilde{\mathbf{B}}_1$, $\tilde{\mathbf{B}}_2$ and $\tilde{\mathbf{B}}_3$, representing the extrapolated difference spectra are presented in Figure 3.7D. $\tilde{\mathbf{B}}_1$ is the initial absorbance change right after the flash, and suggests that the initial bleach led to the formation of the I_1 intermediate (positive absorbance change near 480 nm). $\tilde{\mathbf{B}}_2$ is the difference spectrum with respect to the ground state after the first transition. Inspection of Figure 3.7D shows that below 390 nm $\tilde{B}_2(\lambda)$ is zero, i.e. has no contribution from intermediates absorbing in the UV like I_2'. Inspection of $B_1(\lambda)$, $B_2(\lambda)$ and $\tilde{B}_2(\lambda)$ thus allows the conclusion that I_1' is the direct decay product of I_1. We note that this conclusion was already evident from the experimental time traces at 390, 400, 410 and 420 nm of Figure 3.7A.

We now use the second constraint described in Materials and Methods (section 2.4.1), that I_2' does not absorb beyond 410 nm, and consider eq 2.34 only in the range $\lambda > 410$ nm; i.e., we drop the rows for the shorter wavelengths. Then the third column of the reduced matrix **A**, corresponding to the spectrum of I_2', is the null vector: $(\mathbf{A})_3 = \vec{0}$. Since $(\mathbf{A})_3$ is zero, one can solve eq 2.34 for $(\tilde{\mathbf{C}}^{-1})_3$. In this way, we determine the third column of $\tilde{\mathbf{C}}^{-1}$. Provided that the number of wavelength points is larger than 3, eq 2.34 is an overdetermined system of linear equations, for which the least squares solution may be found by multiplication with the pseudoinverse of $\tilde{\mathbf{B}}$ from the left and rearranging, which is eq 2.36. Using the well established ground state spectrum $\vec{A}_p$ and the measured $\tilde{\mathbf{B}}$ spectra, we find from eq 2.36, for the three elements of the third column of $\tilde{\mathbf{C}}^{-1}$: + 0.103, - 4.52, 7.56. Using the first constraint, the sum of these matrix elements equals η^{-1}. In this way, the fraction of cycling molecules, $\eta = 0.318$ is determined. Finally, using $\tilde{\mathbf{B}}$ and $\vec{A}_p$ for the whole spectral

range allows us to calculate the spectrum of I_2' from $(\tilde{\mathbf{C}}^{-1})_3$ using eq 2.34. The result is shown in Figure 3.8A (■).

Further progress can be made by noting that only I_1 contributes to $\tilde{\mathbf{B}}_1$ (Figure 3.7D). Thus the elements $\tilde{C}_{21} = y_1$ and $\tilde{C}_{31} = z_1$ of $\tilde{\mathbf{C}}$ defined by eq 2.30 are given by $y_1 = z_1 = 0$. This allows us to calculate the elements of the first column of $\tilde{\mathbf{C}}^{-1}$ of eq 2.33. The result is $\tilde{C}^{-1}_{11} = 1/x_1$, $\tilde{C}^{-1}_{21} = 0$, $\tilde{C}^{-1}_{31} = 0$. Since the sum of these elements equals 1/η (conservation constraint, eq 2.35), we have $x_1 = \eta = 0.318$. With $(\tilde{\mathbf{C}}^{-1})_1$ now completely known, we can calculate the spectrum of I_1 from $(\tilde{\mathbf{C}}^{-1})_1$, $\tilde{\mathbf{B}}$ and $\bar{A}_p$ using eq 2.34. The result is shown in Figure 3.8A (□).

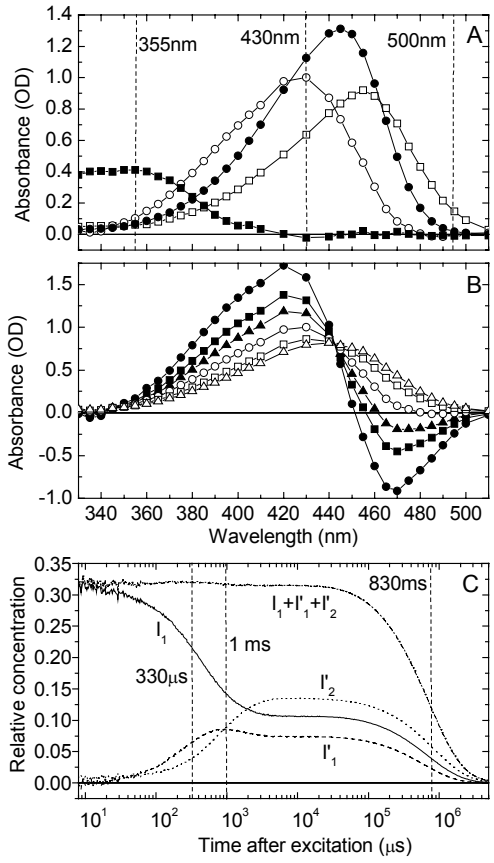

Figure 3.8: (A) Intermediate spectra of I_1 (□), I_1' (○) and I_2' (■) calculated from the extrapolated difference spectra of Figure 3.7D. ●: spectrum of the dark state P for comparison. Vertical dashed lines indicate the wavelengths of the blue (430 nm), violet (355 nm) and green (500 nm) excitation flashes used. (B) I_1' spectra for various allowed values of y_2 as described in the text. y_2= 0.05 (●), y_2 = 0.07 (■), y_2 = 0.09 (▲), y_2 = 0.13 (○), y_2 = 0.21 (□) and y_2 = 0.3 (Δ). (C) Time-courses of the relative concentrations of I_1 (—), I_1' (---), and I_2' (....) calculated according to eq 2.18 with y_2 = 0.13. The time-courses of the sum of the relative concentrations of I_1, I_1' and I_2' is indicated by —· —. The vertical dashed lines indicate the time constants from the global SVD fit of Figure 3.7A.

To calculate the spectrum of the third spectral species, I_1', we proceed in a similar fashion. From Figure 3.7D and as discussed above, $\tilde{\mathbf{B}}_2$ has no contribution from I_2'. Thus z_2 = 0. The elements x_2, y_2, z_2 of the second column of $\tilde{\mathbf{C}}^{-1}$ can now be expressed in terms of x_2, y_2, and η with the help of $\tilde{\mathbf{C}}^{-1}\tilde{\mathbf{C}} = \mathbf{I}$ as shown in eq 2.39. Using the conservation constraint eq 2.35, $x_2 + y_2 = \eta$, we finally obtain for the elements of the second column of $\tilde{\mathbf{C}}^{-1}$ of eq

2.40, $\tilde{C}_{12}^{-1} = -(\eta - y_2)/\eta y_2$, $\tilde{C}_{22}^{-1} = 1/y_2$, $\tilde{C}_{32}^{-1} = 0$. So, all elements of $\tilde{\mathbf{C}}^{-1}$ are determined now, the only free parameter remaining is y_2. Since x_i, y_i and z_i can only assume positive values and $x_2 + y_2 = \eta$, y_2 is restricted to values between 0 and η. The spectrum of I_1' can now be calculated from $(\tilde{\mathbf{C}}^{-1})_2$, $\tilde{\mathbf{B}}$ and $\vec{A}_p$ using eq 2.34. The results are shown in Figure 3.8B for six values of y_2 from 0.05 to 0.3 (~η). Since the extinction coefficient has to be positive, physically meaningful absorption spectra are only obtained for $y_2 \geq 0.13$. Of the spectra with $y_2 \geq 0.13$ in Figure 3.8B we pick the one associated with $y_2 = 0.13$, since it has a spectral bandwidth which is most similar to that of the other intermediates and P. As shown in Figure 3.8B, for y_2 considerably larger than 0.13, the spectral bandwidth becomes much larger than for P and I_1, which is unlikely to be correct. The spectrum of I_1' for $y_2 = 0.13$ is redrawn in Figure 3.8A (○). Its λ_{max} value is at about 425 nm. We note this spectrum is confirmed by an independent analysis method (scaled subtraction method) presented in the next section.

Since the spectra of intermediates are determined, the time courses of the intermediates may be calculated using eq 2.18. The time-dependence of the relative concentrations of the I_1, I_1' and I_2' intermediates are shown in Figure 3.8C. As expected from the data (Figure 3.7A), I_1 partially decays to I_1' in 330 μs. I_1 and I_1' then further decay around 1 ms to an $I_1/I_1'/I_2'$ equilibrium. This equilibrium finally decays to P in 830 ms. Also shown is the sum of the relative concentrations of these intermediates (dash-dot line). To a very good approximation, this sum is constant over the entire time range prior to the decay to P, as it should be. Its value is very close to $\eta = 0.318$, the fraction cycling, showing the internal consistency of the analysis.

The matrix containing the relative contributions of the intermediates, $\tilde{\mathbf{C}}$ of eq. 2.30, it's inverse, $\tilde{\mathbf{C}}^{-1}$ of eq. 2.33, and the coefficient matrix, **C** of eq. 2.17, calculated in this analysis are

$$\tilde{\mathbf{C}} = \begin{pmatrix} 0.318 & 0.188 & 0.108 \\ 0 & 0.13 & 0.078 \\ 0 & 0 & 0.132 \end{pmatrix},$$

$$\tilde{\mathbf{C}}^{-1} = \begin{pmatrix} 3.144 & -4.55 & 0.103 \\ 0 & 7.69 & -4.52 \\ 0 & 0 & 7.563 \end{pmatrix} \text{ and}$$

$$\mathbf{C}=\begin{pmatrix} 0.13 & 0.08 & 0.108 \\ -0.13 & 0.052 & 0.078 \\ 0 & -0.132 & 0.132 \end{pmatrix} \text{ respectively.}$$

3.2.1.2 Scaled subtraction method

The method presented in the previous section for the spectra and time courses of the intermediates is rigorous but not intuitive. A less rigorous but more transparent method is presented below which confirms that the spectra of intermediates I_1, I_1' and I_2' presented in Figure 3.8A are correct.

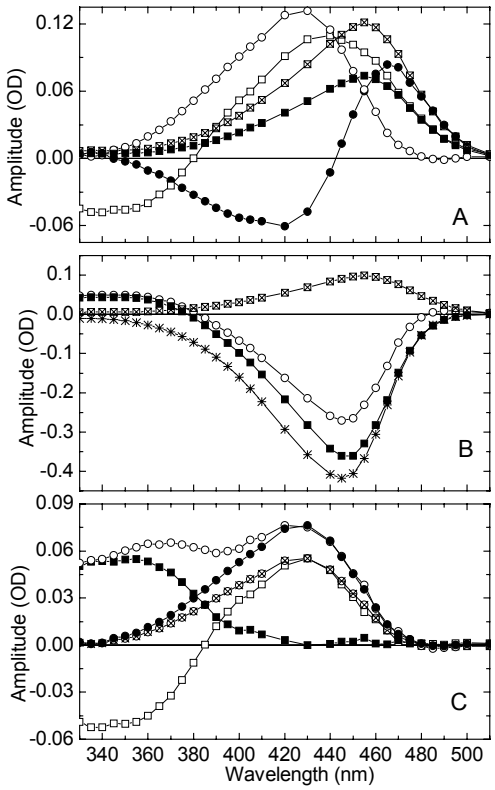

Figure 3.9: (A) In the scaled subtraction method, the I_1 spectrum of Figure 3.8A is scaled down (☒) in such a way that its long wavelength shoulder ($\lambda \geq 485$ nm) fits optimally to the corresponding shoulder of the amplitude spectrum $B_1(\lambda)$ (●). The spectrum of I_1' (○) was obtained by subtracting the ☒ spectrum from the ● spectrum and inverting this difference. The I_1 spectrum is also scaled down (■) to match its long wavelength shoulder ($\lambda \geq 485$ nm) with that of the $B_2(\lambda)$ (□) amplitude spectrum. The amplitude spectrum plotted in 3C (□) was obtained by subtracting the ■ spectrum of this panel from the □ spectrum. (B) The $\mathbf{B}_3$ amplitude spectrum (○) has to be corrected for the contribution of the ground state spectrum, P in addition to I_1, because the rise of P is the final step of photocycle. The down scaled I_1 spectrum (☒) was subtracted from $\mathbf{B}_3$ (○) amplitude spectrum which is: ■ spectrum, and has contributions from I_1', I_2' and P. The scaled and inverted dark spectrum, P (✳) overlaps $\lambda \geq 465$ nm region of this spectrum. The amplitude spectrum plotted in 3C (○) was obtained by subtracting scaled and inverted dark spectrum, P (✳) from ■ spectrum of this panel. (C) The open squared spectrum (□) obtained from the $\mathbf{B}_2$ amplitude spectrum, in A represents the partial decay of I_1' and rise of I_2'. The I_1' spectrum is scaled down (☒) in such a way that its long wavelength shoulder ($\lambda \geq 430$ nm) fits optimally the corresponding shoulder of the □ amplitude spectrum. The I_2' spectrum (■) was obtained by subtracting the ☒ spectrum from the □ spectrum and inverting this difference. The ○ spectrum of this panel is obtained from the $\mathbf{B}_3$ amplitude spectrum in B, which represents the mixture of I_1' and I_2' spectra. Also shown is the down scaled I_1' spectrum (●), where its shoulder ($\lambda \geq 430$ nm) fits with the shoulder of ○ amplitude spectrum.

None of the amplitude spectra of Figure 3.7C: $\mathbf{B}_1$ (330 µs, ●), $\mathbf{B}_2$ (1 ms, □) and $\mathbf{B}_3$ (830 µs, ○) scale to the dark spectrum even in the spectral range λ≥450 nm. Rather all these amplitude spectra show I_1 contributions (positive for λ≥500 nm). So the contribution of the I_1 spectrum must be subtracted from these amplitude spectra. The resulting amplitude spectrum after correction of the I_1 contribution is either the pure I_1' spectrum (from $\mathbf{B}_1$) or a mixture of the I_1' and I_2' spectra (from $\mathbf{B}_2$ and $\mathbf{B}_3$) as shown below.

The scaled subtraction method requires accurate knowledge of the I_1 spectrum. It is an experimental fact that the I_1-P difference spectrum (absorbance difference ~ 1µs; e.g. Figure 3.1C(▲) and 3.7D(▲)) is almost independent of pH, i.e. the amount of I_1 in the µs time range is pH independent. This can be taken as the measure of the amount of the cycling molecules. Thus, the I_1 spectrum at pH 6 can be taken as the I_1 spectrum at pH 10. As we observed here, at alkaline pH I_1' contributes in the ms range which makes it difficult to calculate the excitation efficiency of the blue flash. This is simpler at pH 6 where I_2' contributes on the ms time scale and doesn't absorb for λ≥430 nm, thus making it possible to scale the dark spectrum for λ≥430 nm range to the difference spectrum of the transient absorbance changes of the normal cycle measured at 10 ms for same wavelength range. The spectrum of I_1 can be calculated from the 1 µs difference spectrum of the normal cycle by adding this scaled amount of the ground-state spectrum. For further analysis, the I_1 spectrum of Figure 3.8A is used.

The starting point for this procedure is the amplitude spectrum $B_1(\lambda)$ (Figure 3.9A, ●) for the 330 µs transition from I_1 to I_1'. We assume that this transition only involves the I_1 and I_1' intermediates. This is strongly supported by the fact that this amplitude spectrum contains a positive peak around 465 nm presumably due to I_1, a negative peak around 420 nm presumably due to I_1' and has zero absorbance around 355 nm where I_2' absorbs. For a sequential unidirectional transition between I_1 and I_1', $B_1(\lambda)$ should equal their difference spectrum and experimentally this seems to be the case. This allows us to remove the contribution of I_1 from $B_1(\lambda)$, thereby obtaining the spectrum of I_1'. This procedure is shown in Figure 3.9A. The spectrum of I_1 is scaled (⊠) so that its long wavelength shoulder matches optimally with the $B_1(\lambda)$ spectrum, which assumes that I_1' does not absorb in the matching region. As we see from Figure 3.9A, the match is excellent for λ ≥ 485 nm when the spectrum of I_1 is scaled by a factor of 0.132. Therefore, the extinction coefficient of I_1' is zero beyond 485 nm. Thus, the matching criterion is equivalent to this constraint on the I_1' spectrum. Subtracting this amount of I_1 from $B_1(\lambda)$ and inverting this difference should correct

completely for the I_1 contribution, leaving the I_1' spectrum (○), which is shown in Figure 3.9A. The negative sign of the I_1' spectrum obtained after subtraction of the I_1 contribution from $B_1(\lambda)$ indicates the rise of this intermediate in first transition. When this I_1' spectrum is scaled up by dividing with a factor of 0.132 the result is almost identical to the I_1' spectrum of Figure 3.8A(○) obtained by the matrix method. This shows that the $\mathbf{B}_1$ amplitude spectrum represents the partial decay of I_1 (a factor 0.132 of I_1 from Figure 3.8A) to I_1' (a factor of -0.132). This agreement is not fortuitous, since the constraint of requiring the extinction coefficient to be zero beyond 485 nm is equivalent to the choice $y_2 = 0.13$ (see Figure 3.8B). The corresponding factors of I_1 and I_1' acquired in this analysis are similar to those arranged in the first column of the **C** matrix of the previous section (extrapolated difference method), also arranged in **C** matrix of eq 3.1 below. The rows of **C** matrix defined by eq 2.17, correspond to the relative contributions of a particular intermediate, so that, first, second and third rows correspond to the relative contributions of I_1, I_1' and I_2' intermediates respectively. Similarly, the column of **C** matrix corresponds to the relative contributions of the all intermediates during a particular transition, so that, first, second and third column represent the relative contribution of all I_1, I_1' and I_2' intermediates during the 370 μs, 1 ms and 830 ms transition respectively.

Next, it will be shown that the amplitude spectrum $B_2(\lambda)$ (Figure 3.9A, □) for the 1 ms transition is due to the partial decay of I_1 and I_1' to I_2'. We assume that this transition involves the I_1, I_1' and I_2' intermediates only. This is strongly supported by the fact that this amplitude spectrum contains a broad positive absorption band around 400-500 nm presumably due to I_1 and I_1', a negative peak around 350 nm presumably due to I_2'. It will be shown below that there is no dark recovery during this transition. This implies that there is zero contribution of dark state in this amplitude spectrum. For a sequential unidirectional transition between I_1 and I_1' to I_2', $B_2(\lambda)$ should equal their difference spectrum. Thus the I_1 contribution might be removed from $B_2(\lambda)$, obtaining in that way, the amplitude spectrum containing the contributions from the remaining intermediates I_1' and I_2'. This is also shown in Figure 3.9A. The spectrum of I_1 is down scaled (■) so that its long wavelength shoulder matches with the $B_2(\lambda)$ spectrum (□). The match is excellent for $\lambda \geq 485$ nm when the spectrum of I_1 is scaled by a factor of 0.08. This factor is described below. Subtracting this amount of I_1 should correct completely for the I_1 contribution, leaving the contributions from the remaining intermediates I_1' and I_2', which is plotted in Figure 3.9C (□). Moreover, there is no contribution from the dark spectrum. This is supported by the fact that this amplitude

spectrum of Figure 3.9C (□) contains a positive peak around 430 nm presumably due to the decay of I_1', a negative peak around 350 nm presumably due to the rise of I_2' and has zero absorbance beyond 480 nm where P absorbs. For a sequential unidirectional transition between I_1' and I_2', □ amplitude spectrum should equal their difference spectrum. This allows to remove the contribution of I_1' from the □ amplitude spectrum, thereby obtaining the spectrum of I_2'. This is shown in Figure 3.9C where the spectrum of I_1' is down scaled (⊠) so that its long wavelength shoulder matches with the □ amplitude spectrum, which assumes that I_1' does not absorb in the matching region. This match is excellent for $\lambda \geq 430$ nm, when the spectrum of I_1' is scaled by a factor of 0.055. Therefore, the extinction coefficient of I_2' is zero beyond 430 nm. This factor is described below. Subtracting this amount of I_1' from the □ amplitude spectrum and inverting this difference should correct completely for the I_1' contribution, leaving the I_2' spectrum (■) of Figure 3.9C. The negative sign of the spectrum obtained from the subtraction indicates the rise I_2'. This I_2' spectrum is scaled up by dividing with a factor of 0.135 (the total of 0.08 factor of I_1 and 0.055 factor of I_1'). The resulting spectrum is almost identical to I_2' spectrum of Figure 3.8A(■) obtained by the matrix method. This shows that the $\mathbf{B}_2$ amplitude spectrum is due to the partial decay of I_1 (a factor of 0.08) and I_1' (a factor of 0.055) to I_2' (a factor of - 0.135). No direct recovery to the dark state is observed during the second transition. The corresponding factors of I_1, I_1' and I_2' acquired from the $\mathbf{B}_2$ amplitude spectrum are close to those in the second column of the **C** matrix of the previous section (extrapolated difference method) , and are arranged in the **C** matrix of eq 3.1 below.

The I_1' and I_2' spectra can also be acquired from the $\mathbf{B}_3$ amplitude spectrum of Figure 3.9B (○). In this case, the contribution of ground state spectrum P has to be subtracted in addition to the I_1 contribution. The amount of P (✳) is the same as the amount of P added to calculate the I_1 spectrum from the I_1-P difference spectrum (absorbance difference at 1 μs), which is the excitation efficiency (0.31) times the spectrum of the dark state of Figure 3.8A (●). It will be shown that the amplitude spectrum $\mathbf{B_3}$ for the 830 ms transition is due to the decay of I_1, I_1' and I_2' to P. This is evident from the fact that this amplitude spectrum has a positive absorption near 480 nm and 350 nm, presumably due to I_1 and I_2' respectively, and a negative peak around 450 nm presumably due to P.

The ■ spectrum of in Figure 3.9B is obtained by subtracting the I_1 contribution (⊠) from the $\mathbf{B}_3$ amplitude spectrum (○). The inverted dark spectrum P(✳) is scaled in such a way that it matches the ■ spectrum for $\lambda \geq 465$ nm,. The ■ spectrum is due to the rise of P (the

negative peak around 450 nm), the decay of I_2' (a positive absorption around $\lambda \sim 350$ nm) and I_1' (a mismatch arioundλ ~ 420 nm). Here, only the amount of I_1 (a factor of 0.1) was varied and the other two spectra $\mathbf{B}_3$ and P(✳) are fixed. The criterion for selecting the I_1 contribution in the $\mathbf{B}_3$ amplitude spectrum is critical, where the I_1 spectrum is scaled down to overlap in the $\lambda \geq 500$ nm range. In this spectral region not many measured points are available. However, further optimisation of this factor to 0.1 is attained from successive step of subtraction where the ■ amplitude spectrum overlaps the P (✳) spectrum in the $\lambda \geq 465$ nm range. In this region, many measured points are available making it easier to optimise. The ground state spectrum P(✳) was also subtracted from the ■ amplitude spectrum. The result is a mixture of the I_1' and I_2' spectra as shown in Figure 3.9C (○). The two positive maxima around ~ 430 nm and ~ 360 nm are presumably due to I_1' and I_2', and the ○ spectrum is their sum. The removal of the contribution of I_1' from the ○ spectrum results in the I_2' spectrum as shown in Figure 3.9C, where the spectrum of I_1' is scaled down (●) so that its long wavelength shoulder matches with ○ amplitude spectrum in the $\lambda \geq 430$ nm region. Subtracting this amount of I_1' (with a factor of 0.077) corrects for the I_1' contribution leaving the I_2' spectrum. This I_2' spectrum is very similar to the I_2' spectrum of Figure 3.9C (■) (data not shown). Taken together these subtraction steps show that the $\mathbf{B}_3$ amplitude spectrum has contributions from the decay of I_1 (a factor of 0.1), I_1' (a factor of 0.077) and I_2' (a factor of 0.135) and the rise of P. The corresponding factors of I_1, I_1' and I_2' acquired from the $\mathbf{B}_3$ amplitude spectrum are similar to those in the third column of the **C** matrix calculated in the extrapolated difference method (section 3.2.1.1).

Thus, the spectra of the intermediates I_1, I_1' and I_2' contributing to the photocycle are determined using the scaled subtraction method. The corresponding **C** matrix acquired from this method is:

$$\mathbf{C}= \begin{pmatrix} 0.132 & 0.08 & 0.1 \\ -0.132 & 0.055 & 0.077 \\ 0 & -0.135 & 0.135 \end{pmatrix} \qquad \textbf{(3.1)}$$

which should be compared with the **C** matrix of the previous section (extrapolated difference method). The agreement is excellent

From the known spectra of the intermediates, the time courses can be calculated using eq. 2.18. Thus the two methods, extrapolated difference method and scaled subtraction method, are equivalent.

3.2.2 pH Dependence

To learn more about the nature of the transition between the neutral and alkaline pH regimes, the photocycle kinetics was measured at the seven pH values 8.0, 8.5, 9.0, 9.5, 10.0, 10.5 and 11.0. With excitation at 430 nm, time traces were collected at 14 wavelengths from 370 to 500 nm in steps of 10 nm.

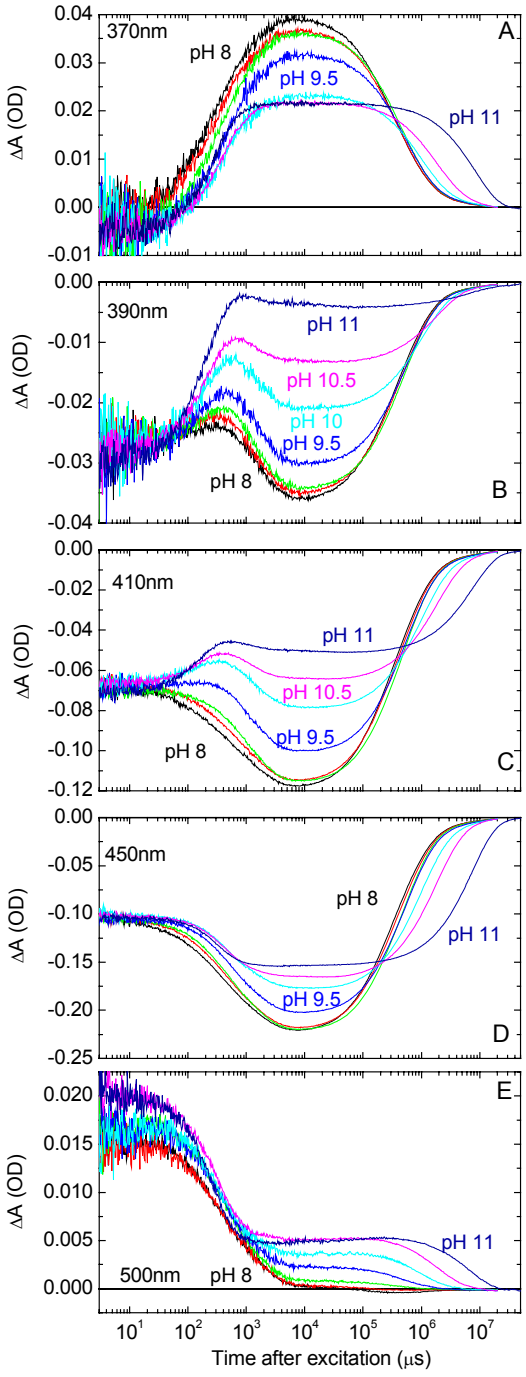

Figure 3.10: pH dependence of the transient absorbance changes after excitation at 430 nm at various wavelengths. (A): 370 nm (characteristic for I_2'), (B): 390 nm (I_2), (C): 410 nm (I_1'), (D): 450 nm (depletion signal, P), (E): 500 nm (I_1). Color code for pH values: black, pH 8; red, pH 8.5; green, pH 9; blue, pH 9.5; light-blue, pH 10; pink, pH 10.5; dark-blue, pH 11. Conditions: 20 mM Tris, 50 mM KCl, 20°C. PYP concentration: 58 μM.

Results for selected wavelengths are shown in Figure 3.10. Note that the panels of Figure 3.10 have very different vertical scales, and correspondingly different signal to noise

ratios. The smallest pH-induced absorbance changes are at 500 nm. The initial absorbance change is almost pH independent at every wavelength, suggesting that the amount of I_1 formed is pH independent.

At each pH, the absorbance changes at all wavelengths could be fitted simultaneously with a sum of three exponentials. The first two time constants were virtually independent of pH. The first time constant varied between 200 and 370 μs in this pH range. For the second time constant, the range was 720 μs to 1.3 ms. As we saw above, the first transition is due to the decay of I_1 to I_1', the second transition due to the decay of I_1/I_1' to the $I_1/I_1'/I_2'$ equilibrium. The data of Figure 3.10 show that the third time constant, the return of the $I_1/I_1'/I_2'$ equilibrium to P, is strongly pH dependent, slowing down with pH. The amplitudes of the time traces around 10 ms, when the $I_1/I_1'/I_2'$ equilibrium is well established, may be used to draw conclusions on the pH dependence of the equilibrium intermediate populations.

Panel A of Figure 3.10 shows that the I_2' population decreases with pH. From panel E we may conclude that the fraction of molecules in I_1 in the ms time range increases with pH. The traces at 450 nm, panel D, indicate that the ground state depletion decreases with pH, consistent with the reduced amount of I_2'. The traces at 390 and 410 nm (panels B and C) are characteristic for I_1'. Here again the pH dependence is consistent with an increase of the I_1/I_1' equilibrium contribution and a decrease in the amount of I_2' with pH.

To obtain the time courses of the intermediates the data at the five pH values from 8.0 to 10.0 in steps of 0.5 were measured at 14 wavelengths from 370 to 500nm in steps of 10 nm. Since hydrolysis occurs at high pH **[Meyer**, **2003]**, fewer data points were collected at pH 10.5 and 11 to reduce the measuring time. At these pH values, data were collected at only 8 wavelengths from 370 to 500 nm. The spectrally superior data at the five pH values between 8 and 10 were arranged by truncating the data matrix measured at each pH (time traces are arranged in the rows), and forming a large matrix as described in section 2.5.1. The number of rows in this large matrix is the number of wavelengths and the number of columns is the sum of the time points from the whole pH range. This combined matrix is subjected to a SVD analysis (eq 2.41). This assumes that the same spectral species contribute over the whole pH range. We then have:

$$(\mathbf{\Delta A}_{pH8}, \ldots.., \mathbf{\Delta A}_{pH10}) = \mathbf{U}^T\mathbf{D}\ (s)\ (\mathbf{V}_{pH8}, \ldots., \mathbf{V}_{pH10})$$

The first five singular values were: 17.03, 2.54, 0.45, 0.16, 0.12. Since the contributions from s_4 and s_5 are within the noise level, only the first three components are considered as significant. This suggests again the presence of only three spectral components,

presumably I_1, I_1' and I_2'. The time traces of the three SVD components V_i at pH 10 (where significant amounts of I_1' and I_1 are present), weighted with the corresponding singular values s_i, were fitted simultaneously with a sum of three exponentials. From the amplitudes of this fit and the basis spectra U_i, the three amplitude spectra $B_j(\lambda)$ were calculated as described by eq 2.27. Finally the extrapolated difference method was used to calculate the spectra of the intermediates (I_1, I_1', I_2') from these amplitude spectra. The spectra of I_1, I_1' and I_2' obtained in this way (not shown) are, as expected, very similar to those from the separate measurements at pH 10 (Figure 3.8A), but they have the advantage that they are the best average spectra over this whole pH range.

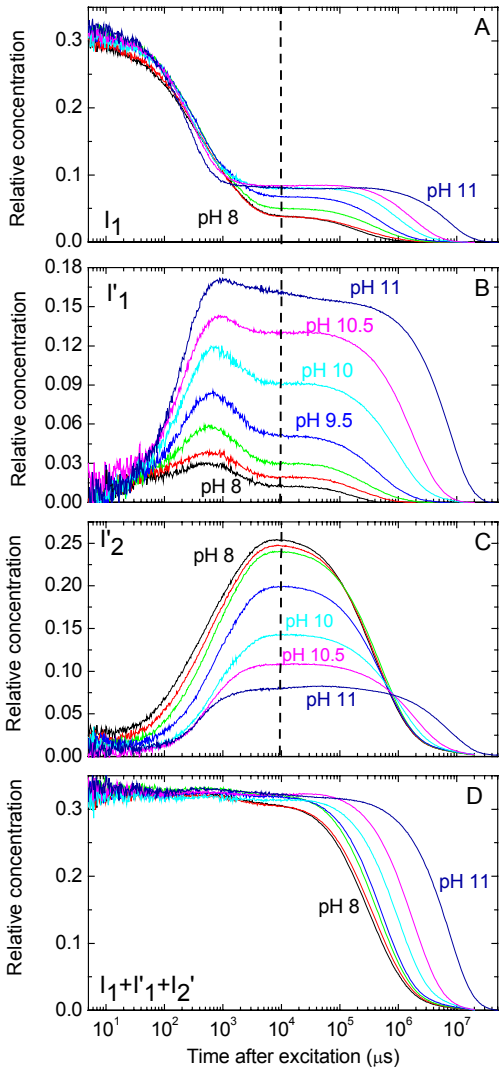

Figure 3.11: Time courses of the relative concentrations of the I_1 (A), I_1' (B) and I_2' (C) intermediates at various pH values calculated from the combined SVD as explained in the text. (D): time course of the sum of the populations of I_1, I_1' and I_2'. Color code as in Figure 3.10.

The time courses of the intermediate concentrations $n_i(t)$ at each pH were then calculated from $\Delta A(\lambda, t)$ at all 14 wavelengths and the intermediate spectra by using eq 2.18. For the two pH values 10.5 and 11.0, where data at only 8 wavelength values were collected,

which were not included in the joint SVD, the same intermediate spectra were used to calculate their time courses, again from eq 2.18.

The resulting time traces are shown in Figure 3.11. The fractions of the molecules in I_1, I_1' and I_2' have the time dependence we expect from the data and from our previous results at pH 10 (Figure 3.8C). The sum of the fractions is plotted in Figure 3.11D. This sum is practically constant in time until the ground state recovery, as required. Moreover, this plateau value is virtually pH independent and equal to the fraction cycling which is similar to that of the previous experiments at pH 10 (Figure 3.8C).

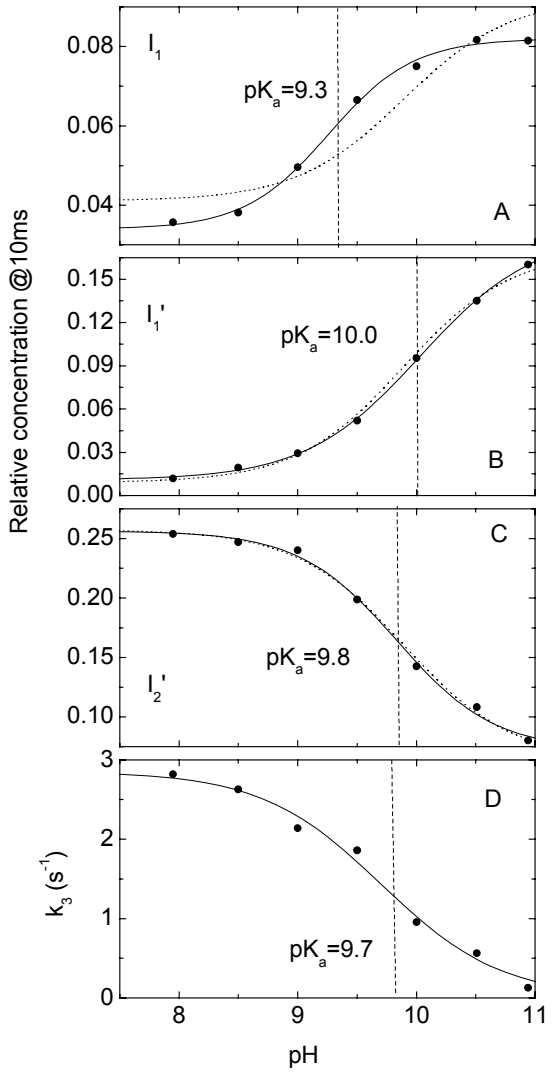

Figure 3.12: pH dependence of the equilibrium concentrations of the I_1, I_1' and I_2' intermediates at 10 ms, derived from Figure 3.11A, B and C, respectively. The dotted curves are simultaneous fits of these titration curves with $pK_a \sim 9.9$ and $n \sim 0.96$. The solid curves are individual fits with the Henderson-Hasselbalch equation. (A): I_1, $pK_a = 9.3$, $n = 1.21$; (B): I_1', $pK_a = 10.0$, $n = 0.9$; (C): I_2', $pK_a = 9.8$, $n = 1.06$. (D): pH dependence of the decay rate k_3 for the ground state recovery. Solid curve is fit with Henderson-Hasselbalch equation and $pK_a = 9.7$, $n = 0.87$.

The pH dependence of the time traces in panels A to C not only confirms what was already suggested by the data at various wavelengths (Figure 3.10), but allows a quantitative analysis of the pH dependence of the intermediate equilibria. From around 5 ms to the ground state recovery, the intermediate concentrations are constant in time and the

intermediates are in equilibrium. The fractions in equilibrium are clearly pH dependent. The main effect is that the fraction in I_1' increases with pH at the expense of I_2'. The increase in I_1 is smaller. The population values at 10 ms (vertical dashed lines in panels A to C of Figure 3.11) were used as a measure for the equilibrium values. The pH dependence of the equilibrium values of the intermediate concentrations at 10 ms is plotted in Figure 3.12. The dotted curves are simultaneous fits of the data of panels A, B and C with the Henderson-Hasselbalch equation with $pK_a = 9.9$ and n = 0.96. The solid curves are individual fits with the Henderson-Hasselbalch equation. The fit parameters are: I_1, $pK_a = 9.3$, n = 1.21; I_1', $pK_a = 10.0$, n = 0.9; I_2', $pK_a = 9.8$, n = 1.06. The global fit is excellent for I_2' and I_1', but only adequate for I_1. Panel D of Figure 3.12 shows the pH dependence of the rate constant for the recovery to the ground state P. This sigmoidal curve yielded a pK_a of 9.7 and a Hill coefficient of 0.87. The high pH end value for this fit was fixed at zero.

From Figure 3.12, we conclude that the populations of I_1 and I_1' increase with pH, whereas the population of I_2' simultaneously decreases. One possible scheme (III), which can explain the observed common pH dependence of the equilibrium populations and the recovery rate (Figure 3.12D) involves a rapid equilibrium between I_1, I_1' and I_2'. Rapid means that the equilibration rates between I_1, I_1' and I_2' are fast with respect to the recovery rates k', $k''$and k''' (see section 2.5.2 or scheme (III) below). The I_1/I_1' equilibrium is assumed to be pH independent, this guarantees that I_1 and I_1' increase in parallel. The I_1'/I_2' equilibrium is pH dependent and the rate constants for the return to P are pH independent.

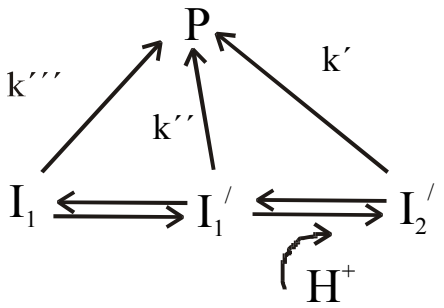

III

Analysis of this reaction scheme shows that the apparent rate constant for the ground state recovery (k_3 of Figure 3.12D) has the observed sigmoidal pH dependence with the highest rate at pH 8 and equal to k', and a pK_a equal to that for the I_1'/I_2' equilibrium. The observed pH dependence of the recovery rate is thus a consequence of the pH dependence of the intermediate equilibria. The data in Figure 3.12D with k_3 almost zero at pH 11 suggest that $k' >> k'', k'''$. Since the protonation of the chromophore changes in this equilibrium, the

simplest interpretation is that this pK_a of ~ 9.9 represents the surface exposed chromophore. The I_1' intermediate thus appears to be the alkaline form of I_2'.

3.2.3 Discussion

From measurements of the pH dependence of the photocycle kinetics of PYP between 8 and 11, the following results were obtained: 1) the spectrum of I_1' with a λ_{max} at about ~ 425 nm, 2) I_1' is the decay product of I_1, 3) from several ms (formation of I_2') to the end of the cycle the three intermediates I_1, I_1' and I_2' are in equilibrium, 4) the pK_a of the pH-dependent equilibrium between I_2' and its precursor I_1' is ~ 10. The pH is thus an important parameter that controls the amount of receptor in the active state, i.e. I_2'.

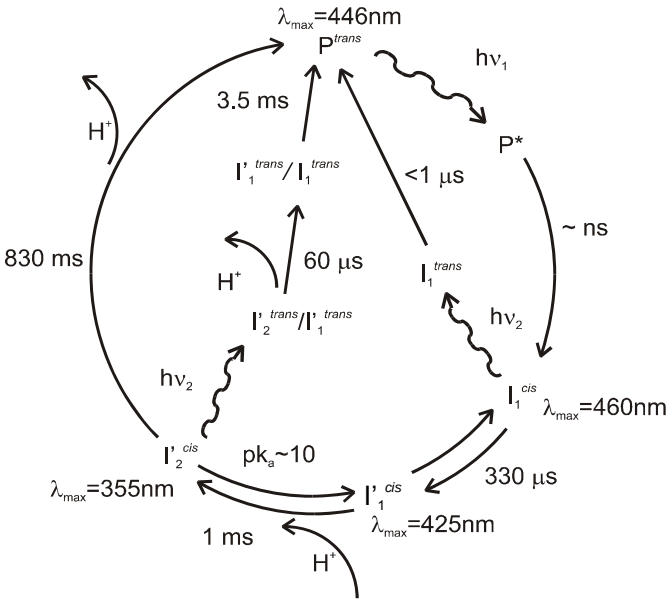

Figure 3.13: Proposed model for the kinetics of the photocycle and photoreversal of PYP at pH 10. Note the equilibria between I_1, I_1' and I_2'. These three intermediates decay together to P. Photoreversal from I_1 and I_2' are described in section 4.3. For each intermediate, the chromophore configuration state, *cis* or *trans*, is denoted in the superscript and described in section 4.3. For clarity the short-lived intermediates I_0 and $I_0^{\ddagger}$ between P* and I_1 are not shown.

Evidence for the I_1' intermediate was also obtained from the $\mathbf{B}_1$ amplitude spectrum of the photoreversal kinetics (see section 4.3). An I_1'-like intermediate was also detected at alkaline pH in the mutant Y98Q **[Borucki, 2005]**. The absorption maximum of the spectrum of I_1' at about ~ 425 nm, lies in between the λ_{max} values of I_1 and I_2'. At neutral pH, three intermediates are required, in the sequence I_1, I_2, I_2' (Figure 3.2C). In I_2' the chromophore is believed to be exposed and protonated. Since at sufficiently high pH, the exposed chromophore can no longer be protonated, the I_1' intermediate may be regarded as the alkaline form of I_2' with deprotonated chromophore but similar structure. Indeed, a wavelength maximum of 425 nm is consistent with a deprotonated partially exposed chromophore. For both the *cis* and *trans* forms, a shift of about 58 nm is observed between the λ_{max} values of the protonated and deprotonated bound exposed chromophore **[Imamoto,**

2004]. The electronic spectra of I_2 and I_2' at pH 7 can be distinguished and the λ_{max} values for I_2 and I_2' are about 372 and 352 nm respectively (Figure 3.2A, **[Otto**, **2005]**). Thus, the deprotonated forms of I_2 and I_2' may be expected to have their λ_{max} values near 430 and 410 nm, respectively. The observed value of 425 nm is therefore reasonable and it seems likely that I_1' has a deprotonated chromophore. This question could be settled by time-resolved vibrational spectroscopy.

Concerning the intermediate nomenclature, we labeled the 425 nm alkaline species, I_1'. The subscript one was chosen since its chromophore is deprotonated, and a prime was added to distinguish it from its precursor I_1. We note that for wild type at neutral pH, heterogeneity in I_1 has been detected by FTIR **[Imamoto**, **2002]**, resonance Raman **[Unno**, **2004]** and X-ray diffraction **[Ihee**, **2005]**. In those cases, the I_1-like intermediates had chromophores that were still hydrogen bonded in the binding pocket, whereas I_1' at alkaline pH refers most likely to a state with a surface exposed chromophore. For the mutant E46Q, we previously introduced an intermediate I_1' between I_1 and I_2 which had a surface exposed chromophore and was in a pH-dependent equilibrium with I_2 **[Borucki**, **2003]**. In that case we had no evidence however that this intermediate absorbed at 425 nm in the pH-range studied.

The results presented here for the photocycle showed that at pH 10, I_1 decays partially to I_1' (330 µs). I_1 and I_1' then decay further to I_2' (1 ms). The $I_1/I_1'/I_2'$ equilibrium finally decays to P in 830 ms. The proposed reaction scheme for the kinetics of the photocycle and the photoreversal (described in section 4.3) at pH 10 is presented in Figure 3.13.

The spectra of I_1, I_1' and I_2' (Figure 3.8A) as well as their time-courses were obtained from the transient absorbance data with the help of the extrapolated difference method **[Borucki**, **1999]**. The assumptions used in this procedure are plausible and explained in detail in Materials and Methods: 1) the absorbance of I_2' is zero beyond 410 nm, 2) the sum of the relative intermediate contributions to the extrapolated difference spectra is constant and equals the fraction cycling. This method was previously successful with bacteriorhodopsin where in addition constraints from linear dichroism were used **[Borucki**, **1999]**. It is validated for PYP by the fact that the spectra of I_2' and I_1 are in excellent agreement with the corresponding spectra at acid/neutral pH of Figure 3.2A, that the sum of the relative intermediate concentrations remains constant during the cycle until the recovery of the groundstate (Figure 3.8C) and that an independent analysis (scaled subtraction) led to the same spectrum for I_1'.

The spectrum of the UV intermediate in Figure 3.8A was assigned to I_2' and not to I_2 , since its wavelength maximum is at 355 nm. The spectra of I_2 and I_2' are known to have their maxima at 372 nm and 352 nm respectively (Figure 3.2A, **[Otto, 2005]**). At neutral pH, the I_2 and I_2' intermediates are in equilibrium, as shown in Figure 3.5C. This equilibrium is pH dependent with a pK_a of 6.2 (Figure 3.5C, **[Otto, 2005]**). Above this pK_a the I_2' intermediate dominates (Figure 3.5C, **[Otto, 2005]**). At alkaline pH we therefore only expect to observe I_2'. The absence of an I_2 intermediate at alkaline pH is furthermore supported by the photoreversal experiments which indicate the presence of only one I_2/I_2' –like intermediate (section 4.3).

The result for the I_1' spectrum is also confirmed by an alternative and more subjective method. This scaled subtraction method has the advantage that it is easier to understand. It requires as input an accurate I_1 spectrum. The agreement between the spectra of I_1' calculated from $\mathbf{B}_1$ using the scaled subtraction method and from the extrapolated difference method was excellent. The amplitude spectra $\mathbf{B}_2$ (1 ms) or $\mathbf{B}_3$ (830 ms) may also be used to extract the I_1' and I_2' spectra as described in Figure 3.9.

In previous work approximate spectra for I_1' were obtained from photostationary light/dark difference spectra at alkaline pH (**[Hendriks**, **1999A]**, **[Imamoto**, **2004]**, **[Hendriks**, **2003]**). These spectra have to be corrected for the contributions from other intermediates (I_1, I_2'), that accumulate at high pH under background illumination. Such measurements suffer moreover from potential artifacts due to the efficient photoreversal of these intermediates (e.g. I_1) by the background illumination (section 4.1 to 4.3). Due to the very slow recovery rates at alkaline pH this correction is essential.

An analysis similar to a version of scaled subtraction method was performed by Imamoto et. al. **[Imamoto**, **2004]**. The absorbance change was measured at pH 10 with 10 ms time resolution and the obtained difference spectrum was very similar to $\mathbf{B}_3$ of Figure 3.9B(○). The I_1 and dark spectrum contributions were subtracted from this difference spectrum. The resulting spectrum is very similar to the I_1'/I_2' spectra of Figure 3.9C(○). A spectrum was presented for PYP_M^{410}, which has a λ_{max} value of 410 nm **[Imamoto**, **2004]** and an extinction coefficient that is only half as large as for our I_1' spectrum of Figure 3.8A. The presented PYP_M (or I_2') and $PYP^{410}{}_M$ (or I_1') spectra in this publication have similar extinction coefficients at their absorbance maxima. However, we obtained very different results as shown in Figure 3.8A. The reason for this difference is that the I_1'/I_2' spectra of Figure 3.9C(○) have to be scaled with different scaling factors (eq 3.1, 0.077 for I_1' and 0.13

for I_2') to compare with I_1 and P the spectra of Figure 3.8A. Those factors can only be obtained from the scaled subtraction procedure of the first ($\mathbf{B}_1$) and second transition ($\mathbf{B}_2$) as described in eq 3.1. Thus, the $PYP^{410}{}_M$ spectrum presented in **[Imamoto**, **2004]** is incorrect as these two transitions are not resolved in the measurements presented this publication.

Hendriks et. al. **[Hendriks**, **1999A]** acquired a photostationary spectrum of pB^{deprot} (deprotonated form of I_2') in the presence of background illumination at pH 10.9 and subtracted a scaled ground state spectrum to remove the contribution of this state from the difference spectrum. The spectrum determined in this way had only six wavelength points and a λ_{max} value of about 420 nm **[Hendriks**, **1999A]**. We observed a very similar spectrum (data not shown), when a scaled ground state spectrum P(✳) of Figure 3.9B(○) is subtracted from the $\mathbf{B}_3$ amplitude spectrum. However, this resulting spectrum is a mixture of I_1, I_1' and I_2' intermediates as shown in Figure 3.9B,C. Thus, the pB^{deprot} spectrum presented in **[Hendriks**, **1999A]** is not the pure I_1' spectrum but rather a mixture of I_1, I_1' and I_2.

Our spectra for I_1' were obtained from the wavelength dependence of the transient absorption data, do not suffer from the problems described above, and provide the correct I_1' spectrum.

These measurements provide for the first time kinetic information on the formation of the I_1' intermediate. The amplitude spectrum $B_1(\lambda)$ (Figure 3.7C), which is derived directly from the data without any assumptions, clearly proves that in the 330 μs transition I_1 decays to I_1', without the formation of I_2'. $B_2(\lambda)$ shows that in the next transition I_1 and I_1' decay to I_2'. These results are model independent. Further analysis, based on the extrapolated difference method and a few plausible assumptions, confirms these results. Both the time traces (Figure 3.7A) and the intermediate time-courses (Figure 3.8C) derived from these data, indicate that I_1' is the decay product of I_1 and decays in equilibrium with I_1 and I_2' to P. In **[Hendriks**, **2003]** the intermediate pB^{deprot} (equivalent to I_1') was introduced between I_2' and P, and in equilibrium with I_2'. It was concluded that pB^{deprot} (I_1') is the decay product of pB (I_2'). Our kinetic data prove, that this is incorrect, and that I_1' is formed from I_1. The photocycle model in Figure 4 of **[Hendriks**, **2003]** is thus also incorrect. pB^{deprot} or I_1' is also presented in **[Yeremenko, 2006]**, in the photocycle model at pH 6.5, although it is mentioned that this state is not characterized in that study. We have shown here that no pB^{deprot} or I_1' exist at this low pH (Figure 3.3D: 410 nm is the characteristic wavelength for I_1', Figure 3.12B).

Assuming that the spectra of I_1, I_1' and I_2' are pH independent, and that no other intermediates contribute, eq 2.18 was used to calculate the time traces of these intermediates at each pH. Then the stationary equilibrium values at 10 ms were used to derive titration curves for the I_1, I_1' and I_2' populations (Figure 3.12). The results show that with increasing pH the equilibrium concentrations of I_1 and I_1' in the millisecond time range increase at the expense of a corresponding decrease in the I_2' concentration. The common pK_a is ~ 9.9. The pH dependence of the rate constant for the return to the ground state from this equilibrium was sigmoidal with a pK_a of ~ 9.7 (Figure 3.12D), within experimental error equal to the value of the pK_a for the pH dependent change in equilibrium populations. These data were analysed on the basis of scheme (III), in which only the I_1'/I_2' equilibrium is pH dependent. We find that the pH dependence of the recovery rate is a consequence of the corresponding pH dependence of the I_1'/I_2' equilibrium. The pK_a of 9.9 is attributed to the phenol group of the partially exposed chromophore, in agreement with previous assignments (**[Demchuk**, **2000]**, **[Meyer**, **2003]**).

These data are analyzed on the basis of the simple kinetic scheme (III) with only one pK_a. The titration of Figure 3.12 suggested the presence of a common pK_a of ~ 9.9. The poor fit for I_1 (with an individual pK_a of ~ 9.3, Figure 3.12A) is attributed to experimental error (low signal to noise ratio) and the very limited number of pH points. The pH dependence of the equilibrium populations (Figure 3.12) is based on the time traces of Figure 3.11. These depend in turn on the intermediate spectra. It is noted, that some residual freedom remained in these spectra (exact value of the parameter y_2), which leads to corresponding uncertainty in the time traces and pH dependencies. For these reasons we do not want to overinterpret our data, and thus limit this analysis to one common pK_a. It cannot be excluded however that the pK_a of 9.3 is real and that there are two very close pK_a's. This would require a more complex kinetic scheme, such as discussed for the mutant Y98Q **[Borucki**, **2005]**.

It has long been known that the rate constant for the ground state recovery has a bell-shaped pH dependence with pK_a's of 6.4 and 9.4 (**[Genick**, **1997]**, **[Demchuk**, **2000]**). In **[Demchuk**, **2000]** these data were analyzed on the basis of an equilibrium model implying that the recovery of P proceeds via a species with deprotonated chromophore and protonated Glu46, i.e. an I_1-like species. Since the microscopic rate for the transition from this I_1-like state to P was assumed to be pH independent **[Demchuk**, **2000]**, the apparent rate constant of the recovery of P follows the accumulation of the I_1-like state in the equilibrium that is maximal at ~ pH 8.0. We note that no amplitude data were used in this analysis to confirm the assumed accumulation of the I_1-like state. Here it is shown that the accumulation of I_1 in

the equilibrium increases from pH 8 to 10, which is inconsistent with the proposed model **[Demchuk, 2000]**. Moreover, we provide an explanation for the higher pK_a in terms of the pH dependence of the I_1'/ I_2' equilibrium.

We determined the equilibrium concentrations of the intermediates I_1, I_1' and I_2' from their time courses and provided direct kinetic evidence for the existence of their equilibria. In **[Borucki, 2003]** we first demonstrated the equilibrium between I_1 and I_2' at pH 11. Recently the equilibrium concentrations of these intermediates at alkaline pH were obtained from photostationary absorption spectra in the presence of background illumination **[Imamoto, 2004]**. The pH dependencies of $I_1'$and I_2' agree fairly well with our results. A pK_a of 10.2 was obtained for this equilibrium, in good agreement with our value of 9.9. The results for I_1 disagree, however. According to **[Imamoto, 2004]** the fraction of molecules in I_1 rises with pH up to pH 10.2 and then decreases again. Our data points (Figure 3.12A) agree up to pH 10, but do not decrease at higher pH values. The probable reason of discrepancy is explained above. Moreover, we showed recently, that the ionic strength also affects these equilibria **[Borucki, 2005]**, with increasing salt shifting the I_1/I_1' equilibrium towards I_2'. Differences in the amounts of salt added during the titration may thus explain the discrepancy. The steady-state data in **[Imamoto, 2004]** were collected under continuous illumination with light with wavelengths above 430 nm. Another contribution to the discrepancy could thus be photoreversal from I_1 (λ_{max} ~ 460 nm), which would reduce the I_1 population as described in section 4.1 to 4.3, in particular, at the highest pH values where the return to the initial state is slowest.

Based on their data two very close pK_a's were introduced in **[Imamoto, 2004]**. The first one of 10.2 was assigned to the I_1'/I_2' equilibrium, as discussed. The second one of 10.4 was assigned to the I_1/I_2' equilibrium. We note that this assignment is inconsistent since the two distinct pK_a values refer to the protonation of the chromophore, i.e. to only one protonable group. However, the finding of two pK_a values requires the involvement of two protonable groups. Consequently, one of the two pK_a values of **[Imamoto, 2004]** reflects the protonation of a residue that occurs in an equilibrium between I_1 and I_1', which both have a deprotonated chromophore. In our scheme (III), which can explain both the equilibrium and kinetic data of Figure 3.12, we have only one pH dependent equilibrium between I_1' and I_2', and the I_1/I_1' equilibrium is pH independent. The existence of the I_1' intermediate and the absence of the I_2 intermediate at alkaline pH are supported by photoreversal measurements as described in section 4.3.

3.3 Conclusions

The kinetics and intermediates of the photocycle and of the photoreversal were measured by transient absorption spectroscopy in the pH range from 4.6 to 11. SVD analysis of the transient absorption time traces measured in a broad wavelength range (330-510 nm) at pH 7 showed the presence of three spectrally distinguishable species: I_1, I_2 and I_2'. Their spectra were determined by using an advanced data analysis technique, the extrapolated difference method. I_2 and I_2' have absorption spectra, with maxima at 370 ± 5 and 350 ± 5 nm, respectively. Formation of the signaling state is thus associated with a change in the environment of the protonated chromophore, consistent with the observation that the formation of I_2' from I_2 is accompanied by a major conformational change. The signaling state of the photoreceptor photoactive yellow protein is the long-lived intermediate I_2'. The pH dependence of the equilibrium between the transient photocycle intermediates I_2 and I_2' was investigated in acid/neutral pH range (pH 4.6 to 8.4). I_1 decays partially to I_2 in the first transition, and I_2' is formed from I_1 and I_2 during the second transition. I_1, I_2 and I_2' are in equilibrium from ~ 10 ms onwards, and decay together to P in the third transition.

The time courses of the I_1, I_2 and I_2' intermediates were determined from the wavelength dependent transient absorbance changes in the time range from 50 ns to 50 s at each pH. It was assumed that their spectra are pH-independent. The I_1/I_2 equilibrium at ~ 500µs is formed from I_1 during the first transition, is pH dependent with a pK_a of 7, and I_1 as the main species at higher pH. The rate constant k_2 corresponding to the second transition also has a pK_a of ~6.7. The equality of the pK_a's of the pH dependence of decay rate and the equilibrium concentrations follows, if we assume that the equilibration rates between the intermediates are much faster than the decay rate and that the equilibrium decays through one of the species, e.g. I_1 here, consequently $k_2 \sim [I_1]$. After the formation of I_2' (~ 2 ms), the I_1, I_2 and I_2' intermediates are in equilibrium and decay together to the initial dark state. The equilibrium between I_2 and I_2' is pH dependent with a pK_a of 6.4 and I_2' is the main species above this pK_a. The rate constant k_3 for the recovery to the initial dark state also has a pK_a of ~ 6.3. This equality of the equilibrium and kinetic pK_a's suggests that $k_3 \sim [I_2']$.

Since the habitat of *Halorhodospira halophila* is distinctly alkaline the kinetics and intermediates of the photocycle and photoreversal were investigated further in the alkaline region from pH 8 to 11. SVD analysis of the data at pH 10 shows the presence of three spectrally distinct species I_1, $I_1'$and I_2'. The spectra of the intermediates I_1, I_1' and I_2' were obtained in two different ways: extrapolated difference method and scaled subtraction

method. I_1' absorbs maximally at 425 nm. I_1' probably has a deprotonated chromophore and may be regarded as the alkaline form of I_2'. At pH 10, the I_1 intermediate decays in ~ 330 μs in part to I_1' before I_1 and I_1' decay further to I_2' in ~ 1 ms. From the rise of I_2' (~ 1 ms) to the end of the photocycle the three intermediates I_1, I_1' and I_2' remain in equilibrium and decay together to P in ~ 830 ms. Assuming that the spectra of I_1, I_1' and I_2' are pH independent, their time courses were determined. On the ms to s time scale they are in a pH dependent equilibrium with a pK_a of ~ 9.9. With increasing pH the I_1 and I_1' populations increase at the expense of the amount of I_2'. The I_1'/I_2' equilibrium is pH-dependent, while the I_1/I_1' equilibrium is pH-independent. The apparent rate constant for the recovery of P slows down with increasing pH with a pK_a of ~ 9.7. This equality of the equilibrium and kinetic pK_a's suggests that $k_3 \sim [I_2']$ here too. The pK_a of ~ 9.9 is assigned to the deprotonation of the phenol of the surface exposed chromophore in the I_1'/I_2' equilibrium.

The existence of equilibria between transient photocycle intermediates was demonstrated here for the first time using kinetic methods. Spectra for the photocycle intermediates I_1, I_1', I_2 and I_2' were obtained from transient absorption data. In previous work such spectra were obtained from steady-state measurements in the presence of background illumination. Over the whole pH range the rate of recovery k_3 is proportional to the concentration of the signaling state. The amount of the signaling state is controlled by the pH and is maximal near pH 8.

Chapter 4

Photocycle Kinetics Mechanism Through Photoreversal Kinetics

Photoreceptors with chromophores isomerizable around a specific double bond can be switched back (reset) from the active (signaling) and to the inactive state by light. They are photochromic. They can usually be photoreversed from most intermediates. In our experiments with PYP, the sample is excited with two flashes applied at a defined delay (the wavelengths of the two flashes lie within the absorption band of the photocycle intermediates). The first flash (normally a blue flash, ~430nm) starts the cycle. A second flash applied during the cycle leads to the photoreisomerization and a rapid return to the initial state. In this way, the concentrations of cycling molecules are reduced via photoreversal. The photoreversal kinetics may be time resolved by triggering the data acquisition system on the second flash.

In this chapter, the results of the photoreversal kinetics measured with double flash excitation are presented. It will be shown that a second violet flash at 355 nm or a second green flash at 500 nm have a specific effect, respectively on the I_2/I_2' and I_1 intermediates. A photocycle mechanism of WT will be proposed based on these observations. The observations presented in this chapter support the photocycle mechanism derived from measurements with single flash excitation discussed in sections 3.1.3 and 3.2.3.

A relation will be presented to determine the pure photoreversal signal from measurements with single and double flash excitation (section 4.1.1). The dependence of the photoreversal signals on the delay between the flashes, measured with a violet flash as the second flash at pH 6, will be presented in section 4.1.2. This provides information about the temporal variation of the populations of the I_2/I_2' intermediates. It is observed that the I_2/I_2' intermediates are in equilibrium after about ~20 ms during the cycle. Moreover, the pH dependence of the photoreversal kinetics investigated in the pH range 4.6 to 8.4 (section 4.2), indicates that this equilibrium is pH dependent with a pK_a of ~6.1.

The photoreversal intermediates were further characterized spectrally through the wavelength dependent photoreversal signal measured at a particular delay (section 4.1.3). The photoreversal from I_1 is efficient, when selectively excited by a second flash at 500 nm (section 4.1.4) applied with ~ μs time delay. The delay and the wavelength dependence of the photoreversal signals measured at pH 10 (section 4.3) with a second flash at 355 nm indicate that the photoreversal kinetics at this pH differs significantly from the kinetics at pH 6.

4.1 Photoreversal at pH 6

4.1.1 Construction of the Photoreversal Signal from I_2 / I_2'

Typical transient absorption data for the photoreversal reaction from I_2 / I_2' at 340 and 450 nm are shown in panels A and B of Figure 4.1. The delay between the two flashes was 10 ms as indicated by the arrows. At this time, most molecules cycling are in the I_2 / I_2' intermediate state, Figure 3.4A-C. Panel C of Figure 4.1 shows the absorption spectra of the three states P, I_1, and the I_2/I_2' mixture with vertical lines marking the wavelengths of the three excitation flashes.

Panels A and B of Figure 4.1 each contain six time traces labeled BFTB[1], DFTB[1], DFTV[1], BFTV[1], VFTV[1], and PR[1] (photoreversal signal). The first five traces are the data. The photoreversal signal was constructed from the traces DFTV, BFTV, and VFTV as follows. The trace BFTB (black) is the normal single flash trace: *b*lue *f*lash (430 nm) *t*riggered on *b*lue flash. The absorbance increase at 340 nm about 300 μs after excitation is due to the formation of I_2 (Figure 4.1A). The corresponding kinetic component in the ground-state depletion signal is the absorbance decrease at 450 nm due to the I_1 to I_2 transition (Figure 4.1B). The photoreversal reaction is evident from the traces labeled DFTB (red) in panels A and B of Figure 4.1. DFTB stands for *d*ouble *f*lash *t*riggered on the *b*lue flash. At 340 nm (Figure 4.1A) there is a positive spike followed by a large unresolved drop in absorbance at the delay time of 10 ms (marked by arrow). At 450 nm (Figure 4.1B), there is a large unresolved increase in absorbance. Together, these effects are the signature of photoreversal from I_2/I_2' to P: the concentration of I_2/I_2' (absorbing around 350 nm) drops and simultaneously the concentration of the initial dark state P (absorbing around 450 nm) increases. The kinetics of the photo-back-reaction is clearly fast compared to the I_2 to I_2' transition and cannot be resolved by using a logarithmic time base when triggering on the first (blue) flash. The photoreversal from I_2 can be resolved, however, by triggering on the second (violet, 355 nm) flash. This is shown in the traces labeled DFTV (green) in panels A and B of Figure 4.1: *d*ouble *f*lash *t*riggered on

the *v*iolet flash. Note that when the trigger is on the second flash, the zero in the linear time basis (origin of the horizontal axis of Figure 4.1A,B) is the second flash.

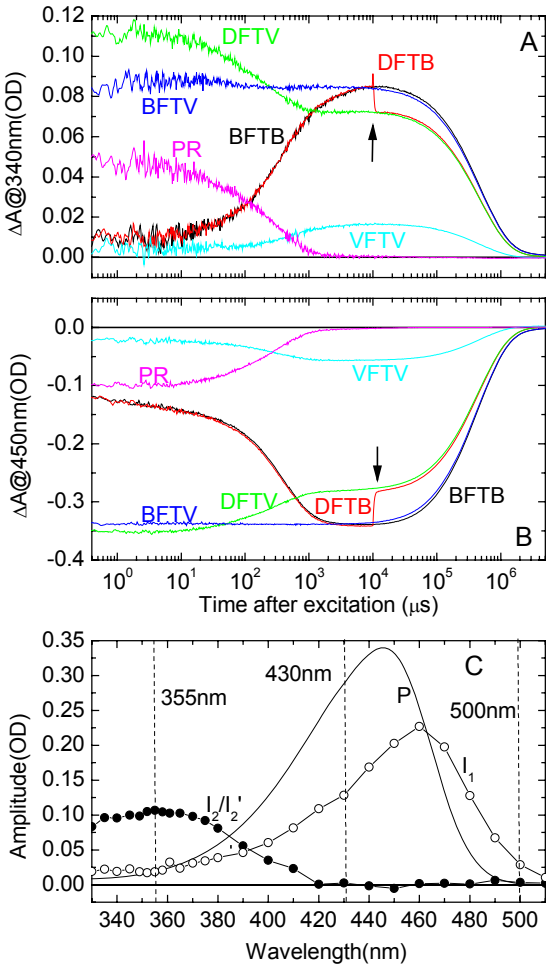

Figure 4.1 Absorbance changes at 340 nm (A) and 450 nm (B) after single (430 or 355 nm) or double flash excitation [430 nm followed by 355 nm 10 ms later (arrow)]. Each trace is the average of 10 flashes. Note the logarithmic time scale. The double flash traces labeled DFTB and DFTV are triggered on the first flash (430 nm) and on the second flash (355 nm), respectively. If the trigger is on the second flash, that flash sets the zero time point on the horizontal time axis. Single flash signals with either blue (B, 430 nm) or violet (V, 355 nm) excitation and triggered on the first (BFTB) or second flash (BFTV, VFTV) are displayed as well. These are needed to construct the photoreversal signal (PR) according to eq 4.2, with $f_1 = 0.76$ and $f_2 = 0.73$. Conditions: WT, pH 6, 20 °C, 20 mM Tris, and 50 mM KCl. PYP concentration, 64μM. (C) Absorption spectra of P, I_1, and the I_2/I_2' mixture, together with markers indicating the wavelengths of the blue (430 nm), violet (355 nm) and green (500 nm) excitation flashes. The spectra of the I_1 intermediate and the I_2/I_2' mixture were calculated from the single flash data of Figure 4.4B as described in the text.

At the time of the second flash, there exists a mixed population of the intermediates I_1, I_2, and I_2' as well as the remaining population of PYP molecules that were not excited by the first flash, Figure 3.4A-C. The violet flash is able to excite all of these species (see overlapping intermediate spectra in panel C of Figure 4.1 or Figure 3.2A. The spectra of Figure 4.1C were calculated from the data of Figure 4.4B, as described below). Except for the very short delays, the photoreversal from I_1 can be ignored (see below). Therefore, we need only to correct for the fraction of PYP molecules that were not excited by the first, blue flash but were excited by the second, violet flash. The traces labeled VFTV, *v*iolet *f*lash triggered on the *v*iolet *f*lash, show that the excitation of the PYP sample by a single flash, at 355 nm, is quite efficient. Moreover, these traces have the same kinetics as for excitation at 430 nm and contribute in the same time range as the photoreversal changes (compare DFTV with VFTV).

Thus, the double flash signal DFTV has to be corrected for the contribution from those molecules that were not excited by the first, blue flash but by the second, violet flash. To make this correction, we need to know f_1, the fraction of the initial PYP population that was not excited by the first flash and remains in the ground state. Since f_1 equals 1 minus the probability of cycling induced by the first flash, f_1 was determined by measuring the amplitude of the ground-state depletion signal at 450 nm and comparing it with the dark absorption at 450 nm. In this way, typical values for f_1 of 0.76 were obtained. This means that, with our laser system, the first flash drove 24% of the molecules through the photocycle. The remaining 76% could be excited by the second, violet flash. The dependence of f_1 on the delay is shown in Figure 4.2B. Since no significant thermal relaxation from I_2 back to the ground state occurs up to about 10 ms, f_1 remains constant up to that time (Figure 4.2B). With delays beyond this value, a growing number of molecules return to the initial state, thus f_1 increases to a final value of 1.

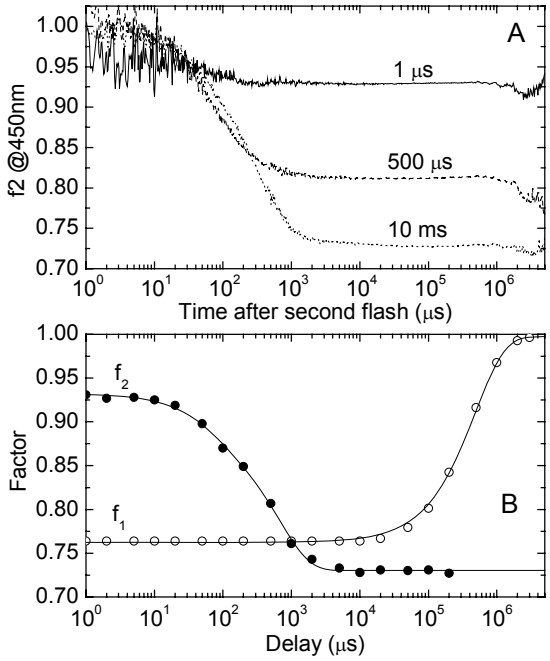

Figure 4.2 (A) Correction factor $f_2(t)$ calculated according to eq 4.1 for delays of 1 µs, 500 µs, and 10 ms. The plateau values are plotted in panel B for various delays. (B) Correction factors f_1 and f_2 for various values of the time delay between the flashes. f_1 is the fraction of PYP molecules not excited by the first flash. f_2 is the fraction of cycling PYP molecules not excited by the second flash.

To obtain the true photoreversal signal, the double flash absorption change also has to be corrected for the contribution from the first flash of those molecules in the cycle that are not excited by the second flash and thus complete the thermal cycle. The trace BFTV (*b*lue *f*lash *t*riggered on *v*iolet flash) corresponds to a single blue flash excitation triggered at the time point where the second, violet flash would have occurred in the double flash excitation. This trace has to be weighted by f_2, the fraction of cycling PYP molecules not excited by the second flash. f_2 was determined in a similar way as f_1 from the amplitudes of the depletion signal at 450 nm at times after completion of the photoreversal kinetics. Its calculation is

based on the assumption, borne out by the experimental data, that the photoreversal kinetics are faster than the thermal decay of I_2 to P. $f_2(t)$ is defined as the value of the ratio:

$$f_2(t) = \frac{\Delta A_{DFTV}(t) - f_1 \Delta A_{VFTV}(t)}{\Delta A_{BFTV}(t)} \qquad \textbf{(4.1)}$$

and evaluated at 450 nm.

At times after completion of the photoreversal reaction, the numerator is the amplitude of the depletion signal after photoreversal (DFTV) corrected for the contribution from the molecules that were not excited by the first flash but by the second violet flash (VFTV). The denominator is the amplitude of the depletion signal in the normal single flash photocycle, i.e., in the absence of photoreversal. This ratio is exactly the fraction of molecules cycling that continues along the thermal photocycle after the second flash, i.e., the fraction not excited by the second flash. Using the time traces DFTV, VFTV, and BFTV as well as the value of f_1, $f_2(t)$ was calculated according to eq 4.1 as a function of time. In Figure 4.2A, $f_2(t)$ is plotted for delays of 1 μs, 500 μs, and 10 ms. At times after completion of the photoreversal reaction (>~2 ms), $f_2(t)$ reaches a constant time-independent value (see Figure 4.2A). This constant f_2 is the fraction required and used in eq 4.2 below. These values depend on the delay (Figure 4.2A) and are plotted in Figure 4.2B. At short delays (<20 μs), f_2 is not equal to 1 as one might have expected but to ~0.93. This is due to photoreversal from I_1. Evidence for efficient photoreversal from I_1 with a second flash at 500 nm will be presented below (section 4.1.4). We note that, based on the spectrum of I_1 in Figure 4.1C, some photoreversal from I_1 with excitation at 355 nm is to be expected. Figure 4.2B shows that f_2 decreases between delays of 100 μs and 2 ms from about 0.87 to about 0.74. This is due to the growth of the I_2/I_2' population in this time interval. The photoreversal signals ΔA_{PR} (PR, pink traces) shown in Figure 4.1A,B were obtained from the traces labeled DFTV, VFTV, and BFTV using eq 4.2 and the delay-dependent correction factors f_1 and f_2 of Figure 4.2B **[Druckmann, 1993]**:

$$\Delta A_{PR}(t) = \Delta A_{DFTV}(t) - f_1 * \Delta A_{VFTV}(t) - f_2 * \Delta A_{BFTV}(t) \qquad \textbf{(4.2)}$$

The photoreversal absorbance signals in Figure 4.1A,B, constructed in this way, are exactly zero after completion of the photoreversal reaction and do not contain any contribution from the single, blue flash photocycle as a consequence of the definition of the correction factor f_2. Thus, the f_2 correction used here greatly simplifies the analysis of the photoreversal kinetics by removing the unrelated kinetic components from the normal photocycle prior to analysis. Comparing the DFTV and PR traces in panels A and B of Figure 4.1, the effect of corrections is twofold: the f_1 correction has removed the kinetic contributions from the photocycle intermediates formed by the second flash, and the f_2 correction has

removed the kinetic contribution from those molecules not excited by the second flash but continuing to P along the normal thermal cycle.

4.1.2 Dependence of the Photoreversal Signal on Delay

The experiment shown in Figure 4.1, at a delay of 10 ms, was carried out at 20 additional delays ranging from 1 µs to 3 s, at both 340 and 450 nm. The calculated photoreversal signals, positive at 340 nm and negative at 450 nm, were constructed as described above. Of the corresponding 21 traces, for clarity, only 7 are presented at each wavelength in Figure 4.3A.

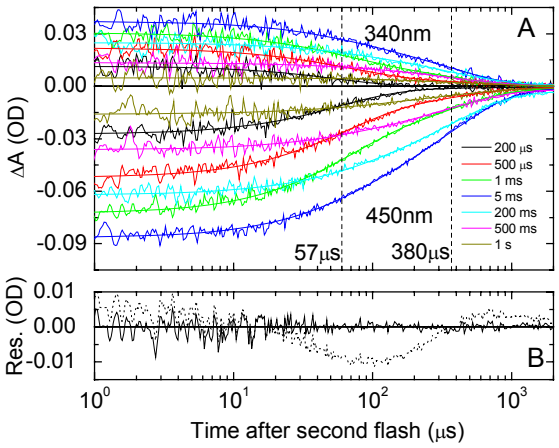

Figure 4.3 (A) Corrected photoreversal signals at 340 and 450 nm at seven delays ranging from 1 µs to 3 s. For clarity, the data at the 14 other delays are not shown. The solid lines represent a two-exponential global fit to all of the data with τ_1 = 57 µs and τ_2 = 380 µs. Conditions: pH 6, 50 mM KCl, 20 °C, and 20 mM Tris. PYP concentration: 64 µM (B) Residuals of the fit to the 450 nm photoreversal signal at a delay of 1 ms. Black dots: one-exponential fit. Black line: two-exponential fit.

We note that a number of these traces cross, indicating that they cannot be fitted simultaneously by a single exponential with a common time constant. For a global fit to all data sets, a sum of two exponentials with comparable amplitudes was required. In Figure 4.3B, is shown, as an example, the residuals at 450 nm for a one-exponential and a two-exponential global fit to the data of Figure 4.3A at a delay of 1 ms. Systematic deviations are apparent in the residuals for the one-exponential fit, while residuals for the two-exponential fit appear to be randomly distributed around zero. The complete set of data at the 2 wavelengths and 21 delays could be fitted with two exponentials with the common time constants τ_1 = 57 ± 5 µs and τ_2 = 380 ± 40 µs (marked by the vertical dashed lines in Figure 4.3A). The fits of individual experiments are represented by the solid lines in Figure 4.3A. The corresponding amplitudes A_1 and A_2 varied with the delay. This dependence is shown in Figure 4.4A.

The amplitudes A_1 and A_2 for the short and long photoreversal time constants show, apart from the sign and scaling factor, the same dependence on delay at 340 and 450 nm. The four discrete sets of amplitudes (A_1 and A_2 at two wavelengths) were fitted simultaneously

with a sum of three exponentials (solid lines in Figure 4.4A). The optimal fit was obtained with time constants of 410 µs, 1.3 ms, and 500 ms identified by dotted vertical lines. The first two time constants, 410 µs and 1.3 ms, are close together and to the eye do not appear to provide a good description of the rise and decay of the A_1 amplitudes. This is a consequence of the partial cancellation of the positive and negative amplitudes associated with these time constants. Since the number of delay values is small, the errors in these time constants are large. The absolute value $|A_1|$ rises with a time constant of 410 µs. $|A_1|$ then decreases (1.3 ms), and in parallel, as expected for a sequential reaction, the amplitude $|A_2|$ rises. The A_1 amplitudes do not decay to zero, however, but reach a constant value after about 5 ms. Finally, $|A_1|$ and $|A_2|$ decay together with a time constant of 500 ms. We note that the positive (340 nm) and negative (450 nm) amplitudes are to a very good approximation scaled mirror images.

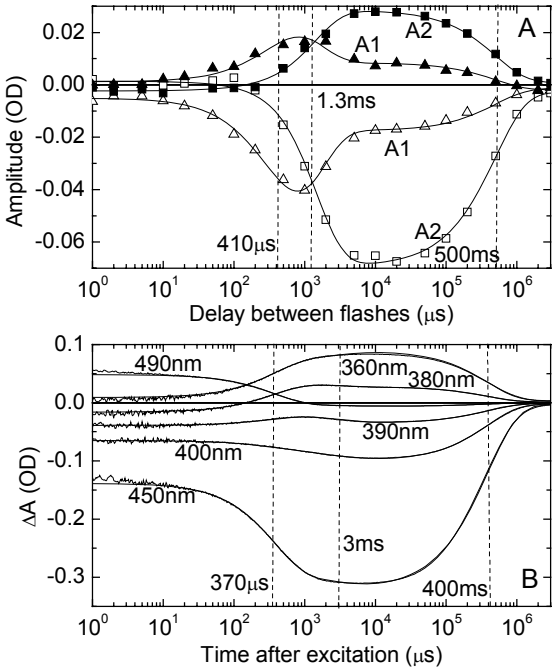

Figure 4.4 (A) Dependence of the amplitudes A_1 and A_2 on the delay. A_1 and A_2 are the amplitudes of the fast (57 µs) and slow (380 µs) photoreversal components, respectively. The two positive amplitudes with filled triangles (A_1) and squares (A_2) are at 340 nm; the two negative amplitudes with open triangles (A_1) and squares (A_2) are at 450 nm. The dashed vertical lines at 410 µs, 1.3 ms, and 500 ms indicate the values of the exponential time constants for a global fit with three exponentials. (B) Single flash (430 nm) absorbance changes for the same sample at 26 wavelengths varying from 330 to 510 nm. For clarity, only the traces at the indicated wavelengths are shown. The vertical dashed lines indicate the positions of the time constants for a global fit to all of the data with a sum of three exponentials; τ_1= 370 µs is the rise time of I_2, τ_2= 3 ms is the rise time of the I_2/I_2' equilibrium, and τ_3= 400 ms is the decay time of I_2/I_2'. The solid lines are the fits.

Figure 4.4B shows for comparison the single flash (430 nm) kinetics at 6 selected wavelengths out of 26 collected from 330 to 510 nm. As it will be shown below, the I_2 and I_2' intermediates are in a thermal equilibrium after 3 ms. The model-dependent intermediate spectra for I_1 and the I_2/I_2' mixture, shown in Figure 4.1C, were calculated from these data in the following way. It was assumed that the cycle is sequential and unidirectional with only I_1

present at 10 μs and only the I_2/I_2' equilibrium mixture at 10 ms. Moreover, it was assumed that the I_2 and I_2' intermediates do not absorb at 446 nm. Using these assumptions, the spectrum of the I_2/I_2' equilibrium was determined by adding, to the difference spectrum at 10 ms [spectrum labeled (*) in Figure 4.5B, calculated from Figure 4.4B], a scaled amount of the ground-state spectrum to make the absorbance around 450 nm zero. The spectrum of I_1 was then calculated from the difference spectrum at 10 μs (from Figure 4.4B) by adding this same amount of the ground-state spectrum.

The complete 26-wavelength data set of Figure 4.4B was subjected to a global fit with three exponentials (solid lines). The three vertical dotted lines indicate the values of the three exponential time constants: 370 μs, 3 ms, and 400 ms. These times correspond to the rise of I_2, the rise of $I_1/I_2/I_2'$ equilibrium, and the return to the initial dark state, Figure 3.2C (blue curve). The presence of the 3 ms component (I_2/I_2' equilibrium) can be clearly discerned in the data in Figure 4.4B (e.g., in the 390 nm trace). The reasonable agreement between these three time constants for I_2 and I_2' (Figure 4.4B) and the corresponding three values of 410 μs, 1.3 ms, and 500 ms for A_1 and A_2 (in Figure 4.4A) together with the dependence of A_1 and A_2 on the delay suggest the following interpretation of the photoreversal kinetics data in terms of a sequential model (Figure 3.6, inner part of the photocycle model). The time constant of 57 μs is assigned to the photoreversal reaction from I_2 (I_2^{cis}). The very rapid photoisomerization from I_2^{cis} to I_2^{trans} is not resolved but leads to the initial positive absorbance change at 340 nm (see Figure 4.1A, difference between DFTV and BFTV at time zero and the positive spike at 10 ms in the DFTB trace). Between I_2^{trans} and P^{trans}, the chromophore deprotonates and returns to the binding pocket with a time constant of 57 μs. The time constant of 380 μs is assigned to the photoreversal reaction from I_2' ($I_2'^{cis}$). After the rapid unresolved photoisomerization to $I_2'^{trans}$, the chromophore has to be deprotonated and the global conformational change has to be reversed. In the sequential model, the delay dependence of A_1 and A_2 should reflect the time courses of the concentrations of I_2 and I_2', respectively. In agreement with this model, A_1 dominates at small delays, and A_2 rises concomitantly with the first decay phase of A_1. The rise time of A_1 (410 μs) agrees well with the rise time of I_2 (370 μs). The rise time of A_2 and the decay time of A_1 (1.3 ms) is only slightly ahead of the rise time of I_2' (3 ms). The common decay time of A_1 and A_2 (500 ms) agrees well with the decay time of I_2' (400 ms). In these respects, the unidirectional sequential model provides a good description for the observations and is summarized in Figure 3.6. On the other hand, if the transition between I_2 and I_2' were unidirectional, the amplitude of A_1 should go to zero in the 1.3 ms decay. This is, however, clearly not the case. The fact that A_1 remains constant after 5 ms at approximately 50% of its

maximal value and finally decays to zero in a second decay phase (500 ms) together with A_2 is direct evidence for the existence of an equilibrium between I_2 and I_2'. I_2 and I_2' coexist after 5 ms and decay together. The amplitude data clearly suggest a thermal back-reaction from I_2' to I_2. Thus, protein rearrangement must be faster than decay of I_2' and I_2 (500 ms), perhaps as fast as 400 µs.

Moreover, the delay dependence of the A_1 amplitude of Figure 4.4A is comparable to the I_2 time course of Figure 3.4B (blue curve). This shows that the 57 µs component is due to the photoreversal from I_2. Similarly, the delay dependence of the A_2 amplitude of Figure 4.4A is very similar to the I_2' time course of Figure 3.4C (blue curve). This shows that the 380 µs component is due to the photoreversal from I_2'.

4.1.3 Wavelength Dependence of the Photoreversal Signal at the Fixed Delays of 1 and 10 ms

To characterize the two photoreversal components with reversal time constants of 57 µs and 380 µs spectrally, the wavelength dependence of the photoreversal signal was investigated at delays of 1 and 10 ms. At a delay of 1 ms A_1 and A_2 have comparable magnitude, whereas at a delay of 10 ms A_2 dominates (see Figure 4.4A). Data were collected at 26 wavelengths from 330 to 510 nm. The photoreversal signals were constructed as described earlier (see panels A and B of Figure 4.1 for examples at 340 and 450 nm at a 10 ms delay). Typical data for the delay of 1 ms and at seven selected wavelengths are displayed in Figure 4.5A together with their global two-exponential fits.

The two common exponential time constants for this independent data set (at 26 wavelengths), at a delay of 1 ms, were 66 ± 5 and 410 ± 40 µs. For the data set at the delay of 10 ms (data not shown), the two time constants were 51 and 390 µs. The rounded average values of 59 and 400 µs are marked by the dotted vertical lines (Figure 4.5A) and are in excellent agreement with the values of 57 and 380 µs determined from the delay data at the two wavelengths 340 and 450 nm (Figure 4.3A). The amplitude spectra A_2 (○ at 10 ms delay, ■ at 1 ms delay) and A_1 (△ at 1 ms delay) are plotted in Figure 4.5B together with the single flash difference spectrum at 10 ms (∗) and the inverted ground-state spectrum (solid line).

Recall that the f_1 and f_2 corrections removed all contributions of the normal photocycle from the double flash signal. The photoreversal signal (PR) thus represents only the absorbance change due to photoreversal. In the previous section on the delay dependence, it was argued that a sequential model provides a good description of the photoreversal kinetics:

I_2^{cis} is photoreversed with the single decay time τ_1 and $I_2'^{cis}$ with the longer single decay time τ_2. We detected no further intermediates between I_2^{trans} and P nor between $I_2'^{trans}$ and P. The corresponding amplitude spectra $A_1(\lambda)$ and $A_2(\lambda)$ for such a two-state sequential model (I_2^{trans} to P and $I_2'^{trans}$ to P) are then equal to the difference spectra between the two states (I_2^{trans}/P and $I_2'^{trans}$/P, respectively). The spectra of I_2^{trans} and $I_2'^{trans}$ may thus be constructed from the A_1 and A_2 amplitude spectra in a simple way. This is illustrated for the A_2 amplitude spectrum at 10 ms in Figure 4.5B,C.

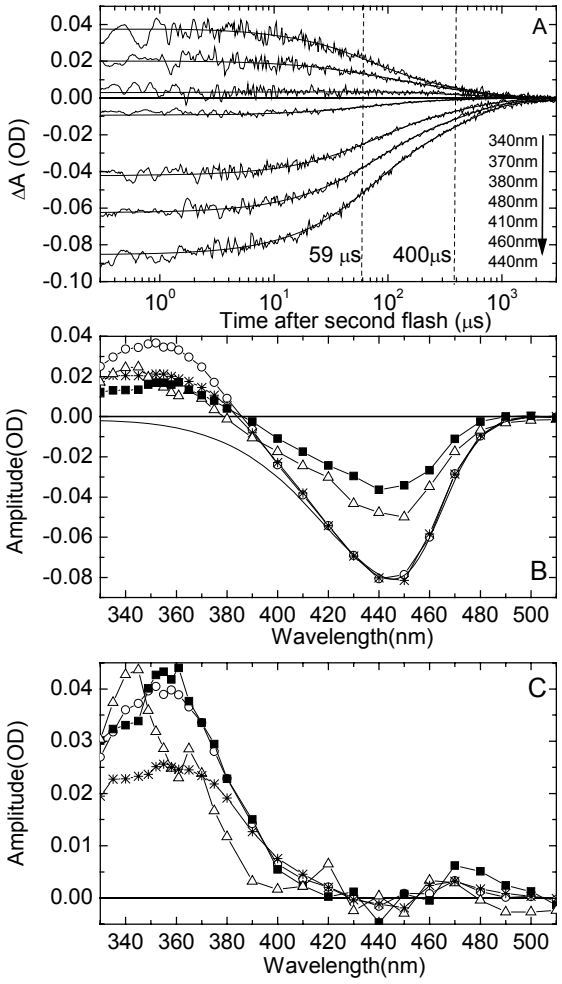

Figure 4.5 (A) Photoreversal signals at seven wavelengths between 330 and 510 nm at the fixed delay of 1 ms. For clarity, similar data at 19 additional wavelengths are not shown. The solid lines are the global fits with a sum of two exponentials with the common time constants τ_1 = 66 μs and τ_2 = 413 μs. A second data set (not shown) was acquired at a delay of 10 ms with global fit parameters τ_1 = 51 μs and τ_2 = 391 μs. The average τ's are marked by the vertical lines. (B) Amplitude spectra $A_1(\lambda)$ and $A_2(\lambda)$ associated with τ_1 and τ_2 obtained from the global fit of (A): (○) A_2 for the 10 ms delay; (■) A_2 for the 1 ms delay; (△) A_1 for the 1 ms delay. For comparison, the absorbance difference spectrum for the single flash experiment at 10 ms after the flash is shown (*, obtained from the data of Figure 4.4B). The A_2 spectrum at 10 ms (○) and the difference spectrum (*) are scaled at 450 nm to the spectrum of the dark state P (solid line). (C) Absorption spectra of $I_2'^{cis}$ (*), $I_2'^{trans}$ (○ at 10 ms delay, ■ at 1 ms delay), and I_2^{trans} (△) calculated from (B).

First A_2 is scaled in such a way that it matches the inverted ground-state spectrum (P) at 450 nm (○). Figure 4.5B shows that the fit of the scaled A_2 spectrum to P is quite good in the wavelength range from 410 to 510 nm. This supports the assumption that, at least in this wavelength range, no states other than P contribute. By adding the ground-state spectrum to the scaled A_2 spectrum, the absorbance in the 410-510 nm range is now reduced to zero and

the $I_2'^{trans}$ spectrum is generated (○ in Figure 4.5C). The same procedure was applied to the $A_2(\lambda)$ amplitude spectrum at 1 ms (■ in Figure 4.5B,C). The corresponding $I_2'^{trans}$ spectrum is within experimental error the same as that derived from A_2 at 10 ms, as it should be. In the same way the I_2^{trans} spectrum (△) was generated from the $A_1(\lambda)$ amplitude spectrum. In agreement with the observation of an instantaneous absorbance increase around 350 nm after the second flash (arrow in Figure 4.1A), the I_2^{trans} and $I_2'^{trans}$ intermediates have considerably higher extinction coefficients than I_2^{cis} (Figure 4.5C). Note that the extinction coefficient is not exactly zero above 410 nm but assumes small positive or negative values. This is due to experimental error in the determination of A_1 and A_2 at individual wavelengths. These errors are of the same magnitude as the differences between the two spectra for the $I_2'^{trans}$ intermediate derived from A_2 at 10 and 1 ms in the UV region.

At first sight, the spectrum for I_2^{trans} (△) appears to be anomalous due to the minimum at 361 nm. We recall that A_1, from which this spectrum is derived, is the amplitude of the fastest photoreversal component and therefore more affected by the flash. The absorption traces at the five wavelengths 349, 353, 355, 358, and 361 nm, closest to the excitation wavelength of 355 nm, are most affected by the flash artifact which leads to an artificially lower absorbance at these five wavelengths. Leaving these five wavelength traces out of the data analysis leads to the same absorbance at the wavelengths at or below 345 nm and at wavelengths at or above 365 nm. We conclude that the apparent minimum at 361 nm is due to the flash artifact. We may therefore conclude that the spectrum of I_2^{trans} is blue shifted with respect to the spectrum of $I_2'^{trans}$ by ~10 nm but has approximately the same maximal extinction coefficient. This blue shift is also apparent from the data points above 365 nm in Figure 4.5C, which are not affected by the flash artifact. From these spectra we estimate λ_{max} values of approximately 345 and 355 nm for I_2^{trans} and $I_2'^{trans}$, respectively.

4.1.4 Photoreversal from I_1 by a Green Flash (500 nm)

From the spectrum of I_1 in Figure 4.1C, it is clear that selective photoreversal from I_1 should be feasible with a second flash around 500 nm. Figure 4.6 shows double flash data at measuring wavelengths of 360 and 450 nm with a first flash, at 430 nm (blue), followed by a second flash, at 500 nm (green), after a delay of 20 μs. At 20 μs, almost all molecules cycling are in I_1 as shown in Figure 3.4A-C. As expected, the green flash alone (GFTG[1], *g*reen *f*lash data acquisition *t*riggered on *g*reen flash) leads to very small effects due to the low absorbance of P at 500 nm. The photoreversal effect from I_1 can be most clearly discerned in the depletion signal (Figure 4.6B, 450 nm), since at this wavelength both I_1 and the initial dark

state P absorb strongly, with the extinction coefficient of P being much larger than that of I_1 at this wavelength (Figure 4.1C).

At 20 μs, a large positive absorbance change is observed (DFTB; the negative spike is the flash artifact), corresponding to the I_1 to P transition. This instantaneous positive absorbance step is not resolved when triggering on the first flash (DFTB). Triggering on the second flash (DFTG, not shown) also did not resolve this absorbance change. Thus, we can only conclude that photoreversal from I_1 is faster than 1 μs. The reduction in the number of cycling molecules at 20 μs by the 500 nm flash leads to a corresponding reduction in the amplitude of the depletion signal at 10 ms, since fewer I_2 molecules are formed.

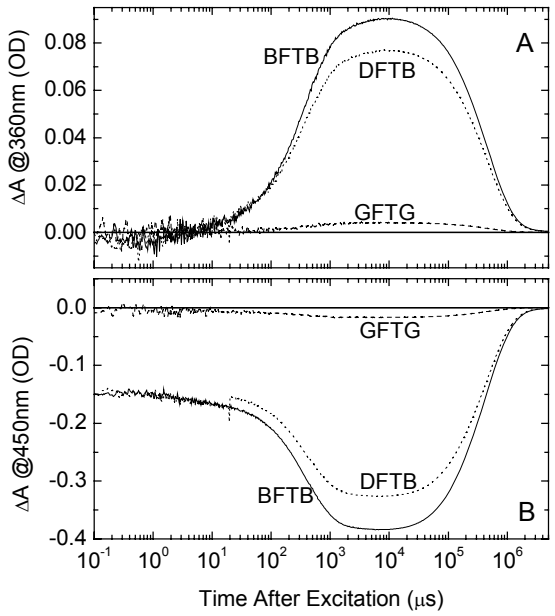

Figure 4.6 Photoreversal from I_1. The first flash (at 430 nm) was followed after 20 μs by a second flash (at 500 nm). Conditions: pH 6, 20 °C, 20 mM Tris, and 50 mM KCl. (A) Absorbance change at 360 nm. The trace labeled BFTB is the response after a blue single flash. DFTB labels the double flash response triggered on the first, blue flash. The trace labeled GFTG is the response after a single green flash. (B) Absorbance change at 450 nm. The meaning of the labels is as in (A). The positive unresolved absorbance change at 20 μs is due to about 18% photoreversal from I_1 to the initial dark state P.

In Figure 4.6A (360 nm), no absorbance change is observed at 20 μs (apart from the negative spike), since the extinction coefficients of I_1 and P are quite small and similar at this wavelength (see Figure 4.1C). At 10 ms after the flash, the double flash amplitude (DFTB) is reduced by ~18% with respect to the single flash amplitude (BFTB). This reduction factor is the same as for the depletion signal at 10 ms and is due to the reduction in the population of I_2 caused by the photoreversal of the preceding intermediate I_1. Additional experiments were carried out at delays of 300 ns, 10 μs, and 10 ms (data not shown). At 300 ns and 10 μs, the amplitude of the photoreversal signal from I_1 was about the same as at 20 μs. This is as expected since I_1 has a rise time of about 3 ns and decays to I_2 in 300 μs, Figure 3.4A. At a delay of 10 ms, photoreversal from I_1 could not be detected, since, at this delay, I_1 contribution is below detection limit in photoreversal signal. Photoreversal from I_1^{cis} is represented in Figure 3.6.

4.2 pH Dependence of the Photoreversal Kinetics at Acid and Neutral pH

The I_2 and I_2' intermediates are in a pH dependent equilibrium from about ~ 20 ms until the end of the cycle as shown by Figure 3.4 B,C. This pH dependence was further investigated in double flash experiments with a violet flash (355 nm, selective for I_2/I_2'; I_1 absorbs to a much smaller extent at this wavelength (see Figure 3.2A)) as the second flash at a delay of 20 ms (maximum of I_2/I_2' population during cycle, Figure 3.4B,C). The photoreversal kinetics was measured at only two wavelengths (340 and 450 nm) and at the following fifteen-pH values: 4.6, 4.8, 5.1, 5.4, 5.7, 6.0, 6.3, 6.6, 6.75, 6.9, 7.35, 7.7, 7.9, 8.1, and 8.4.

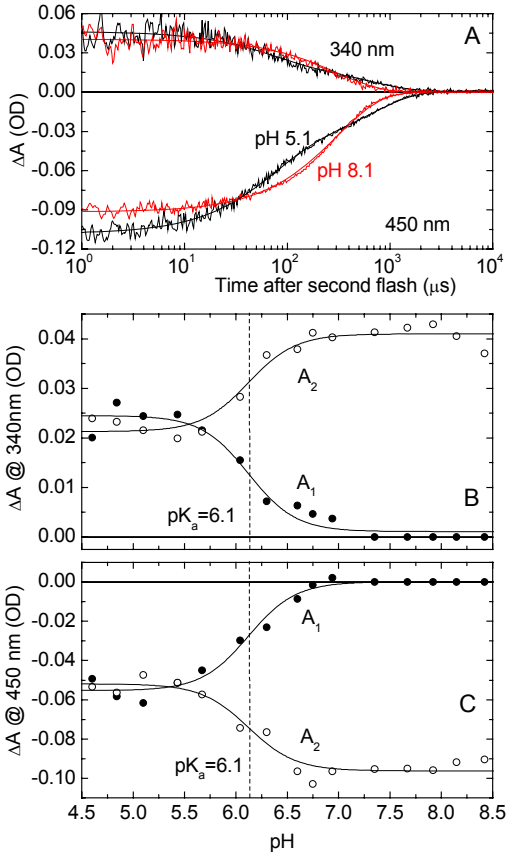

Figure 4.7: (A) Photoreversal signals, at 340 nm (positive) and 450 nm (negative) at pH 5.1 (black) and 8.1 (red), calculated using eq 4.2. For clarity, the data obtained at 13 other pH values ranging from 4.6 to 8.4 are not shown. The solid curves represent a simultaneous exponential fit to the 340 nm and 450 nm traces. Conditions: 20°C, 50 mM KCl and 50 mM MES, PYP concentration: 53 μM. The delay between first (blue, 430nm) and second (violet, 355nm) flashes is 20 ms. (B), (C) pH dependence of the photoreversal amplitudes A_1 and A_2 at 340nm (B) and 450nm (C). A_1(•) and A_2(o) are the amplitudes of the fast (48 to 60 μs) and slow (330 to 770 μs) components, respectively, obtained from the simultaneous fit of the 340 nm and 450 nm traces of panel A. The solid curves of panels B and C represent a common fit to the pH dependence of all four amplitudes with the Henderson-Hasselbalch equation, with a pK_a of 6.1 (dash vertical lines) and a Hill coefficient of 1.9.

The photoreversal signals at pH 5.1 and 8.1 are shown in Figure 4.7A. For clarity, only the traces at two of the fifteen pH values are shown together with their simultaneous fits (solid lines). As at pH 6 (Figure 4.5A), the kinetics required two exponentials over the pH range from 4.6 to 6.9. These two phases can be clearly discerned in the data at pH 5.1. From pH 7.3 on, only the slow component was required. The fast time constant was virtually pH-independent, varying between 48 and 63 μs. The second time constant varied between 330

and 770 μs in the pH range investigated. Comparing the time traces in Figure 4.7A, it is clear that there are significant differences between pH 5.1 and 8.1. The total initial photoreversal signal is somewhat larger at pH 5.1 than at 8.1, suggesting that more I_2/I_2' can be photoreversed.

The amplitude data provide further insight. The pH dependence of the amplitudes A_1 and A_2 (for the corresponding time constants τ_1 and τ_2) are plotted in Figure 4.7B (340 nm) and C (450 nm). These figures confirm that, with increasing pH, A_1 becomes smaller approaching zero around pH 7 at both wavelengths, whereas A_2 shows a corresponding increase. The solid curves are simultaneous fits of the amplitudes at 340 and 450 nm with the Henderson-Hasselbalch equation, with $pK_a = 6.1$ and $n = 1.9$. The amplitudes A_1 and A_2 were assigned to photoreversal from I_2 and I_2', respectively (Figure 4.4A). The results of Figure 4.7B and C thus suggest that, with increasing pH, the I_2/I_2' equilibrium shifts from I_2 at pH 4.6 to I_2' at pH 8.4. These results, from the pH dependence of the photoreversal amplitudes, thus support the observations from the photocycle as described in Figure 3.5C, where a pK_a of 6.4 was obtained.

4.3 Photoreversal from I_2' at pH 10, dependence on delay and wavelength

I_1, I_1' and I_2' contribute to the photocycle at pH 10 and are in equilibrium beyond about ~ 3 ms during photocycle, Figure 3.8C. The delay dependence of the photoreversal kinetics was investigated at this pH with a violet flash (355 nm, selective for I_2'; I_1' and I_1 absorb to a much smaller extent at this wavelength (see Figure 3.8A)) after a variable time delay. The pure photoreversal signal was calculated from the DFTV, VFTV and BFTV and the f_1 and f_2 factors using eq 4.2.

The photoreversal signals were measured at 365 and 450 nm at 19 delays ranging from 500 ns to 5 s. A selection of 6 of these traces at each wavelength is shown in Figure 4.8A. The solid lines are from a two-exponential global fit to the data at all 19 delays. The data clearly show the presence of two phases with exponential decay constants of $\tau_1 = 60$ μs and $\tau_2 = 3.5$ ms, identified by the dashed vertical lines.

The corresponding amplitudes A_1 (60 μs component) and A_2 (3.5 ms) are plotted as a function of the delay in Figure 4.8B. The positive amplitudes refer to the photoreversal signal at 365 nm, the negative amplitudes to the signal at 450 nm. The solid lines in Figure 4.8B are simultaneous fits to the delay dependence of the amplitudes with a sum of two exponentials. The optimal fit was obtained with exponential time constants of 1.1 ms (rise) and 680 ms (decay). The 1.1 ms rise time corresponds closely with the 1 ms rise time of I_2' (Figure 3.8C).

In view of the small number of delay times, the 680 ms decay time agrees well with the 830 ms decay time of I_2' (Figure 3.8C).

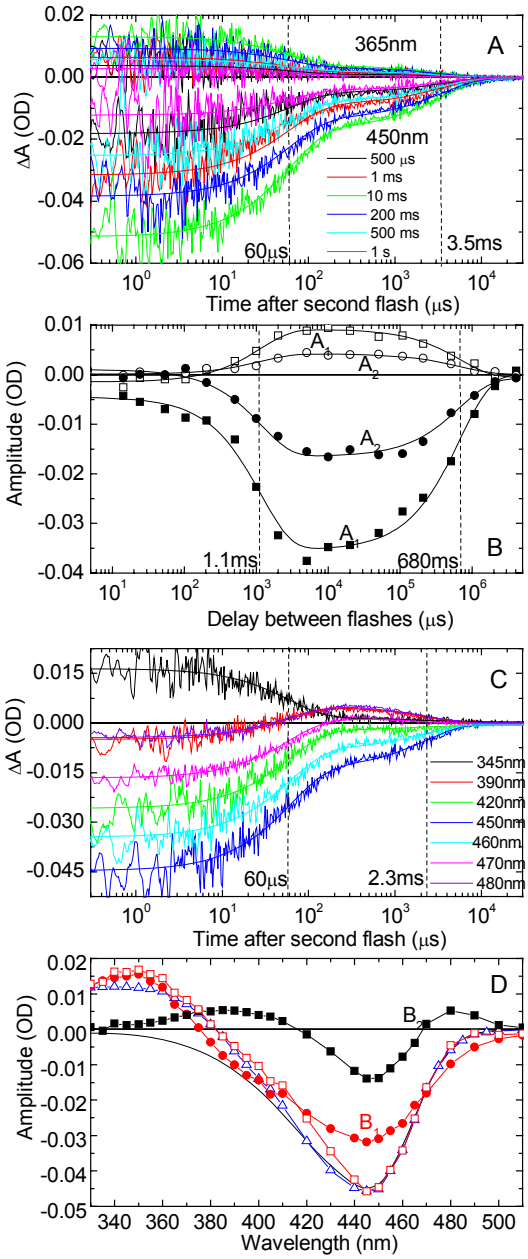

Figure 4.8: (A) Photoreversal signals, at 365 nm and 450 nm at six delays ranging from 500 µs to 1 s (first flash at 430 nm, second flash at 355 nm). For clarity, the data at 13 other delays are not shown. The solid lines represent a two-exponential global fit to all of the data with τ_1 = 60 µs and τ_2 = 3.5 ms marked by the dashed vertical lines. Conditions: pH 10, 20 °C, 50 mM KCl and 20 mM Tris. PYP concentration: 58 µM. (B) Dependence of the photoreversal amplitudes A_1 and A_2 on the delay. A_1 and A_2 are the amplitudes of the fast (60 µs) and slow (3.5 ms) components, respectively, obtained from the global fit of the delay data of panel A. The two positive amplitudes with open squares (A_1) and circles (A_2) are for the data at 365 nm; the two negative amplitudes with filled squares (A_1) and circles (A_2) are for the data at 450 nm. The dashed lines at 1.1 ms and 680 ms indicate the values of the time constants for a global fit with two exponentials. The solid curves represent the fit. (C) Photoreversal signals at seven wavelengths between 330 and 510 nm at the fixed delay of 10 ms. For clarity, similar data at 23 additional wavelengths are not shown. The solid lines are the global fits with a sum of two exponentials with the common time constants τ_1 = 60 µs and τ_2 = 2.3 ms, marked by the vertical dashed lines. (D) Amplitude spectra $B_1(\lambda)$ and $B_2(\lambda)$ associated with τ_1 and τ_2 obtained from the global fit of (B): B_1 (close red circles), B_2 (■), sum of B_1 and B_2 (open red squares) and down scaled $I_2'^{cis}$ – P difference spectrum (blue open triangles). The solid curve is a scaled P spectrum.

The delay dependence of A_1 and A_2 in Figure 4.8B thus closely matches the time course of the I_2' intermediate (Figure 3.8C). The slow ms component A_2 has a much smaller amplitude than A_1 (about 40%).

To characterize the spectral intermediates involved in photoreversal, its kinetics were measured at 30 wavelengths from 330 to 510 nm at the fixed delay of 10 ms (where the photoreversal amplitude is maximal, Figure 4.8B). The time traces at seven selected wavelengths are shown in Figure 4.8C. The solid lines are from a simultaneous fit to all 30 traces with two exponentials. The two exponential time constants are τ_1 = 60 μs and τ_2 = 2.3 ms and are identified by vertical dashed lines in Figure 4.8C. The agreement with the delay data (panel A) is excellent. The corresponding amplitude spectra $B_1(\lambda)$ (red balls) and $B_2(\lambda)$ (■) associated with these two exponentials are plotted in Figure 4.8D. The sum of $B_1(\lambda)$ and $B_2(\lambda)$ (open red squares) is also plotted. This sum equals the initial absorbance change after the second flash with respect to the initial dark state P.

The fact that both A_1 and A_2 have the same delay dependence and rise and decay in parallel with I_2', suggests that at alkaline pH photoreversal proceeds via $I_2'^{cis}$ under our experimental conditions. From Figure 3.8A we note that the extinction coefficient of I_1' at 355 nm is only about a fourth of that of I_2'. According to Figure 3.8C, the relative concentration of I_1' is only about half that of I_2' at the delay of 10 ms. Together these factors lead to an expected photoreversal signal from I_1' below the detection limit. Similar arguments hold for I_1. As shown in Figure 4.8D, the initial absorbance change (open red squares) fits reasonably well with the scaled ($I_2'^{cis}$ – P) difference spectrum (blue open triangles, Figure 4.5B) for wavelengths larger than 440 nm. Below 440 nm however, significant systematic deviations are apparent. Around 345 nm, this difference is presumably due to the higher extinction coefficient of $I_2'^{trans}$ with respect to $I_2'^{cis}$, Figure 4.5C. The positive discrepancy in the range 390 to 440 nm is most likely due to a contribution from the I_1' intermediate. This suggests that the second flash initially produces $I_2'^{trans}$ from which some $I_1'^{trans}$ is generated before the start of the data acquisition. This I_1' contribution could arise from rapid equilibrium with $I_2'^{trans}$ after reisomerization. Comparison of $B_1(\lambda)$ with the scaled spectrum of P (Figure 4.8D) indicates that, in the fast component, an I_2-like intermediate ($I_2'^{trans}$) decays and an I_1-like intermediate rises (negative mismatch near 490 nm). This transition is probably associated with proton release from the chromophore. The fact that at pH 10 it is accelerated (60 μs) with respect to pH 6 (380 μs) is consistent with faster deprotonation at the higher pH. The $B_2(\lambda)$ spectrum shows that in the subsequent slow transition the $I_1^{trans}/I_1'^{trans}$ equilibrium decays to P. This is supported by the positive contributions to B_2 around 390 nm (I_1') and 480 nm (I_1). The photoreversal transition from $I_2'^{cis}$ to P consists of three sequential steps: rapid unresolved isomerization of $I_2'^{cis}$ and formation of an $I_2'^{trans}/I_1'^{trans}$ equilibrium, the 60 μs transition from

$I_2'^{trans}/I_1'^{trans}$ to $I_1'^{trans}/I_1^{trans}$ (chromophore deprotonation), followed by the return to P in ~ 3 ms. The proposed reaction scheme is shown in the inner part of the photocycle model of the Figure 3.13.

Comparing these results at pH 10 Figure 4.8A, with previous results at pH 6, Figure 4.5A, striking differences are apparent. At pH 10, the two time constants are more widely separated and τ_2 is increased by a factor of about ten (58 and 380 µs at pH 6; 60 µs and 3.5 ms at pH 10). The dependence of both amplitudes A_1 and A_2 on the delay is the same at pH 10 and requires only two exponential time constants 1.1 ms and 680 ms, which closely match the rise and decay times of I_2', Figure 3.8C. At pH 6, the delay dependencies of A_1 and A_2 were very different, requiring three exponentials and suggesting photoreversal from sequential I_2 and I_2' intermediates, Figure 4.4A. Moreover they showed that I_2 and I_2' are in equilibrium. In contrast to the case at pH 6, the slow ms component A_2 has a smaller amplitude than A_1 (about 40%). Whereas both amplitude spectra at pH 6 had only contributions in the 330 – 380 nm region from I_2 and I_2' intermediates, at pH 10 B_1 has a spectrum corresponding to I_2 or I_2' , but B_2 has contributions from I_1' and I_1. The data at pH 10 provide no evidence for a sequential I_2 to I_2' step nor for an I_2/I_2' equilibrium. It is concluded that at pH 10 very little or no I_2 remains. At this pH there is only one intermediate with a protonated chromophore, I_2', and I_1' and I_2' are in equilibrium.

Using a second green flash (495 nm) and a delay of 20 µs, efficient photoreversal from I_1 at pH 10 is detected, with a time constant for the return to P of less than 1 µs (data not shown). This result is the same as that obtained at pH 6 (Figure 4.6). The photoreversal from I_1 is represented in Figure 3.13.

4.4 Discussion

From measurements of the photoreversal kinetics of PYP, the following results were obtained: 1) I_2 and I_2' can be distinguished from their corresponding photoreversal time constants, 2) the delay dependence of the photoreversal amplitudes indicate that I_2 and I_2' are in equilibrium beyond ~10 ms, 3) this equilibrium is pH dependent with pK_a ~6.1, as determined from the pH dependence of the photoreversal amplitudes, 4) I_2^{trans} and $I_2'^{trans}$ have higher extinction coefficients than I_2^{cis} and $I_2'^{cis}$ respectively, and *cis* to *trans* photoisomerization is faster than 50 ns, 5) efficient photoback reaction from I_1 is feasible with a green flash, 6) no I_2 is detected at pH 10.

Using double flash excitation with a variable time delay between the blue (430 nm) and violet (355 nm) flashes, the kinetics of the photoreversal from the I_2^{cis} and $I_2'^{cis}$ intermediates to the initial dark state P were investigated. Figure 3.6 summarizes key aspects of the PYP photocycle and the integration of the photoreversal processes into the overall photocycle in the acid/neutral pH range. Photoisomerization to the I_2^{trans} and $I_2'^{trans}$ intermediates is the first step in photoreversal and is expected to be very rapid (on the order of a few picoseconds, **[Heyne, 2005]**). We could not resolve these isomerization reactions, but we detected them by the instantaneous positive absorbance change in the 350 nm range immediately after the second flash (positive spike in trace DFTB and positive difference between traces DFTV and BFTV at time zero in Figure 4.1A). This initial *cis-trans* isomerization has been observed in previous single flash studies with a photo-steady-state mixture of I_2/I_2' and P but could not be resolved either **[Hendriks, 1999]**. We note that our experiments do not provide definitive evidence that the initial unresolved absorbance is due to isomerization. This is the most likely explanation, however. In all photoreceptors studied to date, photoisomerization occurred in the excited state and was the first event after excitation. Indeed, light-induced isomerization is time-resolved with femtosecond IR spectroscopy **[Heyne, 2005]**, and is found to occur in 3 ps, Figure 1.6.

Using a logarithmic time base and triggering on the second flash, we could time-resolve the slower dark phases of the photoreversal kinetics of I_2 and I_2'. From the data analysis of photoreversal signals, we obtained two exponential kinetic processes with time constants $\tau_1 = 57$ µs and $\tau_2 = 380$ µs (from the delay dependence) and $\tau_1 = 59$ µs and $\tau_2 = 400$ µs (from the wavelength dependence), which can be attributed to the dark phases of the photoreversal reactions of the I_2 and I_2' intermediates, respectively. In a sequential model, the delay dependence of the amplitudes A_1 and A_2, for the dark phases of the photoreversal reactions, should then reflect the time course of the I_2 and I_2' populations. Comparison of the corresponding time constants showed good agreement, except possibly for the rise of A_2 (1.3 versus 3 ms for the rise of I_2'). An exact agreement is not to be expected in view of the large errors in the time constants for the delay dependence of A_1 and A_2. This is due to the limited number of delay times (21 delay times between 1 µs and 3 s; see Figure 4.4A). Fitting these few data points over six decades of time with three exponentials necessarily leads to considerable errors. The fact that A_2 rises simultaneously with the decay of A_1 provides strong evidence for the sequential model.

In a unidirectional sequential model, the A_1 amplitude should decay to zero in parallel with the rise of A_2. Instead, A_1 drops to only about 50% of its maximal value around 5 ms,

remains constant, and finally decays together with A_2 to zero in 500 ms. This suggests the presence of a thermal back-reaction from I_2' to I_2 and the corresponding existence of an I_2/I_2' equilibrium (Figure 3.6). Since chemical reactions are generally reversible, a strictly unidirectional photocycle is unlikely to be correct. In fact, evidence for a pH-dependent equilibrium between the I_1 and I_2 intermediates in wild type and in the mutant E46Q was recently presented **[Borucki, 2003]**, **[Imamoto, 2004]**.

The photoreversal method provides a powerful tool to prove directly the existence of thermal back-reactions. Suppose the intermediate I_n is photoreversed and the delay is set such that both the I_n and I_{n+1} states are populated. The second flash, which selectively excites I_n, leads to an instantaneous decrease in the concentration of I_n. If a back-reaction with I_{n+1} exists, the concentration of I_n will increase again by chemical relaxation of the I_n/I_{n+1} equilibrium. This allows a determination of the rate of the back-reaction. This idea was successfully applied to the equilibrium between the M and N intermediates of bacteriorhodopsin using the photoreversal from M **[Druckmann, 1993]** and should find application to PYP as well. Since the absorption spectra of I_2 and I_2' are very similar, the 355 nm flash used here cannot perturb the postulated I_2/I_2' equilibrium. Application to the I_1/I_2 equilibrium is more promising since these intermediates have very different absorption spectra, allowing selective excitation.

Comparing the spectra of I_2^{trans} and $I_2'^{trans}$ in Figure 4.5C with those of I_2^{cis} and $I_2'^{cis}$, we conclude that the extinction coefficient of I_2' is much higher in the *trans* than in the *cis* form. This result confirms the experimental observation of Figure 4.1A that, at 340 nm (and neighboring UV wavelengths), there is a large instantaneous and unresolved increase in absorbance due to the *cis-trans* isomerization (difference between DFTV and BFTV traces at 1 µs). The origin of this difference in oscillator strength between the *trans* and *cis* forms of the protonated chromophore is not well understood, but the effect is large and seems to be common. For example, in the mutant E46Q, the dark *trans* form of the chromophore also has a much larger extinction coefficient around 350 nm than the I_2^{cis} form in the normal photocycle **[Borucki, 2003]**.

The absorption maxima of I_2^{cis} (~ 370 nm) and $I_2'^{cis}$ (~ 350 nm) differ by about 20 nm as shown in Figure 3.2A. Our analysis of the A_1 and A_2 amplitude spectra, resulting in intermediate spectra of I_2^{trans} (λ_{max} ~ 345 nm) and $I_2'^{trans}$ (λ_{max} ~ 355 nm) of Figure 4.5C, shows that these spectra also differ. The spectrum of I_2^{trans} is blue shifted with respect to that of $I_2'^{trans}$ by roughly 10 nm. These observations are consistent with the view that the chromophore environment differs in the I_2 and I_2' states. Apart from the value of the

extinction coefficient at corresponding λ_{max} values, the $I_2'^{trans}$ and $I_2'^{cis}$ spectra are comparable in terms of the spectral shape and the value of the absorbance maxima. However, the I_2^{trans} and I_2^{cis} spectra are quite different in the value of the absorbance maxima, in addition to the value of the extinction coefficient at their λ_{max}.

The dark phase of photoreversal, involving chromophore deprotonation, movement of chromophore back into the binding pocket, and reversal of global conformational change, is quite rapid: ~58 μs for I_2 and ~400 μs for I_2'. Moreover, these reversals occur in a single concerted step. The difference in the photoreversal kinetics of these two I_2 intermediates is a consequence of the different structure of the two states. Reversal from I_2 involves chromophore deprotonation and a coupled movement of the chromophore back into the binding pocket and is thus rapid (58 μs). In the reversal from I_2', the global conformational change has to be reversed as well, leading to slower kinetics. Our data thus provide a first estimate of about 400 μs for the time constant of the protein refolding reaction. In the thermal decay of I_2 which occurs in a few hundred milliseconds, the isomerization is rate-limiting, and the reaction appears to occur with a single time constant.

It has been argued that I_2 and I_2' are difficult to distinguish with electronic absorption spectroscopy since their spectra are similar. The most convincing evidence for the existence of different I_2 intermediates (protonated chromophore) comes from time-resolved FTIR measurements **[Xie, 2001]**, **[Brudler, 2001]**. I_2 and I_2' can also be distinguished by the ability of I_2' to bind dyes **[Borucki, 2002]**, **[Hendriks, 2002]** when a hydrophobic surface patch is exposed as a result of the conformational change **[Meyer, 1989]**. Here we showed that I_2 and I_2' can be differentiated kinetically using the double flash method with variable time delay, which was applied here for the first time to PYP.

Using a second flash at 500 nm, we directly showed photoreversal from I_1. This reaction is fast (<1 μs) and possibly faster than our time resolution of about 50 ns. It is not surprising that the photoreversal kinetics from I_1 are much faster than from I_2. In the earlier I_1 intermediate, the chromophore remains deprotonated with the hydroxyl of the chromophore hydrogen-bonded to E46 and Y42. Thus, only the isomerization around the C_7=C_8 double bond has to be photoreversed. In I_2 and I_2', the cycle has advanced much further: chromophore protonation, loss of hydrogen bonds, surface exposure of the chromophore, and global conformational change. All of this has to be reversed in addition.

In recent work on the M intermediate of the light-driven proton pump bacteriorhodopsin, we were able to demonstrate a similar kinetic heterogeneity of the M substates by photoreversal kinetics **[Dickopf, 1997]**. In the photoreversal from M,

reisomerization and chromophore protonation are involved. As was the case for the I_2 intermediate of PYP, two photoreversal time constants were observed in BR (100 and 600 ns), which could be assigned to two sequential M intermediates that differed in the protonation state of the proton release group **[Dickopf, 1997]**, **[Druckmann, 1992]**.

In previous work **[Hendriks, 1999]** the photoreversal kinetics from I_2 were investigated with single flash (355 nm) experiments on a photostationary mixture of I_2, I_2', and P at pH 5.6. This low pH was required to accumulate a sufficiently high population of I_2/I_2' under steady illumination, thus limiting this method to the low pH range. The observed exponential time constant was 147 μs at 20 °C and represents the average value over the I_2 and I_2' populations in the initial photo-steady-state mixture under these conditions. Likewise, the observed spectrum of I_2^{trans} was a superposition of the spectra of I_2^{trans} and $I_2'^{trans}$. The efficient excitation of the remaining 30% in the ground state by the 355 nm flash was ignored (see trace VFTV in Figure 4.1A,B). The value of 147 μs (measured at pH 5.6) lies between our value of 57 μs for I_2 and 380 μs for I_2' (measured at pH 6), as expected for an average value. For the mutant M100A, which has a lifetime for I_2' of ~18 min at pH 6, nearly 100% of the PYP molecules are accumulated in the I_2/I_2' equilibrium under steady illumination **[Devanathan, 1998]**. Using single flash excitation, an exponential time constant for photoreversal of 231 μs was obtained, consistent with the results presented here. The fact that the wild-type and M100A photoreversal kinetics are similar is not surprising, since current thinking is that M100 catalyzes the reisomerization but does not affect other steps in the photocycle **[Devanathan, 1998]**. Thus, photoreversal kinetics should be similar to wild type and is consistent with the above interpretation.

Measurements of the pH dependence of the photoreversal kinetics of I_2 and I_2' at a delay of 20 ms (Figure 4.7) provide further support for the pK_a of the I_2 / I_2' equilibrium. The kinetics is characterized by a fast (50-60 μs) and a slow (300-800 μs) component, which are due to photoreversal from I_2 and I_2' respectively, Figure 4.5A. The corresponding amplitudes are pH dependent (Figure 4.7B,C) with a pK_a of 6.1 in good agreement with the value of 6.4 obtained from the photocycle kinetics, Figure 3.5C. The amplitude for I_2 goes to zero beyond pH 7.3. The photoreversal data thus suggest that no I_2 remains at alkaline pH, whereas the photocycle data indicate that some I_2 remains since $[I_2]/([I_2] + [I_2'])$ is about 0.25 at pH 8.6 (Figure 3.5C). We note that the end value of the I_2 population at high pH in Figure 3.5C is quite sensitive to the exact choice of the I_1 spectrum. We found that only three intermediates I_1, I_1' and I_2' are present alkaline pH above pH 8, i.e. no I_2 as shown Figure 3.11.

Our results for photoreversal with the second flash at 355 nm are very different at pH 10 and pH 6. At pH 6, we observed photoreversal from two sequential intermediates I_2 and I_2' that were in equilibrium, and had their own photoreversal time (58 µs and 380 µs for I_2 and I_2' respectively). At pH 10, there is only one intermediate with protonated chromophore, I_2'. The photoreversal kinetics has again two phases (60 µs and 3.5/2.3 ms). However, their interpretation is very different. The first unresolved step is again the rapid isomerization from $I_2'^{cis}$ to $I_2'^{trans}$. Some $I_1'^{trans}$ is also already present around 50 ns after the second flash, possibly from rapid equilibration with $I_2'^{trans}$. In the 60 µs phase, $I_2'^{trans}$ decays to I_1^{trans}. This transition is associated with chromophore deprotonation. In the next, slower phase (3.5 ms), I_1^{trans} and $I_1'^{trans}$ decay to P. The associated amplitude spectrum B_2 provides clear evidence for the participation of I_1- and I_1' -like intermediates in the photoreversal. The photoreversal results thus provide further support for the existence of the I_1' intermediate at alkaline pH.

In future work with the double flash method, it will be of particular interest to investigate the kinetics of the associated proton release and to study the perturbation of equilibrium with selective excitation of one of the equilibrium partners.

4.5 Conclusions

The kinetics of photoreversal from I_1, I_2 and I_2' at pH 6 was measured and analyzed in detail with a violet (at 355 nm) or a green (at 500 nm) flash as the second flash. I_2 and I_2' can be distinguished on the basis of their photoreversal time constants of 57 µs and 380 µs respectively. The time delay between the two flashes was varied from 1 µs to 3 s with a violet flash as the second flash. Temporal variation of the I_2 and I_2' intermediates determined from the delay dependent photoreversal amplitudes is in agreement with their time dependent populations measured in the normal cycle with a single flash excitation experiment. From the delay dependence of the photoreversal amplitudes it was concluded that I_2 and I_2' are in equilibrium beyond ~10 ms.

Moreover, the I_2 and I_2' intermediates are in pH dependent equilibrium in about ~ 20 ms with pK_a ~ 6.1, as determined from the pH dependent photoreversal amplitudes with a violet flash as the second flash. This observation supports the measured pK_a with the single flash excitation experiment from the titration curves of the normal cycle populations at ~ 20 ms time scale.

The initial event just after absorption of the second flash is probably the reisomerization of the chromophore from *cis* to *trans*. This is indicated by the instantaneous

absorbance increase around ~ 350 nm after second flash, in the wavelength dependence of the photoreversal amplitudes at the fixed delays of 1 and 10 ms, when a violet flash is used as the second flash. This might be due to the formation of I_2^{trans} and $I_2'^{\,trans}$ from I_2^{cis} and $I_2'^{\,cis}$ respectively. The chromophore in any intermediate with *trans* configuration is observed to have a higher extinction coefficient than its *cis* counterpart. This *cis* to *trans* isomerization event could not be resolved in this study and is assumed to be faster than our time resolution of 10 ns. The wavelength dependence of the photoreversal amplitudes further indicates that, I_2^{trans} and $I_2'^{\,trans}$ formed just after the second flash, decay to the initial state P, with two separate time constants.

Selective photoreversal from I_1 with a green flash indicated that the photo-backreaction from I_1 to the initial state is faster than 1 μs.

Moreover, the delay and the wavelength dependence of the photoreversal kinetics at pH 10 were measured with a violet flash as the second flash. The delay dependence of the photoreversal amplitudes confirm the rise and decay of the I_2' intermediate, indicating the photoreversal from I_2'. The photoreversal kinetics differ significantly in the acid/neutral and alkaline pH range indicating that different intermediates contribute to the photocycle in the two pH ranges.

These results have established the double flash experiment as a significant technique to elucidate the mechanism of the normal photocycle.

Summary and Outlook

The pH dependence of the photocycle kinetics of photoactive yellow protein was measured and interpreted in terms of a specific reaction mechanism. Transient absorption spectroscopy with single and double flash excitation is used to investigate the photocycle of wild type PYP. The measured transient absorbance changes with a single blue flash excitation in the whole pH range from pH 4.6 to 11, and the time window of 50 ns to 50 s, indicate that four intermediates I_1, I_1', I_2 and I_2' contribute to the photocycle, during three transitions. These intermediates are characterized spectrally from the measured transient absorbance changes using extrapolated difference method and scaled subtraction method. This is the key information to acquire the mechanism of the photocycle kinetics. The measured absorbance maxima of the corresponding intermediates I_1, I_1', I_2 and I_2' are at 460nm, 430 nm, 370 nm and 350 nm respectively. The intermediates, I_1 and I_2' contribute in the whole pH range. However, I_1' and I_2 contribute minimally in the acid (pH 4.6 to 8.4) and alkaline pH (pH 8 to 11) range respectively. The temporal variation of each intermediate is determined from the measured transient absorbance changes and the intermediate spectra. This provides the information about the connectivity among the intermediates. It is observed that these intermediates are in equilibrium, and some intermediate populations are pH dependent during the photocycle.

I_1 decays partially to I_2 during the first transition (~ 400 μs) in the acid/neutral pH range, whereas this intermediate decays in part to I_1' in the alkaline pH range in the same transition. After the second transition (~ ms), the $I_1/I_2/I_2'$-equilibrium is formed in the acid/neutral pH range, in which the I_1/I_2-equilibrium decays further in part to I_2'. However, in the alkaline pH range the I_1/I_1' equilibrium decays forming the $I_1/I_1'/I_2'$ equilibrium during this transition. It is observed that I_2 and I_2' are in a pH dependent equilibrium in the ~ 20 ms time range with a pK_a ~ 6.3 in the acid/neutral pH region. The signaling state I_2' is the main species above this pK_a. Similarly, I_1' and I_2' are in a pH dependent equilibrium with a pK_a ~ 10, in the alkaline pH region during the same time range (~ 20 ms), with the I_1' the main species above this pK_a. Moreover, I_1' is the alkaline form of I_2' with the surface exposed chromophore. The

former pK_a might be assigned to the carboxylate side chain of E46 and the latter to the phenolate oxygen of the chromophore.

The third rate constant k_3 is due to the recovery to P of the $I_1/I_2/I_2'$-equilibrium in the acid/neutral pH range and of the $I_1/I_1'/I_2'$ equilibrium in the alkaline pH range, respectively. This rate is strongly pH dependent with a well known bell-shaped curve with pK_a's of ~ 6.3 and ~ 9.7. These pK_a's are very close to those determined from the intermediate equilibrium populations. In both cases, the recovery rate is proportional to the $[I_2']$ concentration, indicating that the dark state recovery is controlled by the I_2' population of the cycle. Thus the transient accumulation of I_2', the active state of PYP, is controlled by the proton concentration. This is analogous to the case of the photoreceptor rhodopsin, where the equilibrium between the signaling state M_{II} and its precursor M_I is also strongly pH dependent. The habitat of *Hr. Halophila* is alkaline, and this study provides the working pH range of this photoreceptor. The largest accumulation of signaling state is at ~ pH 8.

Moreover, for the first time the well-known pK_a's of the recovery rates are explained in terms of the corresponding pH dependence of the equilibrium intermediate populations. This investigation provides the most extensive data set to date (pH region from pH 4.6 to 11, the time window of 50 ns to 50 s and wavelength range of 320 nm to 510 nm) and analyses this data field in terms of the number of the intermediates, their spectra, connectivity and equilibria. The mechanism of converting photon energy to conformational alteration in PYP presented in this study contributes to understand the signal transduction mechanism of PAS domain superfamily as PYP is proposed as the PAS structural prototype.

The mechanism of the photocycle kinetics acquired with single flash excitation experiments was further supported by double flash excitation experiments, where the kinetics of photoreversal from the I_1, I_2 and I_2' intermediates was investigated. A first flash, at 430 nm, initiated the photocycle. After a variable time delay, the I_1 intermediate was photoreversed by a second flash, at 500 nm, or a mixture of I_2 and I_2' intermediates was photoreversed by a second flash, at 355 nm. The corresponding photoreversal times measured at pH 6 from I_1, I_2, and I_2' are <1 μs, 59 μs and 400 μs respectively. The first step in photoreversal is rapid *cis-trans* isomerization of the chromophore. By varying the delay from 1 μs to 3 s, it was possible to excite selectively the intermediates I_1, I_2, and I_2'. The good agreement of the delay dependence of the two amplitudes, A_1 and A_2 (respective photoreversal times of 59 μs and 400 μs), with the time dependence of the I_2 and I_2' populations provided strong evidence for the sequential model. The persistence of A_1 beyond delay times of 5 ms and its decay, together with A_2 around 500 ms, suggest moreover that I_2 and I_2' are in thermal equilibrium. This was

the first evidence for this equilibrium, which was later supported by measurements of the normal cycle. Depending on the progression of the photocycle, reversal becomes slower with the time delay, thus mirroring the individual steps of the forward photocycle. In this way, the kinetics and equilibria of the single flash cycle may be probed by photoreversal.

Moreover, measurements of the pH dependence of the photoreversal kinetics in the pH range of 4.8 to 8.5 with a second flash of 355 nm applied at a delay of 20 ms confirmed the pK_a value (~ 6.1) of the I_2/I_2' equilibrium obtained from measurements of the single flash cycle. Photoreversal experiments at pH 10 with the second flash at 355 nm indicate the presence of only one I_2-like intermediate, which is assigned on the basis of its λ_{max} value to I_2'. The amplitude spectra of the photoreversal signal support that $I_2'^{trans}$, $I_1'^{trans}$ and I_1^{trans} intermediates participate in this reversal.

Photoreversal from I_2' is slower than from I_2, since, in addition to chromophore protonation, the global conformational change has to be reversed. These data thus provide a first estimate of about 59 µs for deprotonation and 400 µs for the structural change, which also occurs in the thermal decay of the signaling state but is obscured there since reisomerization is rate-limiting.

In future work, these investigations may be extended to key mutants (e.g. E46Q, Y42F, K110A, E12A) and PYP/phytochrome hybrids under various conditions e.g. azide, heavy water, temperature to probe their effect on the photocycle. The extrapolated difference method and the scaled subtraction method might be used to determine the spectra of the intermediates and the associated time courses. Alternatively, the double flash excitation experiment might assist to verify the photocycle kinetics acquired from the single flash excitation experiment.

In particular, photocycle study of K110A and E12A mutants may explain the role of the K110 and E12 salt bridge, during the formation of the signaling state I_2' as proposed in **[Borucki, 2005]**. Still unexplained curved Arrhenius plots for the measured recovery rate as a function of temperature **[Meyer, 1989]** may be explained in terms of the intermediate equilibrium populations. Preliminary experiments for some of these cases have shown interesting observations. For example, there is a large azide effect on the photocycle at pH 6.3, where the recovery is slowed down by a factor of ~ 10 upon addition of 850 mM azide. Whether this effect is just like the salt effect reported in **[Borucki, 2005]**, **[Harigai, 2003]** or whether azide acts as a proton donor/acceptor as observed in bacteriorhodopsin **[Otto, 1989]**, remains to be seen.

Interesting isotope effectes were observed during the course of this Ph. D. work. The dark spectrum is red-shifted by 2 nm, in D_2O and recovery is slowed down by a factor of ~ 2 at pH 6. These observations are similar to those reported in **[Hendriks, 2003]**. Moreover, by measuring the proton inventory plots of various transitions as acquired for bacteriorhodopsin **[Brown, 2000]**, it may be possible to distinguish, whether a particular transition involves one or more protons.

Finally, these investigations may be extended to other photoreceptors especially the hybrid proteins containing PYP and phytochrome domains **[Kyndt, 2004]**. A major question here is why these photoreceptors have two chromophore domains. How do these domains interact? Does the blue light absorbed by PYP control or reset the red light sensitive phytochrome domain? The interest here is on the selective excitation of the particular domain (e.g. phytochrome) and observe its effect on the other domain.

Bibliography

1. **[Anderson, 2004]** Anderson S., Crosson S. and Moffat K. (2004) Short hydrogen bonds in photoactive yellow protein. *Acta Cryst.* **60**,1008-1016.
2. **[Baca, 1994]** Baca M., Borgstahl G. E. O., Boissinot M., Burke P. M., Willams DW. R., Slater K. A. and Getzoff E. D. (1994) Complete chemical structure of photoactive yellow protein: Novel thioester-linked 4-hydroxycinnamyl chromophore and photocycle chemistry. *Biochemistry* **33**, 14369-14377.
3. **[Borgstahl, 1995]** Borgstahl G. E. O., Willams D. R. and Getzoff E. D. (1995) 1.4 Å structure of photoactive yellow protein, a cytosolic photoreceptor: unusual fold, active site, and chromophore. *Biochemistry* **34**,6278-6287.
4. **[Borucki, 1999]** Borucki B., Otto H., Heyn M. P. (1999) Reorientation of the retinylidene chromophore in the K, L and M intermediates of bacteriorhodopsin from time-resolved linear dichroism: resolving kinetically and spectrally overlapping intermediates of chromoproteins. *J. Phys. Chem. B* **103**,6371-6383.
5. **[Borucki, 2002]** Borucki B., Devanathan S., Otto H., Cusanovich M. A., Tollin G. and Heyn M. P. (2002) Kinetics of proton uptake and dye binding by photoactive yellow protein in wild type and in the E46Q and E46A mutants. *Biochemistry* **41**,10026-10037.
6. **[Borucki, 2003]** Borucki B., Otto H., Joshi C. P., Gasperi C., Cusanovich M. A., Devanathan S., Tollin G. and Heyn M. P. (2003) pH dependence of the photocycle kinetics of the E46Q mutant of photoactive yellow protein: protonation equilibrium between I_1 and I_2 intermediates, chromophore deprotonation by hydroxyl uptake, and protonation relaxation of the dark state. *Biochemistry* **42**, 8780-8790.
7. **[Borucki, 2003A]** Borucki B., Otto H., Rottwinkel G., Hughes J., Heyn M. P. and Lamparter T. (2003) Mechanism of Cph1 phytochrome assembly from stopped-flow kinetics and circular dichroism. *Biochemistry* **42**,13684-13697.
8. **[Borucki, 2005]** Borucki B., Kyndt J. A., Joshi C. P., Otto H., Meyer T. E., Cusanovich M. A., and Heyn M. P. (2005) Effect of salt and pH on the activation of photoactive yellow protein and gateway mutants Y98Q and Y98F. *Biochemistry* **44**,13650-13663.
9. **[Brown, 2000]** Brown L. S., Needleman R. and Lanyi J. K. (2000) Origins of deuterium kinetic isotope effects on the proton transfers of the bacteriorhodopsin photocycle. *Biochemistry* **39**,938 –945.

10. **[Brudler, 2000]** Brudler R., Meyer T. E., Genick U. K., Devanathan S., Woo T. T., Millar D. P., Gerwert K., Cusanovich M. A., Tollin G. and Getzoff E. D. (2000) Coupling of hydrogen bonding to chromophore conformation and function in photoactive yellow protein. *Biochemistry* **39**, 13478-13486.
11. **[Brudler, 2001]** Brudler R., Rammelsberg R., Woo T. T., Getzoff E. and Gerwert K. (2001) Structure of the I_1 early intermediate of photoactive yellow protein by FTIR spectroscopy. *Nature Struct. Biol.* **8**,265-270.
12. **[Cusanovich, 2003]** Cusanovich M. A. and Meyer T. E. (2003) Photoactive yellow protein : A prototypic PAS domain sensory protein and development of a common signaling mechanism. *Biochemistry* **42**,4759-4770.
13. **[Demchuk, 2000]** Demchuk E., Genick U. K., Woo T. T., Getzoff E. D. and Bashford D. (2000) Protonation states and pH titration in the photocycle of photoactive yellow protein. *Biochemistry* **39**,1100-1113.
14. **[Devanathan, 1998]** Devanathan S., Genick U. K., Canestrelli I. L., Meyer T. E., Cusanovich M. A., Getzoff E. D. and Tollin G. (1998) New insights into the photocycle of *Ectothiorhodospira halophila* photoactive yellow protein: photorecovery of the long-lived photobleached intermediate in the Met100Ala mutant. *Biochemistry* **37**,11563-11568.
15. **[Devanathan, 1999A]** Devanathan S., Brudler R., Hessling B., Woo T. T., Gerwert K., Getzoff E. D., Cusanovich M. A. and Tollin G. (1999) Dual photoactive species in Glu46Asp and Glu46Ala mutants of photoactive yellow protein: a pH driven color transition. *Biochemistry* **38**,13766-13772.
16. **[Dickopf,1997]** Dickopf S. and Heyn M. P. (1997) Evidence for the first phase of the reorientation switch of bacteriorhodopsin from time-resolved photovoltage and flash photolysis experiments on the photoreversal of the M-intermediate. *Biophys. J.* **73**,3171-3181.
17. **[Dickopf, 1998]** Dickopf S., Mielke T. and Heyn M. P. (1998) Kinetics of the light-induced proton translocation associated with the pH-dependent formation of the metarhodopsin I/II equilibrium of bovine rhodopsin. *Biochemistry* **37**,16888-16897.
18. **[Druckmann, 1992]** Druckmann S., Friedman N., Lanyi J. K., Needleman R. and Ottolenghi M. (1992) The back photoreaction of the M intermediate in the photocycle of bacteriorhodopsin: mechanism and evidence for two M species. *Photochem. Photobiol.* **56**,1041-1047.

19. [**Druckmann, 1993]** Druckmann S., Heyn M. P., Lanyi J. K., Ottolenghi M. and Zimanyi L. (1993) Thermal equilibrium between the M and N intermediates in the photocycle of bacteriorhodopsin. *Biophys. J.* **65**,1231-1234.
20. **[Düx, 1998]** Düx P., Rubinstenn G., Vuister G. W., Boelens R., Mulder F. A. A., Hard K., Hoff W. D., Kroon A. R., Crielaard W., Hellingwerf K. J. and Kaptein R. (1998) Solution structure and backbone dynamics of the photoactive yellow protein. *Biochemistry* **37**,12689-12699.
21. **[Genick, 1997A]** Genick U., Borgstahl G. E. O., Ng K., Ren Z., Pradervand C., Burke P. M., Srajer V., Teng T. Y., Schildkamp W., McRee D. E., Moffat K. and Getzoff E. D. (1997) Structure of a protein photocycle intermediate by millisecond time-resolved crystallography. *Science* **275**,1471-1475.
22. **[Genick, 1997]** Genick U. K., Devanathan S., Meyer T. E., Canestrelli I. L., Williams E., Cusanovich M. A., Tollin G. and Getzoff E. D. (1997) Active site mutants implicate key residues for control of color and light cycle kinetics of photoactive yellow protein. *Biochemistry* **36**,8-14.
23. **[Genick, 1998]** Genick U. K., Soltis M. S., Kuhn P., Canestrelli I. L. and Getzoff E. (1998) Structure at 0.85 Å resolution of an early protein photocycle intermediate. *Nature* **392**,206-209.
24. **[Groot, 2003]** Groot M. L., van Wilderen L. J. G. W., Larsen D. S., van der Horst M. A., van Stokkum I. H. M., Hellingwerf K. J. and van Grondelle R. (2003) Initial steps of signal generation in photoactive yellow protein revealed with femtosecond mid-infrared spectroscopy. *Biochemistry.* **42**,10054-10059.
25. **[Harigai, 2003]** Harigai M., Imamoto Y., Kamikubo H., Yamazaki Y. and Kataoka M. (2003) Role of an N-terminal loop in the secondary structural change of photoactive yellow protein. *Biochemistry* **42**,13893-13900.
26. **[Hendriks, 1999]** Hendriks J., van Stokkum I. H. M. and Hellingwerf K. J. (1999) Kinetics of and intermediates in a photocycle branching reaction of the photoactive yellow protein from *Ectothiorhodospira halophila*. *FEBS Lett.* **458**, 252-256.
27. **[Hendriks**, **1999A]** Hendriks J., Hoff W. D., Crielaard W. and Hellingwerf K. J. (1999) Protonation deprotonation reactions triggered by photoactivation of photoactive yellow protein from *Ectothiorhodospira halophila. J. Biol. Chem.* **274**,17655-17660.

28. **[Hendriks, 2002]** Hendriks J., Gensch T., Hviid L., van der Horst M. A., Hellingwerf K. J., and van Thor J. J. (2002) Transient exposure of hydrophobic surface in the photoactive yellow protein with Nile red. *Biophys. J.* **82**,1632-1643.
29. **[Hendriks**, **2003]** Hendriks J., van Stokkum I. H .M. and Hellingwerf K. J. (2003) Deuterium isotope effects in the photocycle transitions of the photoactive yellow protein. *Biophys. J*. **84**,1180-1191.
30. **[Henry, 1992]** Henry E. R. and Hofrichter J. (1992) Singular value decomposition: application to the analysis of experimental data. *Methods Enzymol.* **210**,129-192.
31. **[Hellingwerf, 2003]** Hellingwerf K. J., Hendriks J. and Gensch T. (2003) Photoactive yellow protein, a new type of photoreceptor protein: will this "yellow lab" bring us where we want to go?. *J. Phys. Chem.* **107**,1082-1094.
32. **[Heßling, 1993]** Heßling B., Souvignier G. and Gerwert K. (1993) A model-independent approach to assigning bacteriorhodopsin's intramolecular reactions to photocycle intermediates. *Biophys. J.* **65**,1929-1941.
33. **[Heyne, 2005]** Heyne K., Mohammed O. F., Usman A., Dreyer J., Nibbering E. T. J. and Cusanovich M. A. (2005) Structural evolution of the chromophore in the primary stages of trans/cis isomerization in photoactive yellow protein. *J. Am. Chem. Soc.* **127**,18100-18106.
34. **[Hoff, 1994]** Hoff W. D., Düx P., Hard K., Devreese B., Nugteren-Roozant I. M., Crieland W., Boelens R., Kaptein R., Van Beeumen J. and Hellingwerf K. J. (1994) Thiol ester-linked p-coumaric acid as a new photoactive prosthetic group in a protein with rhodopsin-like photochemistry. *Biochemistry* **33**,13959-13962.
35. **[Hoff, 1999]** Hoff W. D., Xie A., Van Stokkum I. H. M., Tang X. J., Gural J., Kroon A. R. and Hellingwerf K. J. (1999) Global conformational changes upon receptor stimulation in photoactive yellow protein. *Biochemistry* **38**, 1009-1017.
36. **[Ihee, 2005]** Ihee H., Rajagopal S., Srajer V., Pahl R., Anderson S., Schmidt M., Schotte F., Anfinrud P. A., Wulff M. and Moffat K. (2005) Visualizing reaction pathways in the photoactive yellow protein from nanoseconds to seconds. *PNAS* **102**,7145-7150.
37. **[Imamoto, 1997]** Imamoto Y., Mihara K., Histomi O., Kataoka M., Tokunaga F., Bojkova N. and Yoshihara K. (1997) Evidence for proton transfer from Glu-46 to the chromophore during the photocycle of photoactive yellow protein. *J. Biol. Chem.* **272**, 12750-12908.

38. **[Imamoto, 2001]** Imamoto Y., Koshimizu H., Mihara K., Hisatomi O., Mizukami T., Tsujimoto K., Kataoka M. and Tokunaga F. (2001) Roles of amino acid residues near the chromophore of photoactive yellow protein. *Biochemistry* **40**,4679-4685.
39. **[Imamoto**, **2001A]** Imamoto Y., Mihara K., Tokunaga F. and Kataoka M. (2001) Spectroscopic characterization of the photocycle intermediates of photoactive yellow protein. *Biochemisty* **40**,14336-14343.
40. **[Imamoto, 2002]** Imamoto Y., Kamikubo H., Mihara K., Shimizu M. and Kataoka M. (2002) Light induced global conformational change of photoactive yellow protein in solution. *Biochemistry* **41**,13595-13601.
41. [**Imamoto, 2004]** Imamoto Y., Harigai M. and Kataoka M. (2004) Direct observation of the pH-dependent equilibrium between L-like and M intermediates of photoactive yellow protein. *FEBS Letters* **577**,75-80.
42. **[Joshi, 2005]** Joshi C. P., Borucki B., Otto H., Meyer T. E., Cusanovich M. A. and Heyn M. P. (2005) Photoreversal kinetics of the I_1 and I_2 intermediates in the photocycle of photoactive yellow protein by double flash experiments with variable time delay. *Biochemistry* **44**,656-665.
43. **[Kenneth, 1990]** Connors, K. A. (1990) Chemical Kinetics. VCH publishers, New York.
44. **[Kim, 1995]** Kim M., Mathies R. A., Hoff W. D. and Hellingwerf K. J. (1995) Resonance Raman evidence that the thioester-linked 4-hydroxycinnamyl chromophore of photoactive yellow protein is deprotonated. *Biochemistry* **34**,12669-12672.
45. **[Kroon, 1996]** Kroon A. R., Hoff W. D., Fennema H. P. M., Gijzen J., Kommen G., Verhoeven J. W., Crielaard W. and Hellingwerf K. J. (1996) Spectral tuning, fluorescence, and photoactivity in hybrids of photoactive yellow protein, reconstituted with native or modified chromophores. *J. Biol. Chem.* **271**,31949-31956.
46. **[Kyndt, 2003]** Kyndt J. A., Vanrobaeys F., Fitch J. C., Devreese B. V., Meyer T. E., Cusanovich M. A. and Van Beeumen J. J. (2003) Heterologous production of *Halorhodospira halophila* Holo-photoactive yellow protein through tandem expression of the postulated biosynthetic genes. *Biochemistry* **42**,965-970.
47. **[Kyndt, 2004]** Kyndt J. A., Meyer T. E. and Cusanovich M. A. (2004) Photoactive yellow protein, bacteriophytochrome, and sensory rhodopsin in purple phototrophic bacteria. *Photochem. Photobiol. Sci.* **3**,519-530.

48. **[Lee, 2001]** Lee B. C., Croonquist P. A., Sosnick T. R. and Hoff W. D. (2001) PAS domain receptor photoactive yellow protein is converted to a molten globule state upon activation. *J. Biol. Chem.* **276**,20821-20823.
49. **[Meyer, 1985]** Meyer T. E. (1985) Isolation and characterization of soluble cytochromes, ferredoxins and other chromophoric proteins from the halophilic phototrophic bacterium *Ectothiorhodospira halophila*. *Biochim. Biophys. Acta* **806**,175-183.
50. **[Meyer, 1987]** Meyer T. E., Yakali E. and Cusanovich M. A. (1987) Properties of a water-soluble, yellow protein isolated from a halophilic phototrophic bacterium that has photochemical activity analogous to sensory rhodopsin. *Biochemistry* **26**,418-423.
51. **[Meyer, 1989]** Meyer T. E., Tollin G., Hazzard J. H. and Cusanovich M. A. (1989) Photocycle of the photoactive yellow protein from the purple phototrophic bacterium, *Ectothiorhodospira halophila*: quantum yield of photobleaching and effects of temperature, alcohols, glycerol, and sucrose on the kinetics of photobleaching and recovery. *Biophys J.* **56**,559-564.
52. **[Meyer, 1991]** Meyer T. E., Tollin G., Causgrove T. P., Cheng P. and Blankenship R. E. (1991) Picosecond decay kinetics and quantum yield of fluorescence of the photoactive yellow protein from the halophilic purple phototrophic bacterium, *Ectothiorhodospira halophila*. *Biophys. J.* **59**,988-991.
53. **[Meyer, 1993]** Meyer T. E., Cusanovich M. A. and Tollin G. (1993) Transient proton uptake and release is associated with the photocycle of the photoactive yellow protein from the purple phototrophic bacterium, *Ectothiorhodospira halophila*. *Arch. Biochem. Biophys.* **306**, 515-517.
54. **[Meyer, 2003]** Meyer T. E., Devanathan S., Woo T., Getzoff E. D., Tollin G. and Cusanovich M. A. (2003) Site-specific mutations provide new insights into the origin of pH effects and alternative spectral forms in the photoactive yellow protein from *Halorhodospira halophila*. *Biochemistry* **42**,3319-3325.
55. **[Miller, 1993]** Miller, A., Leigeber, H., Hoff, W. D. and Hellingwerf, K. J. (1993) A light-dependent branching reaction in the photocycle of the yellow protein from *Ectothiorhodospira halophila*, *Biochim. Biophys. Acta* **1141**,190-196.
56. **[Molina, 2001]** Molina V., Merchan M. (2001) On the absorbance changes in the photocycle of the photoactive yellow protein: A quantum-chemical analysis. *PNAS* **98**,4299-4304.

57. **[Ohishi, 2001]** Ohishi S., Shimizu N., Mihara K., Imamoto Y. and Kataoka M. (2001) Light induces destabilization of photoactive yellow protein. *Biochemistry* **40**,2854-2859.

58. **[Otto, 1989]** Otto, H., Marti, T., Holz, M., Mogi, T., Lindau, M., Khorana, H. G. and Heyn M. P. (1989) Aspartic acid-96 is the internal proton donor in the reprotonation of the Schiff base of bacteriorhodopsin. *Proc. Natl. Acad. Sci. U.S.A.* **86**,9228-9232.

59. **[Otto, 2005]** Otto H., Hoersch D., Meyer T. E., Cusanovich M. A. and Heyn M. P. (2005) Time-resolved single tryptophan fluorescence in photoactive yellow protein monitors changes in the chromophore structure during the photocycle via energy transfer. *Biochemistry* **44**,16804-16816.

60. **[Pan, 2004]** Pan D., Philip A., Hoff W. D., Mathies R. A. (2004) Time-resolved resonance Raman structural studies of the pB′ intermediate in the photocycle of photoactive yellow protein. *Biophys. J.* **86**, 2374-2382.

61. **[Perman, 1998]** Perman B., Srajer V., Ren Z., Teng T. Y., Pradervand C., Ursby T., Bourgeois D., Schotte F., Wulff M., Kort R., Hellingwerf K. J. and Moffat K. (1998) Energy transduction on ns time scale: early structure events in a Xanthopsin photocycle. *Science* **279**, 1946-1950.

62. **[Pellequer, 1998]** Pellequer J. L., Wager-Smith K. A., Kay S. A. and Getzoff E. D. (1998) Photoactive yellow protein : A structural prototype for the three-dimensional fold of the PAS domain superfamily. *PNAS* **95**,5884-5890.

63. **[Ren, 2001]** Ren Z., Perman B., Srajer V., Teng T. Y., Pradervand C., Bourgeois D., Schotte F., Ursby T., Kort R., Wulff M. and Moffat K. (2001) A molecular movie at 1.8 Å resolution displays the photocycle of photoactive yellow protein, a eubacterial blue-light receptor, from nanoseconds to seconds. *Biochemistry* **40**,13788-13801.

64. **[Rubinstenn, 1998]** Rubinstenn G., Vuister G. W., Düx P. E., Boelens R., Mulder F. A. A., Hard K., Hoff W. D., Kroon A. R., Crielaard W., Hellingwerf K. J. and Kaptein R. (1998) Structural and dynamic changes of photoactive yellow protein during its photocycle in solution. *Nature Struct. Biol.* **5**,568-570.

65. **[Sasaki, 2002]** Sasaki J., Kamuchi M., Hamada M., Oka T., and Tokunaga F. (2002) Light induced unfolding of photoactive yellow protein mutant M100L. *Biochemistry* **41**,1915-1922.

66. **[Shimizu, 2006]** Shimizu, N., Imamoto, Y., Harigai, M., Kamikubo, H., Yamazaki, Y. and Kataoka, M. (2006) pH-dependent equilibrium between long lived near-UV intermediates of photoactive yellow protein, *J. Biol. Chem.* **281**,4318-4325.
67. **[Sprenger, 1993]** Sprenger W. W., Hoff W. D., Armitage J. P. and Hellingwerf K. J. (1993) The eubacterium *Ectothiorhodospira halophila* is negatively phototactic, with a wavelength dependence that fits the absorption spectrum of the Photoactive Yellow Protein. *J Bacteriol.* **175**,3096-3104.
68. **[Taylor, 1999]** Taylor B. L. and Zhulin I. B. (1999) PAS domains: internal sensors of oxygen, redox potential, and light. *Microbiol. Mol. Biol. Rev.* **63**,479-506.
69. **[Unno, 2000]** Unno M., Kamauchi M., Sasaki J., Tokunaga F. and Yamauchi S. (2000) Evidence for a protonated and *cis* configuration chromophore in the photobleached intermediate of photoactive yellow protein. *J. Am. Chem. Soc.* **122**, 4233-4234.
70. **[Unno, 2002]** Unno M., Kamauchi M., Sasaki J., Tokunaga F. and Yamauchi S. (2002) Resonance Raman spectroscopy and the quantum chemical calculations reveal structural changes in the active site of photoactive yellow protein. *Biochemistry* **41**,5668-5674.
71. **[Unno, 2003]** Unno M., Kamauchi M., Sasaki J., Tokunaga F. and Yamauchi S. (2003) Assignment of resonance Raman spectrum of photoactive yellow protein in its long-lived blue-shifted intermediate. *J. Phys. Chem. B* **107**,2837-2845.
72. **[Unno**, **2004]** Unno M., Kumauchi M., Hamada N., Tokunaga F. and Yamauchi S. (2004) Resonance Raman evidence for two conformations involved in the L intermediate of photoactive yellow protein. *J. Biol. Chem.* **279**,23855-23858.
73. **[Van Brederode, 1996]** Van Brederode M. E., Hoff W. D., Van Stokkum I. H. M., Groot M.-L. and Hellingwerf K. J (1996) Protein folding thermodynamics applied to the photocycle of the photoactive yellow protein. *Biophys. J.* **71**,365-380.
74. **[Xie, 2001]** Xie A., Kelemen L., Hendriks J., White B. J., Hellingwerf K. J. and Hoff W. D. (2001) Formation of a new buried charge drives a large-amplitude protein quake in photoreceptor activation. *Biochemistry* **40**,1510-1517.
75. **[Yeremenko, 2006]** Yeremenko S., van Stokkum I. H. M., Moffat K. and Hellingwerf K. J. (2006) Influence of the crystalline state on photoinduced dynamics of photoactive yellow protein studied by ultraviolet-visible transient absorption spectroscopy. *Biophys. J.* **90**,4224-4235.

List of Figures

ACKNOWLEDGEMENTS

I would like to express my sincere gratitude to my supervisor Prof. Dr. Maarten P. Heyn for providing an opportunity to work in his group, his support, regular guidance and encouragement during the course of my Ph. D. work.

I am deeply grateful to Dr. Berthold Borucki and Dr. Harald Otto for suggesting the experimental work and their regular guidance of this work from the very beginning to the ending of the project.

My special thanks go to Prof. Dr. Robert Bittl for accepting to be a co-referee of my doctorate thesis and his interest in my work.

All samples of PYP were prepared in the lab of Prof. Dr. Michael Cusanovich at the University of Arizona. I am indebted to him and his coworkers, in particular John Kyndt and Elsa Chen, for a steady supply of high grade PYP wild type and mutants.

I am thankful to Mrs. Ingrid Wallat for helping in the Biochemistry lab and Mrs. Marion Badow for her help in administrative matters.

I am thankful to the colleagues Sven Seibeck, Daniel Höersch and Dirk Opitz from the research group Heyn for helpful discussions.

I would like to acknowledge the German Science Foundation (DFG) for providing the fellowship to carry out this research via grants Sfb 498-TP B1 and GRK 788-TP A9. I am thankful to Prof. Dr. Hans-Heinrich Limbach and Dr. Werner Gans for the support on the behalf of the GRK #788. This has allowed me to attend the American Biophysical Society Meeting and has introduced me to the field of hydrogen bonding.

Finally, I am thankful to my wife Jyoti for her love and continuous support and my sons Shaswat and Swastik who always reduce my tiredness when I returned from work. This small work is dedicated to my parents.

Publications

- Borucki B., Otto H., **Joshi C. P.**, Gasperi C., Cusanovich M. A., Devanathan S., Tollin G. and Heyn M. P. (2003) pH dependence of the photocycle kinetics of the E46Q mutant of photoactive yellow protein: protonation equilibrium between I_1 and I_2 intermediates, chromophore deprotonation by hydroxyl uptake, and protonation relaxation of the dark state. *Biochemistry* **42**, 8780-8790.
- **Joshi C. P.**, Borucki B., Otto H., Meyer T. E., Cusanovich M. A. and Heyn M. P. (2005) Photoreversal kinetics of the I_1 and I_2 intermediates in the photocycle of photoactive yellow protein by double flash experiments with variable time delay. *Biochemistry* **44**,656-665.
- **Joshi C.P.**, Borucki B., Otto H., Meyer T. E., Cusanovich M. A. and Heyn M. P. (2005) Double flash experiments with photoactive yellow protein: photoreversal kinetics of the I_1 and I_2 intermediates, *Biophys. J.* **88**, 508A-508A (Abstract).
- Borucki B., Kyndt J. A., **Joshi C.P.**, Otto H., Meyer T. E., Cusanovich M. A. and Heyn M. P. (2005) Effect of salt and pH on the activation of photoactive yellow protein and gateway mutants Y98Q and Y98F, *Biochemistry* **44**,13650-13663.
- **Joshi C. P.**, Borucki B., Otto H., Meyer T. E., Cusanovich M. A. and Heyn M. P. (2006) Kinetics of the Photocycle and Photoreversal of Photoactive Yellow Protein, *Biophys. J.* **90**, January 2006 (Abstract).
- Borucki B., Kyndt J. A., **Joshi C. P.**, Otto H., Meyer T. E., Cusanovich M. A. and Heyn M. P. (2006) Salt and pH effects on the formation of the signaling state of photoactive yellow protein and the mutants Y98Q and Y98F, *Biophys. J.* **90**, January 2006 (Abstract).
- **Joshi, C. P.**, B. Borucki, H. Otto, T. E. Meyer, M. A. Cusanovich, and M. P. Heyn, (2006) Photocycle and photoreversal of photoactive yellow protein at alkaline pH: kinetics, intermediates and equilibria. *Biochemistry*, in press, web release date: May 17, 2006.
- Borucki B., **Joshi C. P.**, Otto H., Cusanovich M. A. and Heyn M. P. (2006) The transient accumulation of the signaling state of photoactive yellow protein is controlled by the external pH, *Biophysical Journal*, in press.

Presentations

- **C. P. Joshi**, S. R. Pant and K. N. Khanal; *Electrical Resistivity Measurements on Analog Models*; Third National Conference on Science and Technology, 8-11 march

1999 organized by Royal Nepal Academy of Science and Technology, Kathmandu, Nepal (**Poster**).

- B. Borucki, H. Otto, **C. P. Joshi**, C. Gasperi, M. A. Cusanovich, S. Devanathan, G. Tollin and M. P. Heyn; *pH Dependence of the photocycle kinetics of the E46Q mutant of photoactive yellow protein protonation equilibrium between I_1 and I_2 intermediates, Chromophore deprotoanation by hydroxyl uptake and protonation relaxation of dark state*; 15th international conference on hydrogen bond research, 16-21 Sept. 2003, Berlin (**Poster)**; *Programme committee member* of Graduate School on hydrogen bonding and hydrogen transfer 14-16 Sept. 2003, Berlin, and **oral presentation** in graduate school.
- **C. P. Joshi**, B. Borucki, H. Otto, T. E. Meyer, M. A. Cusanovich and M. P. Heyn; *Double flash experiments with photoactive yellow protein: photo reversal kinetics of the I_1 and I_2 intermediates*; 49th Annual Meeting of Biophysical Society, Feb. 12-16 2005, Long Beach, California, USA (**poster**).
- **C. P. Joshi**, B. Borucki, H. Otto, T. E. Meyer, M. A. Cusanovich and M. P. Heyn; *Kinetics of the Photocycle and Photoreversal of Photoactive Yellow Protein*; 50th Annual Meeting of Biophysical Society, Feb. 18-22 2006, Salt Lake City, Utah, USA (**poster**).